(12) INTERNATIONAL APPLICATION PUBLISHED UNDER THE PATENT COOPERATION TREATY (PCT)

(19) World Intellectual Property Organization
International Bureau

(43) International Publication Date
4 October 2012 (04.10.2012)

WIPO | PCT

(10) International Publication Number
WO 2012/135149 A2

(51) International Patent Classification:
A61K 31/53 (2006.01) *A61P 35/00* (2006.01)
A61K 31/5415 (2006.01)

(21) International Application Number:
PCT/US2012/030619

(22) International Filing Date:
26 March 2012 (26.03.2012)

(25) Filing Language: English

(26) Publication Language: English

(30) Priority Data:
61/467,511 25 March 2011 (25.03.2011) US
61/579,519 22 December 2011 (22.12.2011) US
61/583,040 4 January 2012 (04.01.2012) US

(71) Applicant *(for all designated States except US)*: **INDIANA UNIVERSITY RESEARCH AND TECHNOLOGY CORPORATION** [US/US]; 351 West 10th Street, Indianapolis, IN 46204 (US).

(72) Inventors; and
(75) Inventors/Applicants *(for US only)*: **LU, Hua** [US/US]. **ZENG, Shelya** [US/US]. **MEROUEH, Samy** [US/US]; 3387 Modesto Lane, Westfield, IN 46074 (US). **ZHANG, Qi** [CN/—].

(74) Agent: **EMANUELE, John, J.**; Faegre Baker Daniels LLP, 300 North Meridian Street, Suite 2700, Indianapolis, IN 46204 (US).

(81) Designated States *(unless otherwise indicated, for every kind of national protection available)*: AE, AG, AL, AM, AO, AT, AU, AZ, BA, BB, BG, BH, BR, BW, BY, BZ, CA, CH, CL, CN, CO, CR, CU, CZ, DE, DK, DM, DO, DZ, EC, EE, EG, ES, FI, GB, GD, GE, GH, GM, GT, HN, HR, HU, ID, IL, IN, IS, JP, KE, KG, KM, KN, KP, KR, KZ, LA, LC, LK, LR, LS, LT, LU, LY, MA, MD, ME, MG, MK, MN, MW, MX, MY, MZ, NA, NG, NI, NO, NZ, OM, PE, PG, PH, PL, PT, QA, RO, RS, RU, RW, SC, SD, SE, SG, SK, SL, SM, ST, SV, SY, TH, TJ, TM, TN, TR, TT, TZ, UA, UG, US, UZ, VC, VN, ZA, ZM, ZW.

(84) Designated States *(unless otherwise indicated, for every kind of regional protection available)*: ARIPO (BW, GH, GM, KE, LR, LS, MW, MZ, NA, RW, SD, SL, SZ, TZ, UG, ZM, ZW), Eurasian (AM, AZ, BY, KG, KZ, MD, RU, TJ, TM), European (AL, AT, BE, BG, CH, CY, CZ, DE, DK, EE, ES, FI, FR, GB, GR, HR, HU, IE, IS, IT, LT, LU, LV, MC, MK, MT, NL, NO, PL, PT, RO, RS, SE, SI, SK, SM, TR), OAPI (BF, BJ, CF, CG, CI, CM, GA, GN, GQ, GW, ML, MR, NE, SN, TD, TG).

Published:
— *without international search report and to be republished upon receipt of that report (Rule 48.2(g))*

(54) Title: SMALL MOLECULE MODULATORS OF SIRT1 ACTIVITY ACTIVATE P53 AND SUPPRESS TUMOR GROWTH

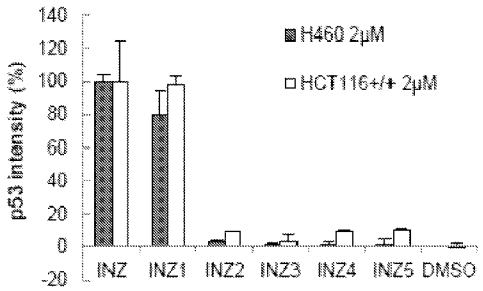

FIG.1C

(57) Abstract: Although -50 % of all types of human cancers harbor wild type TP 53, this p53 tumor suppressor is often deactivated through a concerted action by its abnormally elevated suppressors, MDM2, MDMX, or SIRT1. Reported herein are small molecules such as Inauhzin that effectively reactivates p53 by inhibiting SIRT1 activity, promotes p53 -dependent apoptosis of human cancer cells without causing apparently genotoxic stress. Moreover, Inauhzin stabilizes p53 by increasing p53 acetylation and preventing MDM2 -mediated ubiquitylation of p53 in cells, though not directly in vitro. Remarkably, Inauhzin inhibits cell proliferation, induces senescence and tumor-specific apoptosis, and represses the growth of xenograft tumors derived from p53- harboring H460 and HCT116 cells without causing apparent toxicity to normal tissues and the tumor-bearing SCID mice. As reported herein, Inauhzin is an anti-cancer therapeutic candidate that inhibits SIRT1 activity and activates p53.

WO 2012/135149 A2

SMALL MOLECULE MODULATORS OF SIRT1 ACTIVITY ACTIVATE p53 AND SUPPRESS TUMOR GROWTH

PRIORITY CLAIM

[0001] This application claims the benefit of the following US provisional patent applications: US provisional patent application number 61/467,511, filed on March 25, 2011; US provisional patent application number 61/579,519, filed on December 22, 2011; and US provisional patent application number 61/583,040, filed on January 4, 2012, each of which is hereby incorporated by reference in its entirety as if each were separately incorporated by reference in its entirety.

FIELD OF THE INVENTION

[0002] This invention relates generally to small molecules that inhibit the mediate decacetylase such as SIRT1; increase the activity of p53 and can be used to treat cancers and other disorders characterized by suppressed p53 activity.

BACKGROUND

[0003] The vital importance of the tumor suppressor gene *TP53* in preventing human cancer development and progression is not only demonstrated by the fact that its mutations are detected in 50% of all types of human cancers (Hollstein et al, 1991), but also emphasized by accumulating evidence that the functions and stability of the p53 protein are often abrogated via post-translational mechanisms in the rest of human cancers with wild type *TP53* (Brown et al, 2009; Kruse & Gu, 2009). Cancers need to frequently disarm p53 because it, once activated, triggers cell growth arrest, apoptosis, autophagy, or senescence, which are detrimental to cancer cells (Vogelstein et al, 2000; Vousden & Prives, 2009), and impedes cell migration, metabolism, or angiogenesis, which are favorable to cancer cell progression and metastasis (Vousden & Prives, 2009). These cellular functions of p53 are executed primarily via its transcription-dependent and independent activities (Vousden & Prives, 2009). However, because these functions are also deleterious to normal growing stem cells and developing tissues (Hong et al, 2009), higher eukaryotes have evolved an elegant feedback mechanism to monitor p53 level and activity (Eischen & Lozano, 2009).

[0004] Two chief monitor proteins of p53 are MDM2 (HDM2 in human) (Wu et al, 1993) and MDMX (also known as MDM4) (Shvarts et al, 1996). In a feedback fashion, they work together to directly inhibit the transcriptional activity of p53 (Gu et al, 2002) and mediate p53 degradation via ubiquitin-dependent proteolysis (Haupt et al, 1997; Kubbutat et al, 1997), as MDM2 possesses an E3 ubiquitin ligase activity (Honda et al, 1997) and its mRNA expression is stimulated by p53 (Barak et al, 1993; Wu et al, 1993), thus, keeping p53 level and activity marginally detectable in most of normal mammalian cells or tissues. This feedback regulation as firmly established in mouse models (Jones et al, 1995; Montes de Oca Luna et al, 1995) is subjected to tight regulation (Wade et al, 2010; Zhang & Lu, 2009). On one hand, a variety of cellular genotoxic or non-genotoxic stresses can reverse this feedback inhibition (Kruse & Gu, 2009) via post-translational modifications of either p53 or MDM2/MDMX, such as acetylation (Tang et al, 2008), phosphorylation (Banin et al, 1998; Maya et al, 2001; Shieh et al, 1997), and protein-protein interactions (Zhang & Lu, 2009; Zhang et al, 1998), to ultimately activate p53 that protects cells from transformation and neoplasia. Among the modifications, acetylation and ubiquitylation occur at a similar set of lysine residues within p53 and thus are mutually exclusive, i.e., acetylation of p53 by p300/CBP prevents its degradation by MDM2 and activates its activity, whereas MDM2 inhibits p53 acetylation by p300/CBP (Ito et al, 2001; Kobet et al, 2000; Li et al, 2002). Consistently, deacetylation of p53 by an NAD-dependent deacetylase, SIRT1 (Cheng et al, 2003; Luo et al, 2001; Vaziri et al, 2001), or a class I histone deacetylase, HDAC1 (Luo et al, 2000), facilitates MDM2-mediated p53 degradation and inactivates p53. On the other hand, cancers often hijack this feedback regulation to favor their own growth, as human breast cancers, osteosarcomas, lymphomas or leukemia express high levels of MDM2 or MDMX through distinct mechanisms without p53 mutation (Onel & Cordon-Cardo, 2004). Also, deacetylases are often highly expressed in cancers (Jung-Hynes and Ahmad, 2009; Lim, 2007; Nosho et al., 2009; Ozdag et al., 2006; Tseng et al., 2009). For instance, SIRT1 is highly expressed in cancers largely due to the down-regulation of a gene called hypermethylated-in-cancer-1 (HIC-1) (Tseng et al., 2009; Chen et al., 2005; Wales et al., 1995). HIC-1 encodes a transcriptional repressor that inhibits the expression of SIRT1, but is frequently turned off via hypermethylation of its promoter in cancers (Fleuriel et al., 2009; Fukasawa et al., 2006; Hayashi et al., 2001), though it is a p53 target gene as well (Chen et al., 2005; Wales et al., 1995). In theory, this high level of deacetylases would readily maintain p53 in a deacetylated status in

cancer cells, consequently favoring MDM2/MDMX-mediated degradation. Hence, this highly cancer-pertinent and well-defined p53-MDM2-MDMX pathway offers multiple molecule targets for screening small molecules as potential therapies for wild type p53-harboring cancers.

[0005] Regardless of the intensive endeavor over the past decade, so far, none of the known small molecules that target this p53 pathway has yet been developed into a clinically effective therapy. Thus, identifying more effective small molecules that specifically target this pathway in cancer has still remained challenging and an exciting opportunity to help treat cellular disorders such as cancer. Aspects of the present invention are directed to molecules that interact with this system.

SUMMARY

[0006] As reported herein initial attempts to screen small molecules that may block MDM2/MDMX-p53 binding surprisingly identified a novel small molecule called Inauhzin that effectively activates p53 by inhibiting SIRT1 activity without genotoxicity. Remarkably, Inauhzin suppressed the growth of xenograft tumors derived from p53-containing human lung and colon cancer cells in a p53-dependent fashion. More remarkably, this small molecule was less toxic to normal cells and tissues. Hence, as described herein, Inauhzin is a small molecule that can activate p53 by inhibiting SIRT1 and repressing tumor growth in xenograft tumor models.

[0007] Identification of Inauhzin as a new class of small molecules that can activate p53 and induce p53-dependent apoptosis and senescence without causing genotoxicity as well as suppress tumor growth with little toxicity to normal cells and tissues offers an exciting opportunity in the field of translational cancer research for the development of target-specific anti-cancer therapy either as an individual drug or as a component in combined therapy.

[0001] Some embodiments of the invention include methods of treating abnormal cell growth, comprising the steps of: providing at least one compound, or a pharmaceutically acceptable salt thereof according to the formula:

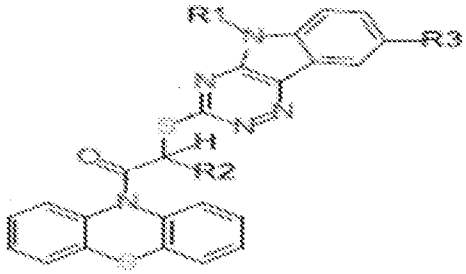

Compound A

wherein: R_1 is selected from the group consisting of -H and $-CH_2CH_3$; R_2 is selected from the group consisting of -H, and $-CH_3$; R_3 is selected from the group consisting of -H and halogens; a R_4 is selected from the group consisting of –H and halogen; and supplying at least one eukaryotic cell that encodes the protein p53; and contacting said compound with said cell. In some embodiments the compound includes the following groups: R_1 is $-CH_2CH_3$; R_2 is –H; R_3 is H; and R_4 is H.

[0002] In some embodiments, the eukaryotic cell contacted with the compound is a cancer cell. In still other embodiments, the eukaryotic cell contacted with the compounds is a pre-cancerous. In yet other embodiments, the eukaryotic cell contacted with the compounds is a normal cell.

[0003] Some embodiments include methods of modulating p53 activity by contacting eukaryotic including mammalian cells with at least one compound such as Compound A.

[0004] In some embodiments, the compound and the eukaryotic contact one other *in vitro*. While in still other embodiments, the compound and the eukaryotic contact one another *in vivo*.

[0005] In still other embodiments, the compound is contacted with a cell that is involved in abnormal cell growth such as disorder of the skin such as psoriasis.

Exemplary embodiments of the invention include, but are not limited to methods of modulating cellular activity, comprising the steps of: contacting a deacylase with an effective amount of compound; or a pharmaceutically acceptable salt thereof of said compound, wherein said compound is:

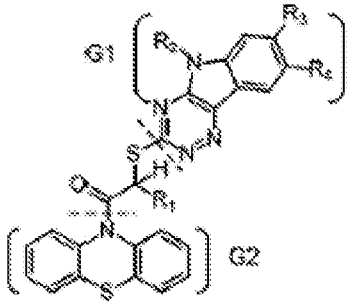

Compound A.

In some embodiments Compound A is comprised of the following groups: R_1 is –H, or –CH_2CH_3; R_2 is -H, or -CH_3; and R_3 is H, or a halogen; and R_4 is H or halogen.

[0006] In some embodiments the deacetylase is SIRT1.

[0007] In some methods the contacting step occurs either in *vitro* or in *vivo*. In some embodiments the contacting step occurs in benign or cancerous tumor cell, or in a normal cell of in an abnormal cell. In some embodiments the cell is a mammalian cell such as a cell from a human being

[0008] Some aspects of the invention include treating patients, comprising the steps of: administering a patient in need thereof a therapeutically effective dose of at least one compound according to formula, or a pharmaceutically acceptable salt thereof:

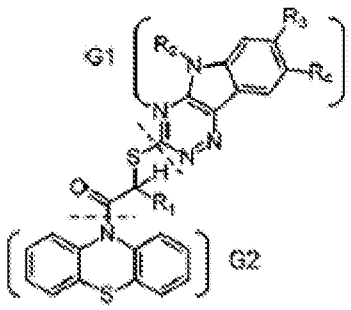

Compound A.

In some embodiments Compound A is comprised of the following groups: R_1 is –H, or –CH_2CH_3; R_2 is -H, or -CH_3; and R_3 is H, or a halogen; and R_4 is H or halogen.

[0009] In some methods that the therapeutically effective dose of the compound about 30 mg kg^{-1} of the mammals' body weight. In some embodiments the patient is a human being or

another mammal and in some embodiments the patient is diagnosed with a cancer such as breast cancer or a precancerous abnormal growth or cell type.

SEQUENCE LISTING

[0008] **SEQ ID NO. 1 5′-CTTCACCTACAGATGCCAACTTTG-3′** hsa-pri-mir-34a, primer.

[0009] **SEQ ID NO. 2; 5′-CCGGTGACTTTGGTCCAATT-3′**

[0010] **SEQ ID NO. 3; 5′-CCGGGCTGTCGATTGG-3′,** hsa-pri-mir-24**.**

[0011] **SEQ ID NO. 4; 5′-GACTCCTGTTCCTGCTGAACTGA-3′.**

BRIEF DESCRIPTION OF THE FIGURES

[0012] **FIG. 1A**. Identification of Inauhzin as a p53 activator. Screening for compounds that increase p53 levels in cells as detected by immunoblotting (IB). H460 cells were harvested for IB after being treated with each of the top 50 compounds (10μM) from computational-throughput screening for 18 hrs as shown in a representative blot here (number denotes each compound; Inauhzin, INZ). 50 μg of total proteins was used per lane (true for the following figures unless indicated).

[0013] **FIG. 1B**. Chemical structures of Inauhzin and some of its analogues INZ**1**-INZ**5**. As disclosed herein, both the triazino [5, 6-b]indo (G1) and phenothiazine (G2) moieties are essential for p53 induction.

[0014] **FIG. 1C.** Cellular activity of INZ analogues was measured using IB that detects p53 levels in H460 and HCT116 cells. The induction levels of p53 were normalized with actin and plotted as percentage of the level of p53 in the cells treated with INZ (mean ± SD, n=3).

[0015] **FIG. 1D.** Dose-dependent activation of p53 pathway by INZ. Cells were treated with INZ or a control compound MI63 for 18 hrs and harvested for IB with the antibodies as indicated. * indicates residual bands from p53 antibody.

[0016] **FIG. 1E.** Cell growth inhibitory activity was evaluated by WST cell growth assays. IC_{50} values are represented as mean ± SD (n=3).

[0017] **FIG. 2A**. Cells were treated with 2μM Inauhzin (INZ) for the indicated time and harvested for IB. * indicates residual signals of p53. Inauhzin induces p53 level and activity as well as p53-dependent apoptosis.

[0018] **FIG. 2B**. H460 cells were treated with 2μM INZ and harvested for real-time PCR (qRT-PCR). Values represent mean ± SD (n=3), p53 and p21.

[0019] **FIG. 2C.** H460 cells were treated with 2μM INZ and harvested for real-time PCR (qRT-PCR). Values represent mean ± SD (n=3), miR34a and miR24.

[0020] **FIG. 2D.** Induction of apoptosis by 2μM INZ analyzed by FACS. The apoptotic cells, identified by sub-G1 DNA content, were presented in the M1 population. Traces obtained with H1299 (p53 null) and $HCT116^{+/+}$ (p53 null) cells.

[0021] **FIG.2E**. Bar graph illustrating quantification of apoptosis of H1299 and H460 cells the results shown are representative of three independent experiments. Values represent mean ± SD (n=3), **p<0.01.

[0022] **FIG. 2F.** Bar graph of β-Galactosidase activity measurd with H460 and $HTC116^{+/+}$ cells. β-Galactosidase activity was measured by the absorbance of 5,5'-dibromo-4,4'-dichloro-indigo at 650 nm generated by the β-Galactosidase staining. Values represent mean ± SD (n=3), **p<0.01. Senescence-associated β-Galactosidase staining was performed in cultured cells for 6 days in the presence of 2 μM INZ or 10 μM Nutlin-3; Inauhzin induces p53-dependent senescence.

[0023] **FIG. 2G.** Representative photomicrographs of the cells by β-Galactosidase staining.

[0024] **FIG. 3A.** IB of H460 cells treated with 2 μM INZ for 18 hrs followed by addition of 50μg/ml cycloheximide (CHX) and harvested at indicated time points for IB. * indicates residual signals of p53. Inauhzin stabilizes p53 and inhibits its ubiquitylation.

[0025] **FIG. 3B.** Plot of remaining p53 versus time measured in cells treated with either DMSO or INZ. The intensity of each band was quantified, and normalized with actin and plotted.

[0026] **FIG. 3C**. IB of H460 cell lysates transfected with His-Ub and treated with INZ for 18 hrs prior to addition of 10μM MG132 and 20μM ALLN for 8 hrs. Cell lysates were subjected to His pull-down by Nickel-NTA agarose and detected by IB with the anti-p53 (DO-1) antibody.

[0027] **FIG. 3D**. IB of HCT116$^{-/-}$ cell lysates transfected with His-Ub, p53 and HA-MDM2 were treated with INZ for 4 hrs, followed by treatment with 10μM MG132 for 8 hrs. Ubiquitylated p53 was purified using Nickel-NTA and detected by IB with the anti-p53 (DO-1) antibody. The expression levels of p53 and HA-MDM2 are shown in the lower panels. Also see **FIG. 11**.

[0028] **FIG. 4**A. Plot of normalized fluorescence versus inhibitor concentration. Titration of INZ and Actinomycin D (ActD) against DNA utilizing ethidium bromide as a fluorescence intercalator; error bars represent standard deviation (n=3). Inauhzin does not directly bind to DNA and does not cause significant DNA damage.

[0029] **FIG. 4B**. Bar graph of the percentage of nuclei with the indicated number of γH2AX foci. Immunofluorescent γH2AX foci in H460 cells treated with 2μM INZ or 10μM Cisplatin (Cis) for 18hrs or 2mM Hydroxyurea (HU) for 8hrs. The quantification expressed as the mean number of foci per cell ± SD is shown in **FIG. 12**. Bar, 20 μm.

[0030] **FIG. 4C.** Images showing the number of γH2AX foci per nuclei in H460 cells. The number of γH2AX foci in INZ treate cells (1.3 ± 0.2 foci per cell, n = 394) is significantly less than that in Cis-treated cells (8.0 ± 1.2 foci per cell, n = 375) (p = 0.0006). HU-treated cells (9.7 ± 0.6 foci per cell, n = 314); DMSO-treated cells (0.28 ± 0.1 foci per cell, n = 395). P values were calculated using two-tailed t-test.

[0031] **FIG. 4D**. IB of H460 cell lysates, cells were treated with INZ, Cisplatin (Cis) and Etoposide for 18 hrs. Cell lysates were immunoblotted for phosphorylated p53 at Ser15. Blots were exposed for longer than 15 minutes.

[0032] **FIG. 4E**. IB of H460 cell, lysates, cells were treated with INZ, Cisplatin and Etoposide for 18 hrs. Cell lysates were immunoblotted for phosphorylated p53 at Ser46. Blots were exposed for longer than 15 minutes.

[0033] **FIG. 4F**. IB of H460 cell lysates, cells were induced with 1mM AICAR (AMP analogue, an AMPK activator) and 2μM INZ for indicated times and probed with the indicated antibodies.

[0034] **FIG. 5A.** IB of cell lysates, H1299 or H460 cells were treated with INZ. Etoposide or TSA as indicated. Inauhzin Induces Acetylation of p53, but not Tubulin, Is Affected by Knockdown of SIRT1. Cells Total levels of p53 and acetylated p53 at lysine 382 were assessed by IB (70 μg of total proteins was used per lane; true to all panels in this figure).

[0035] **FIG. 5B**. IB of cells lyaaste, HCT116+/+ cells were INZ or Etoposide (Eto) and probed with antibodies to P53K382Ac, p53 and Actin.

[0036] **FIG. 5C**. IB of lysates made from H460 cells treated with INZ or ETO. Blots were probed with antibodies to MDM2, P53K382Ac, p53 and Actin.

[0037] **FIG. 5D**. IB illustrating P53K382Ac, p53, TubulinK40Ac and Tublin levels in lysates made from H460 and H1299 cells treated with INZ, or TSA.

[0038] **FIG. 5E**. IB illustrating SIRT1, P53K382Ac, p53 and Actin levels measured in lysates made cells treated with INZ or Eto. H460 cells were plated in 6-well plates 18hr prior to infection with SIRT1 shRNA or control GFP shRNA. To increase shRNA knockdown efficiency, cells were infected again 24 hrs later. At 24 hrs after second infection, cells were treated with Etoposide for 6 hrs, followed by the addition of INZ for 12hr.

[0039] **FIGs. 5F**. Bar graph showing % cell growth measured in the presence of different concentrations of INZ and 2 μM Eto. Cells were infected with shGFP or shSIRT1 adenovirus in **FIG. 5E** were seeded at 3,000 cells per well in 96-well culture plates and incubated overnight at 37°C. Cell growth inhibition was measured using WST cell growth assays. IC_{50} values are represented as mean ± standard deviation (n=3). ** indicates $p<0.01$.

[0040] **FIGs. 5G**. Graph of % cell growth measured at various concentrations of INZ in cells treated with GPF shRNA or SIRT shRNA. Insert shows Western Blot probed for SIRT1 and Actin.

[0041] **FIG. 6A.** IB illustrating that Inauhzin inhibits deacetylation of p53 at lysine 382 by SIRT1 *in vitro* in a dose-dependent fashion using acetylated p53 protein as a substrate as described in the Experimental Section.

[0042] **FIG. 6B** Plot of the band intensity of each band for bound SIRT1 as analyzed using IB as a function of SIRT1 levels. Purified SIRT1 was incubated at indicated concentrations with biotinylated Inauhzin that was conjugated with avidin beads in the presence or the absence of 20 μM of non-biotinylated Inauhzin. Purified SIRT7 was used as a negative control. The intensity of each sample was individually compared with the intensity of the samples without SIRT1. The results shown are representative of three independent experiments. Values represent mean ± SD (n=3)

[0043] **FIG. 6C**. Blots of SIRT1, incubated with Biotin, Biotin-INZ, and Biotin-INZ + μM INZ.

[0044] **FIG. 6D**. Blot illustrating the inhibitory effects of Inauhzin, Cambinol and Salermide on SIRT1 activity were measured by the increase of the levels of acetylated p53 at lysine 382 *in vitro*. The percentage of inhibition was calculated as described in the "Experimental Section" and shown in below. Values represent mean ± SD (n=3).

[0045] **FIG. 6E**. Blots illustrating the effect of Inauhzin, Cambinol, Salermide or Tenovin-6 on p53 acetylation and level in H460 cells.

[0046] **FIG. 6F**. Blots illustrating the effect of Inauhzin, Cambinol, Salermide or Tenovin-6 on p53 acetylation and level in $HCT116^{+/+}$ cells.

[0047] **FIG. 7A.** Plot of tumor volume versus days of treatment; mice bearing H460 xenografts were treated with INZ or 5% of DMSO (vehicle) by i.p. at the dose as indicated at every other day (Q.O.D.) for 21 days. Mean tumor volumes ± SEM are shown in curves (left), and tumor weight is shown in columns (right) (n = 5 mice per group; *$p<0.05$). Inauhzin induces p53 and p53-dependent apoptosis *in vivo* and suppresses the growth of human xenograft tumors.

[0048] **FIGs. 7B** Plot of tumor volume versus days of treatment; mice with $HCT116^{p53-/-}$ and $HCT116^{p53+/+}$ tumors were treated with INZ or 5% of DMSO at doses as indicated by i.p.

once every day (Q.D.) for 21 days. Mean tumor volumes ± SEM are shown in curves (left), and tumor weight is shown in columns (right) (n = 7 mice per group; *p<0.05, **p<0.01).

[0049] **FIG. 7C**. Photos for representative mice bearing $HCT116^{p53-/-}$ and $HCT116^{p53+/+}$ tumors are shown.

[0050] **FIG. 7D**. Immunoblot (IB) of proteins extracted from $HCT116^{p53-/-}$ and $HCT116^{p53+/+}$ tumors (see **FIG. 7C**).

[0051] **FIG. 7E**. Representative H&E, BrdU and TUNEL-stained xenograft tumor sections from INZ or vehicle treated mice as presented in (B-D). Bars for 50 (TUNEL) and 20 (BrdU) μm, respectively, these images show that Inauhzin induces apoptosis and inhibits proliferation in xenograft tumors.

[0052] **FIG. 7F**. Bar graph % TUNEL stained (n=4 mice per group analyzed). Mean values ± SEM are indicated, *p<0.05. P values were calculated using two-tailed t test.

[0053] **FIG. 7G**. Bar graph BrdU stained (n=4 mice per group analyzed). Mean values ± SEM are indicated, *p<0.05. P values were calculated using two-tailed t test.

[0054] **FIG. 8.** A model for inauhzin action in cancer cells.

[0055] **FIG. 9**. IB, of cell lysates, cells were treated with different doses of INZ as indicated and harvested 18 hrs post treatment for immunoblotting analyses as described in **FIG. 1**. * indicates residual signals of p53. Inauhzin induces p53 level and activity in wild type p53-harboring cancer cell lines.

[0056] **FIG.10A.** IB of cell lysatse, A549 cells were transfected with scrambled siRNA or p53 siRNA, and 16hrs prior to cell harvesting, cells were treated with 2 μM INZ. Protein levels were measured by IB. * indicates residual p53K382Ac antibody-reacting bands. This figure related to **FIG. 1** illustrates that depletion of p53 prevents growth suppression effect of Inauhzin. A549 cells were transfected with scrambled siRNA or p53 siRNA, and 16hrs prior to cell harvesting, cells were treated with 2 μM INZ.

[0057] **FIG. 10B**. Plot of % cell growth versus concentration of INZ. A549 cells transfected with scrambled siRNA or p53 siRNA followed by exposure to INZ for 72hrs and

evaluated by WST cell growth assays. The IC_{50} value of INZ in the scrambled siRNA and p53 siRNA transfected cells are 4.4 ± 0.5 μM and 18.7 ± 1.7 μM, respectively (Mean ± SD, n=3).

[0058] **FIG. 10C**. IB of lysates from H460 cells transfected with scrambled siRNA (Scr) or p73 siRNA (Si-p73) were treated with 2μM INZ, and analyzed by qPCR.

[0059] **FIG. 10D.** Bar graph of fold induction measured by qRT-PCR. The graph includes data measured for p73 mRNA, p21 mRNA and MDM2 mRNA.

[0060] **FIG 10E**. Plot of % survival of treated cells relative to untreated cells; the data graphed represent average values from four identically treated samples and are expressed as a percentage of surviving cells relative to untreated controls. The dashed line corresponds to 50% cell killing.

[0061] **FIG 11A.** IB, ubiquitylated MDM2 was separated by 8% SDS–PAGE, and detected by immunoblotting; in these assays *in vivo* ubiquitylation assay was performed as described in **FIG. 3E.** These data indicate that Inauhzin does not affect the auto-ubiqutylation of MDM2 and it does not directly inhibit MDM2 ubiqutin ligase activity.

[0062] **FIG 11B.** IB performed on *in vitro* ubiquitylation assays with purified His-MDM2 and GST-p53; ubiquitylation reactions were terminated after 30 minutes, and the extent of p53 ubiquitylation was evaluated by immunoblot analysis with anti-p53 antibody.

[0063] **FIG. 12A.** Representative images of γ-H2AX foci. H460 cells that were treated with 2μM of Inauhzin (INZ), 10μM Cisplatin (Cis) for 18hrs or 2mM Hydroxyurea (HU) for 8hrs, and analyzed by monoclonal anti-p53 antibodies (red) and polyclonal anti- γ-H2AX antibodies (green). Bar, 20 μm. This figure which is related to **FIG. 4**, illustrated that Inauhzin induces high level of p53 without causing a dramatic formation of foci.

[0064] **FIG. 12B**. Bar graph of the number of γ-H2AX foci per nuclei is shown (mean ± SD). INZ treated cells (1.3 ± 0.2 foci per cell, n = 394); Cis treated cells (8.0 ± 1.2 foci per cell, n = 375); HU treated cells (9.7 ± 0.6 foci per cell, n = 314); DMSO treated cells (0.28 ± 0.1 foci per cell, n = 395).

[0065] **FIG. 13 A.** IB analysis of lysates from HCT116+/+ cells transfected with SIRT1 siRNA, using antibodies as indicated. This figure which is related to **FIG. 5,** illustrates that SIRT1 knockdown leads to increased cell death. .

[0066] **FIG. 13 B.** Bar graph of inductions of p21 and MDM2 mRNA levels in $HCT116^{+/+}$ cells transfected SIRT1 siRNA as assessed by qPCR (mean ± SD, n=3).

[0067] **FIG. 13 C.** FACS analysis, graphs of counts versus PI-DNA measured in either $HCT116^{+/+}$ cells or H450 cells treated with blank vector, scrambled siRNA or SIRT1 siRNA.

[0068] **FIG. 13 D.** Bar graph of SubG1 (%) measured in $HCT116^{+/+}$ cells transfected with SIRT1 siRNA for 72 hrs.

[0069] **FIG. 13 E.** Bar graph of SubG1 (%) measured in H460 cells transfected with SIRT1 siRNA for 72 hrs.

[0070] **FIG. 13 F.** Survival curves of $HCT116^{+/+}$ cells transfected with SIRT1 siRNA or scrambled siRNA for the indicated number of days.

[0071] **FIG. 13 G.** Survival curves of H460 cells transfected with SIRT1 siRNA followed by exposure to the indicated concentrations of INZ for 72hrs. The results as shown here are representatives of three independent experiments. Values represent means ± SD (n=3), **$p<0.01$. Surviving cells are determined by WST cell viability assays shown as the absorbance at 450nm. Each data points represent the average value from six samples. Error bars represent standard deviation.

[0072] **FIG. 14A.** IB of recombinant SIRT1 and SIRT7, produced in E. coli BL21-CodonPlus (DE3)-RIPL, and purified through Ni-His columns and stained with Coomassie brilliant blue. This figure is related to **FIG. 6**, illustrates that biotinylated Inauhzin binds to SIRT1 *in vitro*. .

[0073] **FIG. 14B**. IB of lysates from cells treated with different levels of His-SRT1. Deacetylation activity of purified SIRT1 was measured by analyzing in the level of Ac-Lys382-p53 with acetylated p53 as a substrate, which was isolated via immunoaffinity purification. Proteins were detected by IB with antibodies as indicated.

[0074] **FIG. 14C**. Chemical structure of biotinylated Inauhzin (Biotin-INZ).

[0075] **FIG. 14D**. IB of either H46 of HCT116 cells treated with biotinylated Inauhzin. These data indicate that biotinylated Inauhzin induces p53 level and acetylation in H460 and $HCT116^{+/+}$ cells.

[0076] **FIG. 14E**. Blot probed with NeutrAvidin Protein-Horseradish Peroxidase Conjugated (1:1000; Pierce) and anti-SIRT1 antibodies. Purified SIRT1 was incubated at indicated concentrations with biotinylated Inauhzin or biotin overnight at 4 °C. After incubation, each mixture was subjected to Native-PAGE analysis, followed by blotting to PVDF.

[0077] **FIG. 15A.** Bar graph of % inhibition indicating the effect of Inauhzin and its analogues on SIRT1 deacetylase activity *in vitro* using acetylated p53 as a substrate. The inhibitory effect of the Inauhzin analogues on SIRT1 activity was calculated as described herein, this figure is related to **FIGs. 5** and **6**.

[0078] **FIG. 15B.** Curve fitting and IC_{50} determination of INZ performed using Igor Pro 4.01A. *In vitro* deacetylase assays were conducted by Fluor-de-Lys Fluorimetric Assays. These data indicate that Inauhzin inhibits the deacetylase activity of SIRT1, but not SIRT2, SIRT3 or HDAC8 *in vitro*.

[0079] **FIG. 15C.** IB of lysates from H1299 cells that were treated with the amounts of INZ as indicated for 18hrs and probed with the indicated antibodies. These data indicate that Inauhzin induces acetylation of Histone H3 at K9 in H1299 cells.

[0080] **FIG. 15D.** IB of lysates from cells that were treated with the indicated amounts of INZ or TSA and probed with the indicated antibodies.

[0081] **FIG. 15E.** Graph of arbitrary AFU measured in the presence of different levels of INZ ▲25 μM, ■12.5 μM, ■6.25 μM, ■3.125 μM, ●1.5625 μM, ●0.78125 μM, ●0 μM. Each curve represents the FdL acetylated substrate titration (2-200 μM) with a constant NAD^+ concentration of 25μM and various concentration of INZ. The % K_m and % V_{max} values are shown in the Table below. Each data point represents the mean ± SD (n=3).

[0082] **FIG. 15F.** Graph of AFU measured in the presence of different levels of INZ of INZ, ▲25 μM, ■12.5 μM, ■6.25 μM, ■3.125 μM, ●1.5625 μM, ●0.78125 μM, ●0 μM. Each curve represents NAD^+ titration (10-4000 μM) with a constant substrate concentration of 10μM

and various concentration of INZ. The Y-axis of the charts represents arbitrary fluorescent units (AFU). The % Km and % Vmax values are shown in Table below.

[0083] **FIG. 16A.** IB of lysates from H460 cells treated with INZ, Cambinol, Salermide, and Tenovin-1 or Tenovin-6 at the indicated concentrations for 18 hrs and harvested for IB analyses.

[0084] **FIG. 16B.** IB of lysates from $HCT116^{+/+}$cells were treated with INZ, Cambinol, Salermide, and Tenovin-1 or Tenovin-6 at the indicated concentrations for 18hrs and harvested for IB analyses. The data in **FIGs. 16A** and **16B** indicate that Inauhzin is more effective than cambinol and salermide in inhibiting cell growth and less toxic than tenovin-6 towards primary human cells.

[0085] **FIG. 16C.** Table summarizing the inhibitory effect of the compounds on cell growth as evaluated by WST cell growth assays and IC_{50} values were presented as mean ± SD (n=3).

[0086] **FIG. 17A.** Graph of INZ concentration measured in plasma over time (hours). This figure related to **FIG.7** illustrates that Inauhzin effectively distributes to tumors after i.p. administration and potently represses the growth of H460 and HCT116 xenograft tumors.

[0087] **FIG. 17B.** Bar graphs of plasma and tumor concentrations of Inauhzin versus time (hours) determined by HPLC-MS/MS after administration of 30mg/kg by i.p. injection to mice bearing H460 xenografts (mean ± SD, n=2).

[0088] **FIG. 17C.** Representative photographs of $HCT116^{p53-/-}$ and $HCT116^{p53+/+}$ tumors as treated with either vehicle only or with 30 mg kg^{-1} of INZ these images are related in **FIGs. 7A** and **7B**.

[0089] **FIG. 17D** Photomicrographs of tissue from small intestine, spleen or stomach. The tissues were collected 21 days after INZ administration and stained with H&E or DAPI and TUNEL. The bar in the images is, 50 μm. These data illustrate the level of apoptosis in normal tissues following treatment with INZ.

DESCRIPTION

[0090] For the purposes of promoting an understanding of the principles of the novel technology, reference will now be made to the preferred embodiments thereof, and specific language will be used to describe the same. It will nevertheless be understood that no limitation of the scope of the novel technology is thereby intended. Such alterations, modifications, and further applications of the principles of the novel technology being contemplated as would normally occur to one skilled in the art to which the novel technology relates are within the scope of this disclosure and the claims. Unless explicitly noted otherwise, all theories, hypothesis and conjecture is presented by way of illustration solely for the convenience of the reader and not limiting of the invention or any of the embodiments of the invention.

[0091] As used herein, unless explicitly stated otherwise or clearly implied otherwise the term 'about' refers to a range of values plus or minus 10 percent, e.g., about 1.0 encompasses values from 0.9 to 1.1

[0092] As used herein, unless explicitly stated otherwise or clearly implied otherwise the terms 'therapeutically effective dose,' 'therapeutically effective amounts,' and the like, refer to a portion of a compound that has a net positive effect on the health and well being of a human or other animal. Therapeutic effects may include an improvement in longevity, quality of life and the like. These effects also may also include a reduced susceptibility to developing disease or deteriorating health or well being. The effects may be immediately realized after a single dose and/or treatment or they may be cumulatively realized after a series of doses and/or treatments.

[0093] Pharmaceutically acceptable salts include salts of compounds of the invention that are safe and effective for use in mammals and that possess a desired therapeutic activity. Pharmaceutically acceptable salts include salts of acidic or basic groups present in compounds of the invention. Pharmaceutically acceptable acid addition salts include, but are not limited to, hydrochloride, hydrobromide, hydroiodide, nitrate, sulfate, bisulfate, phosphate, acid phosphate, isonicotinate, acetate, lactate, salicylate, citrate, tartrate, pantothenate, bitartrate, ascorbate, succinate, maleate, gentisinate, fumarate, gluconate, glucaronate, saccharate, formate, benzoate, glutamate, methanesulfonate, ethanesulfonate, benzensulfonate, p-toluenesulfonate and pamoate (i.e., 1,1'-methylene-bis-(2-hydroxy-3-naphthoate)) salts. Certain compounds of the invention

may form pharmaceutically acceptable salts with various amino acids. Suitable base salts include, but are not limited to, aluminum, calcium, lithium, magnesium, potassium, sodium, zinc, and diethanolamine salts. For additional information on some pharmaceutically acceptable salts that can be used to practice the invention, please review Berge, *et al.*, 66 J. PHARM. SCI. 1-19 (1977), Haynes, *et al*, J. Pharma. Sci., Vol. 94, No. 10, Oct. 2005, pgs. 2111-2120, and the like.

[0094] The p53 tumor suppressor is one of the most important proteins acting to protect human beings from developing cancer. Although this gene is highly mutated in late stages of cancers, approximately 50% of all types of human cancers still contain wild type p53. In many types of cancer, p53 is deactivated through a concerted action, including abnormally elevated levels of p53 suppressors such as MDM2, MDMX, or SIRT1. SIRT1 is highly expressed in some cancer cells due to the loss of its repressor HIC-1 via promoter. The result is hypermethylation in some cancer cells, which keeps p53 in a deacetylated status and facilitates its ubiquitylation and degradation by MDM2/MDMX. Thus, reactivation of p53 by targeting the activity or level of various p53 suppressors in p53-containing cancers has become an attractive approach for the development of anti-cancer therapy.

[0095] Several small molecules have been identified to target the p53 pathway (Brown et al, 2009). For instance, Nutlin-3, Rita and MI-219 can interfere with the p53-MDM2 binding (Issaeva et al, 2004; Shangary et al, 2008; Vassilev et al, 2004), consequently increasing p53 level and activity. Recently, tenovins were reported to inhibit the activity of SIRT2 and SIRT1, inducing p53 acetylation and activity (Lain et al, 2008). These exciting studies not only consolidate the p53-MDM2 pathway as a valid target, but also provide multiple candidates for development into anti-cancer drugs, though their clinical significance is still under investigation. Since none of the potent inhibitors of the MDM2-p53 binding, such as Nutlin-3 or MI-219 (Shangary et al, 2008; Vassilev et al, 2004), could effectively affect the MDMX-p53 interaction. This interaction motivated a search for small molecules that could interfere with this interaction, hoping to complement the inhibitory effect of existing MDM2 inhibitors on cancer growth by performing a computational 3D structure-based search followed by a cell-based assessment of top candidates. However, this two-step approach unexpectedly revealed a small molecule that suppresses SIRT1 activity and induces the acetylation, level and activity of p53 consequently and

effectively repressing the growth of xenograft tumors derived from human lung and colon wild type p53-containing cancer cells.

Identification of Inauhzin as a Potent Activator of p53 with Defined Functional Moieties

[0096] Comparison of the structures of the MDM2-p53 and MDMX-p53 complexes (Kussie et al, 1996; Popowicz et al, 2007) revealed that the N-terminal hydrophobic pocket of MDMX for p53 binding is much shallower than that of MDM2. This information explained why MDM2 inhibitors failed to affect MDMX-p53 binding and also prompted us to initiate a computational structure-based screening using the AutoDock computer program (Morris et al, 2008) for the docking of virtual compounds that could distinguish the p53 binding sites on MDM2 and MDMX. After initial computational screening of half a million of commercially available compounds from the ChemDiv chemical library, the 50 top candidates were selected for further characterization. These compounds were tested in cell-based assays at 10 μM for their ability to induce p53 levels in human lung carcinoma H460 cells using an immunoblotting (IB) analyses. Unexpectedly, one small molecule, 10-[2-(5H-[1,2,4]triazino[5,6-b]indol-3-ylthio)butanoyl]-10H-phenothiazine (abbreviated as Inauhzin; Figure 1B), induced p53 levels as effectively as actinomycin D (10 nM) and in a much more pronounced manner than did the rest of the compounds tested (**FIG. 1A** and data not shown).

[0097] After confirming this effect of Inauhzin in several different p53-containing human cancer cell lines (Figures 1D and 9; data not shown), the relationship between the structure and p53 induction activity of this compound was investigated in cells. Some 46 commercially available compounds were obtained, which are similar to INZ (**FIG. 1B** and data not shown). The analysis of those compounds in p53 activation in H460 and HCT116 cells by IB (**FIG. 1C** and data not shown) indicated that a unique structure scaffold might be required for the activity of Inauhzin in cells. Both the triazino[5,6-b]indol (G1) and phenothiazine (G2) moieties are essential for p53 induction, as the analogues without either of them failed to induce p53 (data not shown). Also, removal of the ethyl group at the R_1 position (INZ**2-4**) or modification at R_3 on the indol moiety of Inauhzin (INZ**5**) disabled the compound to induce p53 in cells (**FIGs 1B** and **1C**). These results indicate that a specific chemical structure with the intact triazino[5,6-b]indol-3-ylthio)butanoyl]-10H-phenothiazine is crucial for p53 activation in cells and suggest that this

compound may bind to a specific target in cells. Suprisingly, Inauhzin or its close analogue INZ1 which induced p53 did not appear to affect the interaction between either MDMX and p53, or MDM2 and MDMX, or MDM2 and p53 in, *in vitro* fluorescence polarization and cell-based co-immunoprecipitation assays (data not shown).

Inauhzin Inhibits Cell Growth in a p53-dependent Fashion

[0098] To explore the effect of Inauhzin treatment on the p53 pathway in human cancer cells and determine whether Inauhzin reduces cell viability in a p53-dependent fashion, human lung cancer H460, A549, H1299, HT29, colon cancer HCT116, osteosarcoma U2OS and SJSA, breast cancer MCF7, ovarian cancer A2780, IGROV1, and SKOV3, and glioma U87 and U373 cells, as well as human embryonic fibroblast WI-38 and normal human fibroblast NHF cells were first treated with different doses of Inauhzin for 18hrs and then harvested IB. Inauhzin induced p53 level and activity in a dose-dependent fashion and at a dose as low as 0.5 μM as measured by detecting p53 and its targets p21 and Puma, as well as cleaved PARP, which indicates apoptosis (Duriez & Shah, 1997) in p53-containing cancer cells, including HCT116, H460 (Figure 1D), A549, MCF7, A2780, U87 (Figure 9), U2OS and SJSA cells (data not shown). In striking contrast, this effect was not observed in p53-null (H1299, HCT116$^{-/-}$, SKOV3) or p53-mutated (HT29, IGROV1 and U373) cancer cells (**FIGs 1D** and **9**). Intriguingly, it was much less potent in activation of p53 in WI-38 and NHF cells (**FIG. 1D** and data not shown) in comparison of MI-63, a previuosly reported inhibitor of the MDM2-p53 interaction (Ding et al, 2006). Consistent with these results, Inauhzin displayed much higher toxicity towards p53-containing human cancer cells than to either WI-38 and NHF, or p53-mutant and null cancer cells. This is evident by IC_{50} values that in the former cell lines were 7 to 40 fold greater than that in the latter cell lines (**FIG. 1E**). Consistently, silencing p53 with siRNA in A549 or H460 cells not only reduced p21, MDM2, PARP and Puma up-regulation induced by Inauhzin, but also compromised the growth inhibition by Inauhzin treatment (**FIGs. 10A** and **10B** and data not shown). In comparison, knockdown of p73 in H460 cells did not apparently affect p53 level, acetylation and p53-dependent cell growth suppression induced by Inauhzin, although partially impaired the induction of p21 and MDM2 by Inauhzin (**FIGs. 10C-10E**), suggesting that Inauhin can still activate p53 in p73-knocked down cells. Therefore, the ability of Inauhzin to activate the p53 pathway is strongly correlated with its inhibition of cell survival.

Taken together, these results demonstrate that Inauhzin is a potent p53 activator and mediates p53-dependent cytotoxicity through its specific functional groups.

Inauhzin Induces p53-Dependent Apoptosis

[0099] In order to further characterize the effect of Inauhzin on p53 cellular functions, a set of time course experiments using the same aforementioned approaches were carried out using 2 μM Inauhzin. Inauhzin at this concentration was sufficient to significantly induce p53 level and activity (**FIG. 1D**). In these experimetns, Inauhzin induced p53 level in a time-dependent manner as early as 6 hrs post-treatment in both p53-containing H460 and HCT116 cells (**FIG. 2A**). Correspondingly, three of p53 targets, MDM2, p21 and Puma, were also induced in a time-dependent manner in p53-containing H460 and HCT116, but not in p53-null H1299 and HCT116, cells (**FIG. 2A**). Interestingly, Puma was induced earlier (3-6 hrs) and cleaved PARP was detected later on (~12 hrs) (**FIG. 2A**). Apparently, cleaved PARP was p53-dependent as it was not detected in p53-null cells (**FIG. 2A**). The induction of p53 targets was clearly at the transcriptional level as p21 mRNA and miR34a, but not p53 mRNA and miR24, were highly induced in H460 cells (**FIGs. 2B** and **2C**).

[00100] Inauhzin was tested to determine if it preferentially antagonizes the proliferation of p53-containing cells, and whether the compound induces apoptosis in p53 wild-type, but not null, cells. As shown in **FIGs. 2D** and **2E**, Inauhzin at 2 μM induced drastic apoptosis in a time-dependent fashion in both p53-containing H460 and HCT116 cells by 30-40% increase of apoptotic cells, but not in p53-deficient H1299 and HCT116 cells. These results, in perfect line with the above results (**FIGs. 1**, **2A** and **2B**), demonstrate that Inauhzin not only induces p53 level, but also stimulates its transcriptional activity. Consequently, leading to p53-dependent apoptosis in a time-dependent fashion. This compound was tested to determine if it promotes p53-dependent senescence as measured by the production of senescence-associated β-galactosidase. Notably, Inauhzin induced senescence in H460 or HCT116$^{p53+/+}$, but not in HCT116$^{p53-/-}$, cells, though to a much less degree than did Nutlin-3 (**FIGs. 2F** and **2G**) (Efeyan et al, 2007). These results demonstrate that Inauhzin inhibits cell proliferation by triggering both apoptosis and senescence in p53-containning cells, though it predominantly induces p53-dependent apoptosis.

Inauhzin Stabilizes p53 without either Directly Inhibiting MDM2-mediated Ubiquitylation or Causing Genotoxicity

[00101] The fact that Inauhzin induces the protein, but not mRNA, level of p53 (**FIGs. 1** and **2**) suggests that this compound might regulate the stability of the p53 protein. To test this hypothesis, the half-life of endogenous p53 after the treatment of H460 or HCT116 cells with this compound was measured. As shown in **FIGs. 3A** and **3B**, 2 μM Inauhzin extended the half-life of p53 from 30 minutes to more than 3 hrs (**FIGs. 3A** and **3B**). This effect was specific to p53, as the half-life of p21 was not apparently influenced (**FIG. 3A**) even though its level was remarkably elevated due to the activation of p53 (**FIGs. 1D** and **2A**). Next, it was determined if Inauhzin stabilizes p53 by inhibiting its ubiquitylation in cells. Indeed, the ubiquitylation of both endogenous (**FIG. 3C**) and exogenous (**FIG. 3D**) p53 proteins was markedly inhibited by 2 μM Inauhzin. However, the auto-ubiquitylation of MDM2 was not significantly affected by the treatment of Inauhzin (**FIG. 11A**). Moreover, Inauhzin did not appear to directly affect MDM2-mediated p53 ubiquitylation when it was titrated from 2 to 50 μM in an *in vitro* ubiquitylation assay using purified proteins (Figure 11B). Taken together, these results demonstrate that Inauhzin is able to prevent p53 from MDM2-mediated ubiquitylation and proteasomal degradation and also suggest that it may utilize a cellular mechanism that protects p53 without either directly inhibiting MDM2 activity toward p53 or interfering with MDMX- or MDM2-p53 interaction (data not shown).

[00102] To elucidate possible cellular mechanisms underlying the protection of p53 by Inauhzin from proteolysis in cells, this compound was tested to determine if it causes general genotoxicity to cells by conducting *in vitro* non-sequence-specific DNA-binding, *in vivo* immunofluorescence staining for H2AX Ser139 phosphorylation (γH2AX) and cellular p53 phosphorylation assays. These results indicate that Inauhzin is not genotoxic. First, it was a considerably poor DNA-binding agent in comparison with actinomycin D, as the former hardly bound to DNA at 2 μM (**FIG. 4A**), a dose that markedly induced p53 (**FIGs. 1** and **2**), while the latter bound to 50% of DNA molecules even at 0.3 μM (**FIG. 4A**). Also, even though 2 μM Inauhzin effectively induced p53 levels in cells compared to 10 μM cisplatin, it did not appear to cause significant γH2AX focus formation, which is often used as a marker for DNA damage

(Paull et al, 2000). As shown in **FIGs. 4B**, **4C**, and **12**, more than 80% of H460 cells treated with 10 μM cisplatin or 2 mM hydroxyurea were detected with more than 10 foci per nucleus, whereas only less than 1.5% of H460 cells treated with 2 μM Inauhzin contained such a high level of foci and ~75 % of Inauhzin-treated cells were basically free of foci.

[00103] Furthermore, the level of p53 phosphorylation at either serine 15 or serine 46 in Inauhzin-treated H460 cells was not observed compared to the cells treated with Cisplatin or Etoposide for 18hrs (**FIGs. 4D** and **4E**). Phosphorylation of p53 at serine 15 or serine 46 was previously shown to be responsive to severe DNA damage (Banin et al, 1998; Oda et al, 2000; Shieh et al, 1997). Finally, Inauhzin did not activate AMPK (Figure 4F), which was also reported to activate p53 by phosphorylating serines 15 and 46 (Jones et al, 2005). All together, these results exclude the possibility that Inauhzin might activate a kinase cascade that mediates p53 phosphorylation by causing DNA damage or activating AMPK.

Inauhzin Inhibits SIRT1 Activity and Induces Acetylation of p53, but not Tubulin

[00104] Previous studies have indicated that p53 is also modulated by reversible acetylation, which is inverse to ubiquitylation (Li et al, 2002) because the two post-translational modifications occur at similar lysine residues within p53. Hence, whether Inauhzin would influence p53 acetylation in cells was tested. At 2 μM Inhauhzin induced p53 acetylation at lysine 382 as detected by anti-acetylated K382 antibodies, which correlated well with the increment of p53 levels (**FIG. 5A**) and more markedly than did Etoposide at 10 μM (**FIG. 5B** and **5C**). Interestingly, Inauhzin induced acetylation of p53 in H460 cells, but not tubulin in constrast with trichostatin A (TSA), which induced acetylation of tubulin (**FIG. 5D**) by inhibiting the activity of the HDAC family, such as HDAC1 and HDAC2 (Finnin et al, 1999).

[00105] Because K382 is a target site for SIRT1 (Luo et al, 2001; Vaziri et al, 2001), whether knockdown of SIRT1 might affect Inauhzin-induced p53 acetylation at K382 was investigated. As shown in **FIG. 5E**, knockdown of SIRT1 in H460 cells induced p53 acetylation and protein level in the presence of 2 μM Etoposide. However, additional treatment of the cells with 2 μM Inauhzin failed to further induce p53 acetylation and level compared to the cells without SIRT1 knockdown. Consistently, knockdown of SIRT1 also impaired the ability of Inauhzin to synergize the inhibition of cell growth by Etoposide (**FIG. 5F**). By contrast, in the

absence of Etoposide, Inauhzin synergized the negative effect of SIRT1 knockdown on cell growth, as the IC_{50} value for Inauhzin in cell growth analysis decreased by ~17 fold when SIRT1 was partially depleted via SIRT1 shRNA (**FIG. 5G**). Similar to Inauhzin treatment (**FIGs. 1**, **2**, **5A**, and **5B**), knockdown of SIRT1 using SIRT1 specific siRNA induced the level and activity of p53 as well as p53 acetylation, leading to p53-dependent apoptosis and cell growth suppression in $HCT116^{+/+}$ and H460 cells (**FIG. 13**). These results indicate that Inauhzin might induce p53 acetylation and suppress cell growth by inhibiting SIRT1 activity in cells.

[00106] To validate this possibility, the effect of Inauhzin on SIRT1 activity was tested by conducting *in vitro* assays using acetylated p53 protein as a substrate and purified His-SIRT1 (**FIGs. 14A-B**) as described in the "Experimental Procedures" was measured. As shown in **FIG. 6A**, Inauhzin inhibited SIRT1 deacetylase activity in a dose dependent fashion and effectively inhibited this activity at a concentration of only 3μM. This inhibition was specific to Inauhzin and its chemical analogue INZ1 (methyl substituted R1), which activated p53 (**FIGs. 1B-C**) and decreased SIRT1 activity in a dose-dependent fashion (**FIG. 15A**). By contrast, the analogues INZ5 (bromide substituted on R3) and INZ 15 or INZ 18 (lack of G1, data not shown) that failed to induce p53 did not significantly inhibit SIRT1 activity even at the highest concentration that was tested (20 μM).

[00107] To obtain the evidence supporting the inhibition of SIRT1 by Inauhzin through their direct interaction, biotin was conjugated to the R1 position of Inauhzin since the analysis of the structure-activity relationships of Inauhzin revealed that R1 could be substituted with a different chemical group. Suprisingly, biotinylated Inauhzin was as effective as Inauhzin in the induction of p53 acetylation and level in both H460 and HCT116 cells (**FIGs. 14C-D**) and in inhibition of SIRT1 activity *in vitro* using acetylated p53 protein as a substrate (data not shown). Newly synthesized biotin-Inauhzin was used to determine if SIRT1 could bind to Inauhzin *in vitro* by performing a set of biotin-avidin pull down assays using SIRT7 (**FIG. 14A**) as a control. SIRT7 was recently reported to deacetylate p53 as well (Lavu et al, 2008). As shown in **FIG. 6C**, SIRT1, but not SIRT7, specifically bound to biotin-Inauhzin in a dose dependent manner. This binding was markedly reduced by 20 μM Inauhzin, further validating the specificity of the Inauhzin-SIRT1 binding (**FIGs. 6B-C**). Additionally, biotin-Inauhzin formed complexes with

SIRT1 *in vitro* as detected by native PAGE analyses (**FIG. 14E**). These observations suggest that Inauhzin inhibits SIRT1 activity by directly binding to this deacetylase.

[00108] Consistence with the results showing that Inauhzin induces acetylation of p53K382 (**FIGs. 5** and **6**) and Histone H3K9 (**FIG. 15C**), but not tubulin K40 (**FIG. 5D**), Inauhzin selectively inhibited the activity of SIRT1, but not SIRT2, SIRT3 or HDAC8, with the IC_{50} of 0.7-2μM using Fluor-de-Lys fluorimetric assays (**FIG. 15B**). Because, K382 of p53 and K9 of Histone H3 have been indicated as acetylated target sites for HDAC1 (DiTacchio et al, 2011; Luo et al, 2000), the inhibitory effect of Inauhzin on HDAC1 was tested. Flag-HDAC1 was prepared from H1299 cells transfected with Flag-HDAC1 by immunoaffinity purification and the deacetylase assay was performed similarly using acetylated p53 protein as a substrate. In contrast to the complete rescue of p53 acetylation by 1μM of TSA, (a drug known to selectively inhibits HDAC, but not the Sirtuins), Inauhzin had little effect on HDAC1 activity at 5 μM,and only a mild effect at 25 μM, on HDAC1 activity (**FIG. 15D**). These results, together with the results of **FIGs. 5** and **6**, indicate that Inauhzin appears to be more specific to SIRT1 than to other members of the HDAC family.

[00109] To further delineate biochemical mechansims underlying the inhibition of SIRT1 activity by Inauhzin, competition assays with limited titration of the compound, acetylated p53 peptide substrates and NAD^+, a co-factor of SIRT1 (Tanny et al, 1999) was carried out. As shown in **FIG. 15E**, Inauhzin did not compete with the substrate, as both of V_{max} and K_m values were not changed significantly by increasing amounts of Inauhzin. However, in the case of NAD^+, Inauhzin reduced both V_{max} and K_m values in a dose-dependent manner (**FIG. 15F**), suggesting that this compound might utilize an uncompetitive mechanism to inhibit SIRT1 activity. All together, these results demonstrate that Inauhzin is able to inhibit SIRT1 activity *in vitro* and in cells, consequently leading to p53 aceylation and activation, and also suggest that it might employ an uncompetitive mechanism influencing the binding of NAD^+ to SIRT1.

Inauhzin Is More Effective than Cambinol or Salermide in Inhibition of SIRT1 Activity and Activation of p53

[00110] Inauhzin was compared to some published SIRT1 inhibitors (Heltweg et al, 2006; Lain et al, 2008; Lara et al, 2009) by performing *in vitro* p53-deacetylation and cellulous p53-

activation assays. Inauhzin was shown to be more effective in inhibiting SIRT1 activity than either cambinol or Salermide in *in vitro* assays using acetylated p53 proteins as a substrate, as neither of the latter two compounds could inhibit SIRT1 activity at the 6 μM level, the level at which Inauhzin markedly recovered p53 acetylation (**FIG. 6D**). Consistently, Inauhzin was also more effective than these two compounds in the induction of p53 acetylation and level in H460 (**FIGs. 6E** and **16A**) and HCT116 cells (**FIGs. 6F** and **16B**) as well as in the inhibition of cancer cell growth (**FIG. 16C**). These results demonstrate that Inauhzin is a better bioactive inhibitor of SIRT1 and a more effective activator of p53 than these two known SIRT1 inhibitors. Even though Tenovin-6 was able to induce p53, it was less effective than Inauhzin in the induction of p53 acetylation and level in the colon and lung cancer cells as tested here (**FIGs. 6E-F** and **16A-B**). Also, Tenovin-6 was much more toxic than Inauhzin to human primary embryonic fibroblasts (WI-38) and normal human fibroblasts (NHF-1) (**FIG. 16C**). Together, these results indicate that Inauhzin is tumor selective and more effective in inhibiting SIRT1 activity and activating p53.

Inauhzin Suppresses Growth of Human Xenograft Tumors Harboring p53.

[00111] In order to investigate the biological significance of the activation of p53 by Inauhzin, a set of animal experiments to evaluate the effect of this compound on the growth of human xenograft tumors was carried out. First, Inauhzin was tested to determine if it would affect the growth of xenograft tumors derived from H460 cells in severe combined immunodeficiency (SCID) mice since this compound markedly induced p53 level and activity at 2 μM as well as p53-dependent apoptosis in this cell line (**FIGs. 1** and **2**). Once H460 xenograft tumors grew into the size of 100 mm^2, 30mg/kg of Inauhzin via i.p. injection was administered once every other day (Q.O.D.) to the mice for 3 weeks.

[00112] Referring now to **FIG. 7A**. The tumors grew significantly more slowly in the Inauhzin treated animals than in those animals treated with respective vehicle (5% DMSO) ($p < 0.05$). Inauhzin significantly reduced the average tumor weight at the end of the experiment by nearly 40% ($p < 0.05$, **FIGs. 7A** and **17C**). Through this experimental period, both groups of animals had been healthy except bearing tumors and without apparent changes in their behavior, food appetite and body weight. At the end of the experiment, 1, 2, 4, 8, 10 hrs after the last dose,

sera was obtained; tumors were harvested at 4 and 8 hrs. Quantitative HPLC-MS/MS (API 4000, Applied Biosystems) analysis of the sera revealed that the average level of Inauhzin peaked at 1.5 μg/ml (equivalent to 3μM concentration) 1hr after the i.p. administration (**FIG. 17A**). The result was consistent with earlier obtained pharmacokinetics results (data not shown). Inauhzin levels achieved in the tumors more than 2 fold higher than that in the plasma at 4 hrs and then decreased by 8 hrs (**FIG. 17B**), indicating Inauhzin was able to penetrate tumors and persist within tumor tissues after i.p. administration. Moreover, Inauhzin-treated H460 tumors displayed elevated p53 compared to the vehicle-treated tumors by Immunoblotting (data not shown). These results suggest that Inauhzin has good tumor tissue penetration and is able to inhibit tumor growth by inducing p53.

[00113] In order to further assess the tumor suppression activity of Inauhzin and determine if the p53 pathway contributes to this tumor suppression function of this compound *in vivo*, p53-containing and p53-null HCT116 cells were implanted into the same SCID mouse (one at each side of its back) to generate $p53^{+/+}$ and $p53^{-/-}$ tumors, as shown in the representative **FIG. 7C**, to minimize possible variations between the two cell lines caused by individual animals. The strategy of drug administration was also modified since the animals in H460 xenograft experiments did not show any apparent abnormality. Once palpable tumors were detected, pairs of mice were randomized to receive either 30mg/kg (n=7) once per day (Q.D.) or vehicle (5% DMSO). As a result, Inauhzin was more effective in retarding the tumor growth in $HCT116^{+/+}$ tumors, as it more significantly reduced tumor growth and weight by ~70% at the end of the experiment (**FIG. 7B**). Furthermore, this inhibition was p53-dependent, as Inauhzin had moderate effect on the growth of $HCT116^{-/-}$ tumors (**FIGs. 7B** and **17C**). Inauhzin-treated $HCT116^{+/+}$ tumors were significantly smaller than their respective controls of vehicle treatment ($p<0.01$), whereas there were marginal difference between Inauhzin and vehicle treatments in p53-null HCT116 xenografts ($p>0.1$). Correspondingly, p53 level and activity as indicated with induction of cleaved PARP were highly induced in Inauhzin-treated p53-harboring, but not in p53-null, HCT116 tumors (**FIG. 7D**). This induction in the p53-harboring tumors was also well correlated with a significant increase in apoptosis within the tumor as measured by TUNEL assays and a marked decrease in proliferation as measured by BrdU staining (**FIGs. 7E-G**). However, there was no significant difference observed in apoptosis and proliferation between

Inauhzin and vehicle treatments in p53-null HCT116 xenografts. Remarkably, Inauhzin also potently induced apoptosis specifically in tumor cells (**FIGs. 7E-F**) without measurable cell death in the high proliferative of normal tissues (Small intestine, spleen and stomach) (**FIG. 17D**). Collectively, these results demonstrate that Inauhzin effectively induces apoptosis and suppresses tumor growth in p53-harboring tumors.

[00114] Referring now to **FIG. 8,** upon stress, p53 is significantly acetylated by p300 and thus prevented from ubiquitylation and degradation mediated by MDM2/MDMX. SIRT1 deacetylates p53, not only inhibiting its activity, but also rendering p53 into an ideal substrate for MDM2/MDMX-mediated ubiquitylation and degradation. Inauhzin can induce p53 acetylation and level, hence reactivating p53 by inhibiting SIRT1 deacetylase activity, as SIRT1 is often highly expressed in cancers or cancer cells due to the lack of expression of its repressor HIC-1 via promoter hypermethylation as indicated in dotted lines; Otherwise, in normal cells where its promoter is not hypermethylated, HIC-1 can be induced by p53 to repress SIRT1 expression at the mRNA level in response to stress. As disclosed herein, Inauhzin is a novel small molecule that possesses the ability to induce p53 levels and activity, leading to p53-dependent apoptosis. As a result, this compound inhibits the growth of xenograft tumors from p53-containing lung and colon cancer cell lines, but exhibits minimum effect on tumors from p53-null HCT116 cells. A rationale-based strategy and a reverse target-identification approach (identifying the target(s) of a compound after unveiling its cellular phenotype or biological activity), suggests a likely mechanism that can account for the activation of p53 by this compound; i.e., inhibition of SIRT1 activity (**FIG. 8**).

[00115] Without being bound by any single theory or hypothesis, the initial biochemical analyses indicates that Inauhzin does not appear to compete with a substrate for the active site of SIRT1, but might affect the binding of NAD^+ to SIRT1 via an uncompetitive mechanism, though this mode of action needs to be further investigated.

[00116] It is intriguing that Inauhzin does not effectively induce p53 level and activity in human embryonic fibroblast WI-38 cells and human fibroblast NHF cells (**FIG. 1D** and data not shown). Likewise, it is also much less toxic to these normal cells even though they contain wild-type p53 (**FIGs. 1E** and **16**). This is distinct from MDM2 inhibitors, such as Nultin or MI-63, both of which can activate p53 in normal fibroblast cells (Shangary et al, 2008). Although the

SIRT inhibitor, Tenovin-1, was also reported to resist in the normal human dermal fibroblasts (Lain et al, 2008), the comparison of its analogue tenovin-6 with Inauhzin revealed that the latter is much less toxic than the former to primary human fibroblast cells (**FIG. 16C**). Although it remains to be investigated why Inauhzin does not activate p53 in normal fibroblast cells, it is possible that in the absence of stress, SIRT1 might not be needed to inactivate p53 as p53 is not acetylated by p300/CBP in normally growing cells. Consistent with this assumption, it was recently shown that SIRT1 has no significant role in the growth of murine embryonic stem (ES) cells under normal conditions, but SIRT1 could control mitochondrial localization of p53 by deacetylating it in response to oxidative stress in ES cells (Han et al, 2008). Another possibility is that SIRT1 might be more active in some cancer cells than in normal cells. Indeed, SIRT1 is highly expressed in several human cancers, including lung, colon and prostate cancers due to the inactivation of its repressor HIC-1 (Fleuriel et al, 2009; Fukasawa et al, 2006; Nakae et al, 2006; Tseng et al, 2009). HIC-1 suppresses the expression of SIRT1 at the transcriptional level in response to p53 activation (Chen et al, 2005; Wales et al, 1995), but is often turned off in cancers due to promoter hyper-methylation (Fleuriel et al, 2009; Fukasawa et al, 2006; Hayashi et al, 2001) (**FIG. 8**). Thus, knockdown of SIRT1 by siRNA or inhibition of SIRT1 activity by Inauhzin conveys a more significant effect on p53 activation in cancer cells than in normal cells (**FIGs. 13** and **16**). Because of this, Inauhzin is much less toxic to normal cells, and this feature would be conducive to clinical therapy, as it would minimize its side effect on cancer-bearing patients.

[00117] Over the past decade or so, several small molecule inhibitors of the Sirtuin family have been reported (Alcain & Villalba, 2009). Some of them were quite potent in test tubes (Trapp et al, 2007) and effective in yeast or plants (Grozinger et al, 2001). However, none of them has been reported to be bioactive suppressors of tumor growth in animal models until recently when tenovins were identified to inhibit SIRT2 as well as SIRT1 with a relatively weak activity (Lain et al, 2008). Tenovins induce p53 acetylation and activity resulting in suppression of xenograft melonoma and Burkitt's lymphoma growth *in vivo* at 50-90 mg/kg via IP. By contrast, Inauhzin is a specific and more potent inhibitor of SIRT1 (**FIGs. 5**, **6**, **15** and **16**) and also considerably effective in exerting p53-dependent suppression of xenograft lung and colon cancer growth *in vivo* at 30 mg/kg via i.p (**FIG. 7**). More importantly, Inauhzin exhibits higher

selectivity between cancer cells and normal cells compared to Tenovin-6 (**FIG. 16C**). This discrepancy might be due to the following possibilities: 1) Tenvoins affect multiple members of the Sirtuin family; 2) Inauhzin and Tenovins perhaps inhibit SIRT1 through different mechanisms or bind to different forms of SIRT1 in different cellular locations (Byles et al, 2010; Lynch et al, 2010; Nasrin et al, 2009), and, for example, Inauhzin might bind to phosphorylated SIRT1 which is more active in cancer cells (data not shown); 3) Tenovin and Inauhzin might be transported through cellular membranes by distinct transporters, whose expression levels could be different between normal and cancer cells. Also, as demonstrated herein, Inauhzin was more effective than two other known SIRT1 inhibitors, Cambinol or Salermide, in inhibiting SIRT1 activity *in vitro* and in activating of p53 in cells (**FIGs, 6D-F** and **16**). Although another SIRT1-specific inhibitor, EX527, which effectively inhibited SIRT1-mediated p53 acetylation *in vitro*, had little influence on p53 acetylation and level in MCF7 cells (Peck et al, 2010), it did affect the SIRT1-p53 pathway in rodent tissues (Velasquez et al, 2011). These seemingly contradictory results suggest that EX527 might not be permeable to certain cancer cell lines, such as MCF7 cells. By contrast, Inauhzin was able to activate p53 in all of the p53-containing cancer cells that were tested, including MCF7 cells (**FIGs. 1**, **2**, and **9**). Therefore, this comparison of Inauhzin with existing known small molecule SIRT1 inhibitors indicates that Inauhzin distinguishes itself with following features: 1) it is more effective in inhibiting SIRT1 activity *in vitro*; 2) it is more potent at activating p53 in cells; 3) it is less toxic to normal cells and tissues; and 4) it is more bioactive and bioavailable to all of the cancer cell lines tested. Based on these special characters, Inauhzin appears to be a good candidate for further developing into an anti-cancer drug.

[00118] Although other potential protein targets for Inauhzin may exist, the results disclosed herein clearly demonstrate that this compound specifically triggers p53-dependent apoptosis and suppression of cell proliferation in both cultured cells and xenograft tumors. Another p53 family member, p73, was previously shown to be a target for SIRT1 (Dai et al, 2007). Indeed, knockdown of p73 partially impaired the induction of p21 and MDM2 levels by Inauhzin (**FIG. 10C**); this could partially explain why p21 induction by this compound occurred earlier than p53 induction in **FIG. 2A**. However, depletion of p73 by siRNA did not appear to affect the induction of the level, acetylation and apoptotic activity of p53 by Inauhzin (**FIGs. 10C-E**), indicating that this compound indeed suppresses cell growth by mainly activating p53 and inducing p53-dependent apoptosis (**FIG. 1-8**), which is in line with the previous reports showing the close link of p53 acetylation with p53-dependent apoptosis (Tang et al, 2006). Therefore, as disclosed herein Inauhzin, which is structurally distinct from any of the published Sirtuin inhibitors, appears to be the first SIRT1 inhibitor that can induce p53 acetylation, level and activity without causing genotoxicity and disrupting MDM2/MDMX-p53 interaction in cancer cells, leading to p53-dependent apoptosis and suppression of tumor growth (**FIG. 8**). This unexpected finding not only validates the negative regulation of p53 by SIRT1 in cancer cells, but also divulges a new class of target-specific small molecules as another highly promising contender for future therapy of p53-bearing human lung, colon and prostate cancers that highly express SIRT1 (Jung-Hynes & Ahmad, 2009; Nosho et al, 2009), although it has been debating if SIRT1 plays a role in cancer development and whether SIRT1 would be an appropriate target for cancer therapy (Bosch-Presegue & Vaquero, 2011; Fang & Nicholl, 2011; Herranz & Serrano, 2010; van Leeuwen & Lain, 2009). Since SIRT1 is also involved in aging and metabolic disorders (Guarente, 2000), identification of Inauhzin as an inhibitor of SIRT1 would offer a useful tool for studying molecular events or mechanisms underlying these diseases and a potential candidate for their therapeutic development. Finally, it would be important and interesting to explore if Inauhzin could synergize the anti-cancer effect of the known small molecules that target the p53 pathway or of the existing chemotherapy or radiotherapy in the near future.

Materials and Methods

[00119] The compounds for the cell-based screen, Inauhzin and its analogues were purchased from Asinex, ChemDiv and ChemBridge. Inauhzin and Inauhzin1-5 were re-validated by LC/MS on an Agilent 1200 LC/MS system (Agilent Technology) at the Chemical Genomics Core Facility on the campus. Inauhzin used for the animal experiments was synthesized, purified and identity verified by ChemBridge Inc. The minimum purity of all compounds is higher than 90%. MI-63 was generously provided by Shaomeng Wang (University of Michigan). Actinomycin D, Cisplatin, Etoposide and Trichostatin A (TSA) were purchased from Sigma. 5-Aminoimidazole-4-carboxamide-1-β-D-ribofuranoside (AICAR) was purchased from Toronto Research Chemicals Inc., North York, Ontario, Canada. Cambinol, Salermide and Tenovin-6 were from Cayman Chemical Company. Tenovin-6 was also provided by Sonia Lain (University of Dundee) as a gift. Biotinylated INZ was synthesized and characterized by NMR and LC-MS (Supplemental information).

Cell Viability Assay

[00120] To assess cell growth, the cell counting kit (Dojindo Molecular Technologies Inc., Gaithersburg, Maryland) was used according to manufacturer's instructions. Cell suspensions were seeded at 5,000 cells per well in 96-well culture plates and incubated overnight at 37°C. Compounds were added into the plates and incubated at 37°C for 72 hrs. Cell growth inhibition was determined by adding WST-8 at a final concentration of 10% to each well, and the absorbance of the samples was measured at 450 nm using a Microplate Reader (Molecular Device, SpecrtraMax M5^{e}).

In Vivo Ubiquitylation Assay

[00121] For detection of ubiquitylation of endogenous p53, H460 cells in the 60mm plates were transfected with $(His)_6$-ubiquitin (His-Ub) (3 μg). At 24 hrs after transfection, cells were treated with various concentrations of Inauhzin for 18 hrs, and then 10 μM MG132 and 20 μM ALLN for 8 hrs. For detection of ubiquitylation of exogenous p53, $HCT116^{-/-}$ cells were transfected with His-Ub (3 μg), p53 (0.2 μg), HA-MDM2 (2 μg) expression plasmids as indicated in Figure 3D and Figure 11A. At 36hrs after transfection, cells were treated with

Inauhzin for 4 hrs followed by addition of 10 μM MG132 for 8 hrs. Cells were harvested and split into two aliquots, one for IB and the other for His pull-down by Nickel-NTA agarose (Thermo Scientific) as described previously (Dai et al, 2006; Sun et al, 2007) and analyzed by IB.

Immunofluorescence for Detection of H2AX Ser139 Phosphorylation (γH2AX) Foci

[00122] H460 cells at 50-70% confluence were treated with 2μM of Inauhzin (INZ) or 10μM Cisplatin (Cis) for 18hrs or 2mM Hydroxyurea (HU) for 8hrs. Cells were fixed in 4% formaldehyde/PBS for 10 min, permeabilized and blocked with 0.3% Triton-100, 8%BSA/PBS. The primary antibodies used were polyclonal Phospho-Histone H2A.X (Ser139) antibodies in 1:250 dilution (20E3, Cell signaling) and monoclonal p53 antibodies (DO-1, Santa Cruz Biotechnology) according to the manufactural instruction. Alex488 secondary antibodies were used to detect protein signals (Invitrogen). Images were taken with a Zeiss Axiovert 200M fluorescent microscope and measured using AxioVision 4.7.2.0 software.

Deacetylation Activity Assays Using Full-length Acetylated p53 Proteins as a Substrate

[00123] H1299 cells were transfected with Flag-p53 plasmid and then infected with p300 adenovirus (Zeng et al, 2003) for 24hrs. The cells were treated with 0.4μM TSA for 18hrs and harvested for purification of p53 proteins by using anti-Flag M2 agarose (sigma). Bound proteins were eluted in TBS buffer (50mM Tris-HCl, pH 7.4, 150mM NaCl) containing 0.2 mg of synthetic Flag peptides/ml, and then dialyzed in deacetylation buffer (50 mM Tris-HCl, pH 9.0, 137mM NaCl, 2.7mM KCl, 1mM $MgCl_2$, 0.2mM PMSF, 1mM DTT).

[00124] Deacetylation reaction containing purified Flag-p53 proteins and titrated INZ was pre-incubated at room temperature for 10 min and initiated by adding 1.0 unit of SIRT1 enzyme (Enzo Life Sciences) and 50μM NAD+. Reactions were incubated at 30°C for 1hr and stopped by addition of SDS loading buffer. Samples were analyzed by IB and the acetylated Flag-p53 was detected with anti-p53KAc382 antibodies and total Flag-p53 was detected with anti-p53 DO-1 antibodies (North et al, 2005).

[00125] The inhibition experiments of Inauhzin, Cambinol, Salermide on SIRT1 activity were carried out using the same conditions as above. For each sample, the level (band intensity)

of p53KAc382 was quantified and normalized against total p53 levels. Inhibitory activity was calculated as the mean value of negative controls minus the average sample value divided by the mean value of negative controls minus the mean value of positive controls, multiplied by 100. Positive controls (100% inhibition) contained the acetylated p53 protein substrate only (first lane), and negative controls (0% inhibition) contained the substrate and SIRT1 enzymes (second lane). See Figure 6D.

Binding of Biotinylated INZ to SIRT1

[00126] Recombinant SIRT1 and SIRT7 were expressed in E. coli BL21-CodonPlus (DE3)-RIPL and purified through Ni-NTA agarose beads. Purified proteins was stained with Coomassie blue staining and quantified with BSA as a standard. The activity of purified SIRT1 was measured by the decrease in the levels of Ac-Lys382-p53 with acetylated-p53 protein as a substrate. For detection of binding of biotinylated Inauhzin to SIRT1, the indicated concentrations of purified His-SIRT1 was incubated with biotinylated Inauhzin that was conjugated to NeutrAvidin Agarose (Thermo Scientific) at 4^0C overnight by gently agitating in the presence or the absence of 20 μM of free and non-biotinylated Inauhzin. The beads were washed three times with 0.5% (w/v) NP-40, 0.2% (w/v) Tween 20/Tris buffered saline. Equal volumes of 2 × SDS sample buffer were then added to each bead sample. The samples were boiled for 5 min and subjected to SDS-PAGE and immunoblotted with anti-His antibodies.

Mouse Xenograft Studies

[00127] Five-weeks-old female SCID mice were purchased from *In Vivo* Therapeutics (IVT) Core, Indiana University Simon Cancer Center (IUSCC) and housed in a BSL2 environment. Mice were subcutaneously inoculated with 5×10^6 H460 or 3×10^6 HCT116 cells. Tumor growth was monitored every other day with electronic digital calipers (Fisher Scientific) in two dimensions. Tumor volume was calculated with the formula: tumor volume (mm^3) = (length×width^2) / 2(Figg & McLeod, 2004). When the mean tumor volume reached approximately 100 mm^3 after 7-9 days, animals were dosed by i.p. injection with vehicle (5% DMSO) or Inauhzin. Inhibition of tumor growth was calculated on the last day of treatment. To detect p53 activation *in vivo*, tumors were harvested and disrupted in RIPA buffer containing a protease inhibitor mixture (Sigma). Tumor lysates were analyzed by IB. Cell proliferation in

tumors was assessed by BrdU labeling followed by Immunostaining. 200mg/kg body weight of BrdU (Sigma) was administrated to mice via i.p. injection 2 hrs before mice are sacrificed. Apoptosis was examined by TUNEL staining, using the Fluorescein In situ cell death detection kit (Roche) according to manufacturer's instructions. All animal experiments comply with protocols approved by The IUSM Institutional Animal Care and Use Committee (IACUC).

Cell Culture and Plasmids.

[00128] Human lung non-small-cell carcinoma H460, A549, H1299 and HT29 cells as well as human colon cancer HCT116, human breast cancer MCF7, human embryonic fibroblast WI-38, human osteosarcoma U2OS and SJSA, human glioma U87 and U373, and human ovarian cancer A2780, IGROV1, and SKOV3 cells were used in the study. All cells were cultured in Dulbecco's modified Eagle's medium supplemented with 10% fetal bovine serum (PBS), penicillin, and streptomycin, except SJSA cells, which were grown in RPMI-1640 medium containing glucose. The adenovirus-shRNA for SIRT1 was from X. Charlie Dong's Lab (Indiana University) (Wei et al, 2010). Flag-p53 was provided by Wei Gu (Columbia University).

Antibodies

[00129] Antibodies for immunoblotting were as follows: mouse monoclonal anti-p53 (DO-1), rabbit anti-SIRT1 (H300), rabbit anti-p21 (M19), mouse anti-p21 (F5) from Santa Cruz. Anti-p53-Acetylated (lys382), Cleaved PARP, PARP (9542), Puma, rabbit AMPKapha, rabbit Phospho-AMPK-alpha (Thr172) (40H9), rabbit Acetyl-Histone H3 (K9), rabbit Ac-alpha-tubulin (K40), mouse phosphor-p53 (ser46), and phosphor-p53 (ser15) were from Cell Signaling Technologies. 2A10 monoclonal anti-MDM2 antibodies were described previously (Zeng et al, 1999). Antibodies for immunostaining were as follows: rabbit polyclonal anti-p53 (FL-393, Santa Cruz), mouse monoclonal anti-BrdU (IIB5, Santa Cruz).

Immunoblotting

[00130] Cells were seeded in 6-well plates. All compounds were dissolved in DMSO and diluted directly into the medium to the indicated concentrations; 0.1% DMSO was used as a control. After incubation with the compounds for the indicated times, cells were harvested and lysed in 50 mM Tris-HCl pH 8.0, 150 mM NaCl, 5 mM EDTA, 0.5% NP-40 supplemented with

2 mM DTT and 1 mM PMSF. An equal amount of protein samples (50 μg) was subjected to SDS-PAGE and transferred to a PVDF membrane (PALL Life Science). The membranes with transferred proteins were probed with primary antibodies followed by horseradish-peroxidase-conjugated secondary antibody (1:10,000; Pierce). The blots were then developed using an enhanced chemiluminescence detection kit (Thermo Scientific), and signals were visualized by Omega 12iC Molecular Image System (UltraLUM).

FACS Analysis

[00131] Logarithmically growing cells were incubated with either Inauhzin or DMSO for the time points as indicated. Cells were harvested, fixed in 70% ethanol overnight and analyzed by propidium iodide (PI) staining and flow cytometry (FACS Calibur, Becton Dickinson) as previously described (Riccardi & Nicoletti, 2006).

RNA Interference

[00132] Control scrambled siRNA, or siRNA specific to p53, p73, or SIRT1 were purchased from Santa Cruz Biotechnology. These siRNAs (20 to 120 nM) were introduced into cells using METAFECTENE® SI following the manufacturer's protocol (Biontex). Cells were treated with INZ for IB, qRT-PCR and cell viability assays.

Senescence-Associated β-galactosidase Staining

[00133] Cells (3×10^4) were plated in 3.5-cm-diameter plates and treated for 1 week with 2 μM Inauhzin or 10 μM nutlin-3 (synthesized by the IUPUI chemical core facility). Senescence-associated β-galactosidase staining was performed by using Senescence-β-Gal Staining Kit (Cell Signaling Technology) and following the manufacturer's instructions. β-Galactosidase activity was measured by the absorbance of 5, 5'-dibromo-4, 4'-dichloro-indigo at 650 nm generated by the β-Galactosidase staining using a Microplate Reader (Molecular Device, SpecrtraMax M5e).

Reverse Transcription and Real-Time PCR Analyses.

[00134] Total RNA was isolated from cells using Qiagen RNeasy Mini kits (Qiagen, Valencia, CA) and treated with DNase I (Invitrogen). Quantitative real-time PCR was performed on an ABI 7300 real-time PCR system (Applied Biosystems) using SYBR Green Mix (Applied

Biosystems) as described previously(He et al, 2007). All reactions were carried out in triplicate. The relative gene expression was calculated using the ΔCt method following the manufacturer's instruction. The primers for p53, p21, MDM2 and GAPDH were described(Sun et al, 2007). The primers that amplify the mir-34a pri-miRNA, mir-24 pri-miRNA were designed with Primer Express software: hsa-pri-mir-34a, **(SEQ ID NO. 1)** 5′-CTTCACCTACAGATGCCAACTTTG-3′ and **(SEQ ID NO. 2)**; 5′-CCGGTGACTTTGGTCCAATT-3′; hsa-pri-mir-24, **(SEQ ID NO. 3)**; 5′-CCGGGCTGTCGATTGG-3′ and **(SEQ ID NO. 4)**; 5′-GACTCCTGTTCCTGCTGAACTGA-3′.

In Vitro Ubiquitylation Assay.

[00135] His-MDM2 and GST-p53 were purified from *Escherichia coli*. The *in vitro* p53 ubiquitylation reactions were performed at room temperature (20-22°C) in the ubiquitylation buffer: 25mM Hepes (pH 7.4), 10mM NaCl, 3mM MgCl2, 0.05% TritonX-100, 2mM ATP, 200ng Ubiquitin Activating Enzyme E1 (rabbit, Boston Biochem), 50 ng E2 (UbcH5a, human recombinant, Boston Biochem), 10ng ubiquitin (human recombinant, Boston Biochem) and 50ng purified His-MDM2 were incubated with Inauhzin for 20 min. The reaction was initiated by adding the substrate, 50ng of purified GST-53 and quenched by the addition of SDS loading buffer. Ubiquitinated p53s were detected by immunoblotting with the anti-p53 (DO-1) antibody (Li et al, 2002).

DNA Binding Assay.

[00136] To determine whether Inauhzin direct binds to DNA, Fluorescence Intercalator Displacement Analyses were performed as described previously (Goodwin et al, 2006). 2.5μM ethidium bromide and 1.25 μM DNA (calf thymus DNA, Sigma) was mixed with Inauhzin or Actinomycin D in the buffer (50mM Tris, pH7.4, 100mM NaCl). Fluorescence signals were detected after incubation for 15 min at room temperature using a Microplate Reader (Molecular Device, SpecrtraMax M5^{e}).

***In Vitro* Deacetylation Assays**

[00137] Fluor-de-Lys Fluorimetric Assays for SIRT1 (BML-SE239, ENZO), SIRT2, SIRT3 and HDAC8 were performed in 384-well plates using Fluor-de-Lys Drug Discovery Kit

(BML-AK555, AK556, AK518, ENZO) (Lain et al, 2008). Both SIRT2 and SIRT3 use the same Fluor-de-Lys (FdL) substrate, 317-320 of p53 acetylated on lysine 320. SIRT1 requires a different substrate, 379-382 of p53 acetylated on lysine 382 (BML-KI177, ENZO). In this assay, enzyme was added at a concentration of 0.5units/well for SIRT1 and HDAC8, and 1.0 units/well for SIRT2 and SIRT3. FdL substrates and NAD^+ used in the assay were at 10μM and 25μM, respectively. Assays were incubated for 45 min at 37 °C. Resulting fluorescence was measured after further incubation for 15 min at 37 °C with Fluor-de-Lys Developer II (BML-KI176, ENZO) using a Microplate Reader (Molecular Device, SpecrtraMax M5^e) with excitation set at 360 nm and emission measured at 460 nm. IC_{50} data were analyzed using Igor4.01 (Lake Oswego, Oregon, USA).

Preparation and Characterization of Biotinylated Inauhzin

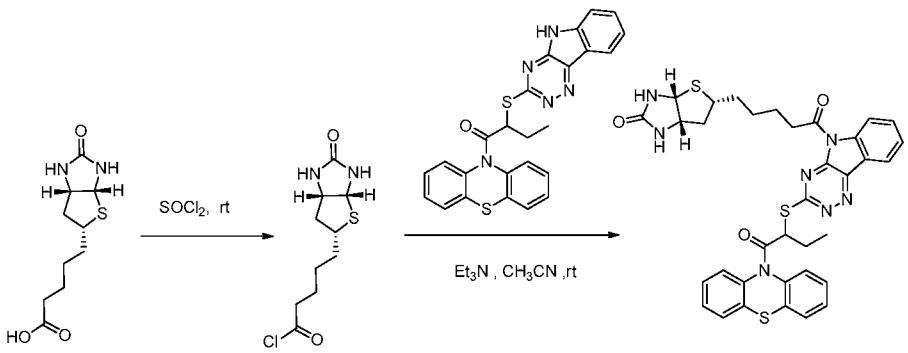

[00138] Biotin (100 mg, 0.410 mM) was placed in a 10 ml reaction flask and cooled to 0 °C. 2.7 ml $SOCl_2$ was added to the flask and allowed to room temperature. The mixture was stirred for 1 h and excess $SOCl_2$ was evaporated. The residue was co-evaporated with 5 ml anhydrous toluene for three times to give the biotin acid chloride. Crude acid chloride was dissolved in 5ml anhydrous CH_3CN. INZ (65 mg, 0.138 mM) was dissolved in 3 ml anhydrous CH_3CN and injected to the above solution through syringe. The mixture was cooled to 0 °C, and 100 μl Et_3N (0.717 mM) was dropped to the mixture. The solution was then allowed to room temperature. TLC was used to monitor the reaction. After 11 hrs, TLC indicated that the reaction was completed. The reaction mixture was diluted with 30 ml ethyl acetate and washed twice by saturated NaCl. The organic phase was separated and dried by anhydrous Na_2SO_4. The organic phase was filtered, concentrated by vacuum and purified through a silica gel column and eluted with DCM/CH_3OH (55:1). The product was obtained in viscous oil (45 mg, 47 % over two

steps). Biotinylated Inauhzin was confirmed by 1HNMR analysis. Its 1HNMR spectrum is as follows (500Mz, $CDCl_3$): δ 8.69(d, J = 8.5, 1H), 8.40 (d, J=7.5, 1H), 7.92(br, 1H), 7.75-7.72(m, 1H), 7.67(d, J=7.0, 1H), 7.59-7.56 (m, 1H), 7.53(d, J=3.0, 1H), 7.40 (br, 1H), 7.35-7.29(m, 3H), 7.18(br, 1H), 5.60(d, J=39.5, 1H), 5.42-5.38 (m, 1H), 5.14(s, 1H), 4.56-4.53 (m,1H), 4.41-4.37(m, 1H), 3.48-3.41(m, 1H),3.35-3.26(m,1H),3.25-3.23(m,1H), 2.98-2.95(m, 1H), 2.76(d, J= 12.5, 1H), 1.90-1.83(m, 4H), 1.79-1.75(m, 1H), 1.70(br, 1H),1.61-1.58(m,2H), 0.98-0.90(m,3H).

Immunofluorescence.

[00139] Tissues were collected in 4% paraformaldehyde, fixed overnight and embedded in paraffin. Antigen retrieval was performed in a hot water bath for 15 min in 10 mM sodium citrate (pH 6.0), cooled for 20 min at 25°C, and washed with PBST (PBS, 0.1% Tween 20). Tissues were permeabilized by incubating the slides in 1% Triton X-100 in PBS for 10 min and then washed again three times in PBST. After blocking for 1 hr at 25°C in blocking buffer (PBS containing 0.2% BSA and 0.2% Triton X-100), slides were incubated overnight in a humidity chamber with a mouse anti-BrdU monoclonal antibody and anti-p53 rabbit polyconal (FL393) diluted 1:100 in blocking buffer. BrdU and p53 were detected with Alexa Fluor 488 (green) goat anti-mouse antibody and Alexa Fluor 546 (red) goat anti-rabbit antibody (Invitrogen), respectively. The slides were then stained with DAPI for nuclei and the images were captured under a Zeiss Axiovert 200M fluorescent microscope. The images were analyzed using AxioVision 4.7.2.0 software from Zeiss.

REFERENCES

Alcain FJ, Villalba JM (2009) Sirtuin inhibitors. *Expert Opin Ther Pat* **19:** 283-294

Banin S, Moyal L, Shieh S, Taya Y, Anderson CW, Chessa L, Smorodinsky NI, Prives C, Reiss Y, Shiloh Y, Ziv Y (1998) Enhanced phosphorylation of p53 by ATM in response to DNA damage. *Science* **281:** 1674-1677

Barak Y, Juven T, Haffner R, Oren M (1993) mdm2 expression is induced by wild type p53 activity. *EMBO J* **12:** 461-468

Bosch-Presegue L, Vaquero A (2011) The dual role of sirtuins in cancer. *Genes & cancer* **2:** 648-662

Brown CJ, Lain S, Verma CS, Fersht AR, Lane DP (2009) Awakening guardian angels: drugging the p53 pathway. *Nat Rev Cancer* **9:** 862-873

Byles V, Chmilewski LK, Wang J, Zhu L, Forman LW, Faller DV, Dai Y (2010) Aberrant cytoplasm localization and protein stability of SIRT1 is regulated by PI3K/IGF-1R signaling in human cancer cells. *International journal of biological sciences* **6:** 599-612

Chen WY, Wang DH, Yen RC, Luo J, Gu W, Baylin SB (2005) Tumor suppressor HIC1 directly regulates SIRT1 to modulate p53-dependent DNA-damage responses. *Cell* **123:** 437-448

Cheng HL, Mostoslavsky R, Saito S, Manis JP, Gu Y, Patel P, Bronson R, Appella E, Alt FW, Chua KF (2003) Developmental defects and p53 hyperacetylation in Sir2 homolog (SIRT1)-deficient mice. *Proc Natl Acad Sci U S A* **100:** 10794-10799

Dai JM, Wang ZY, Sun DC, Lin RX, Wang SQ (2007) SIRT1 interacts with p73 and suppresses p73-dependent transcriptional activity. *Journal of cellular physiology* **210:** 161-166

Dai MS, Shi D, Jin Y, Sun XX, Zhang Y, Grossman SR, Lu H (2006) Regulation of the MDM2-p53 pathway by ribosomal protein L11 involves a post-ubiquitination mechanism. *J Biol Chem* **281:** 24304-24313

Ding K, Lu Y, Nikolovska-Coleska Z, Wang G, Qiu S, Shangary S, Gao W, Qin D, Stuckey J, Krajewski K, Roller PP, Wang S (2006) Structure-based design of spiro-oxindoles as potent, specific small-molecule inhibitors of the MDM2-p53 interaction. *J Med Chem* **49:** 3432-3435

DiTacchio L, Le HD, Vollmers C, Hatori M, Witcher M, Secombe J, Panda S (2011) Histone lysine demethylase JARID1a activates CLOCK-BMAL1 and influences the circadian clock. *Science* **333:** 1881-1885

Duriez PJ, Shah GM (1997) Cleavage of poly(ADP-ribose) polymerase: a sensitive parameter to study cell death. *Biochem Cell Biol* **75:** 337-349

Efeyan A, Ortega-Molina A, Velasco-Miguel S, Herranz D, Vassilev LT, Serrano M (2007) Induction of p53-dependent senescence by the MDM2 antagonist nutlin-3a in mouse cells of fibroblast origin. *Cancer Res* **67:** 7350-7357

Eischen CM, Lozano G (2009) p53 and MDM2: antagonists or partners in crime? *Cancer Cell* **15:** 161-162

Fang Y, Nicholl MB (2011) Sirtuin 1 in malignant transformation: friend or foe? *Cancer letters* **306:** 10-14

Figg WD, McLeod HL (2004) *Handbook of anticancer pharmacokinetics and pharmacodynamics*, Totowa, N.J.: Humana Press.

Finnin MS, Donigian JR, Cohen A, Richon VM, Rifkind RA, Marks PA, Breslow R, Pavletich NP (1999) Structures of a histone deacetylase homologue bound to the TSA and SAHA inhibitors. *Nature* **401:** 188-193

Fleuriel C, Touka M, Boulay G, Guerardel C, Rood BR, Leprince D (2009) HIC1 (Hypermethylated in Cancer 1) epigenetic silencing in tumors. *Int J Biochem Cell Biol* **41:** 26-33

Fukasawa M, Kimura M, Morita S, Matsubara K, Yamanaka S, Endo C, Sakurada A, Sato M, Kondo T, Horii A, Sasaki H, Hatada I (2006) Microarray analysis of promoter methylation in lung cancers. *J Hum Genet* **51:** 368-374

Grozinger CM, Chao ED, Blackwell HE, Moazed D, Schreiber SL (2001) Identification of a class of small molecule inhibitors of the sirtuin family of NAD-dependent deacetylases by phenotypic screening. *J Biol Chem* **276:** 38837-38843

Gu J, Kawai H, Nie L, Kitao H, Wiederschain D, Jochemsen AG, Parant J, Lozano G, Yuan ZM (2002) Mutual dependence of MDM2 and MDMX in their functional inactivation of p53. *J Biol Chem* **277:** 19251-19254

Guarente L (2000) Sir2 links chromatin silencing, metabolism, and aging. *Genes Dev* **14:** 1021-1026

Han MK, Song EK, Guo Y, Ou X, Mantel C, Broxmeyer HE (2008) SIRT1 regulates apoptosis and Nanog expression in mouse embryonic stem cells by controlling p53 subcellular localization. *Cell Stem Cell* **2:** 241-251

Haupt Y, Maya R, Kazaz A, Oren M (1997) Mdm2 promotes the rapid degradation of p53. *Nature* **387:** 296-299

Hayashi M, Tokuchi Y, Hashimoto T, Hayashi S, Nishida K, Ishikawa Y, Nakagawa K, Tsuchiya S, Okumura S, Tsuchiya E (2001) Reduced HIC-1 gene expression in non-small cell lung cancer and its clinical significance. *Anticancer Res* **21:** 535-540

Heltweg B, Gatbonton T, Schuler AD, Posakony J, Li H, Goehle S, Kollipara R, Depinho RA, Gu Y, Simon JA, Bedalov A (2006) Antitumor activity of a small-molecule inhibitor of human silent information regulator 2 enzymes. *Cancer Res* **66:** 4368-4377

Herranz D, Serrano M (2010) SIRT1: recent lessons from mouse models. *Nature reviews Cancer* **10:** 819-823

Hollstein M, Sidransky D, Vogelstein B, Harris CC (1991) p53 mutations in human cancers. *Science* **253:** 49-53

Honda R, Tanaka H, Yasuda H (1997) Oncoprotein MDM2 is a ubiquitin ligase E3 for tumor suppressor p53. *FEBS Lett* **420:** 25-27

Hong H, Takahashi K, Ichisaka T, Aoi T, Kanagawa O, Nakagawa M, Okita K, Yamanaka S (2009) Suppression of induced pluripotent stem cell generation by the p53-p21 pathway. *Nature* **460:** 1132-1135

Issaeva N, Bozko P, Enge M, Protopopova M, Verhoef LG, Masucci M, Pramanik A, Selivanova G (2004) Small molecule RITA binds to p53, blocks p53-HDM-2 interaction and activates p53 function in tumors. *Nat Med* **10:** 1321-1328

Ito A, Lai CH, Zhao X, Saito S, Hamilton MH, Appella E, Yao TP (2001) p300/CBP-mediated p53 acetylation is commonly induced by p53-activating agents and inhibited by MDM2. *EMBO J* **20:** 1331-1340

Jones RG, Plas DR, Kubek S, Buzzai M, Mu J, Xu Y, Birnbaum MJ, Thompson CB (2005) AMP-activated protein kinase induces a p53-dependent metabolic checkpoint. *Mol Cell* **18:** 283-293

Jones SN, Roe AE, Donehower LA, Bradley A (1995) Rescue of embryonic lethality in Mdm2-deficient mice by absence of p53. *Nature* **378:** 206-208

Jung-Hynes B, Ahmad N (2009) Role of p53 in the anti-proliferative effects of Sirt1 inhibition in prostate cancer cells. *Cell Cycle* **8:** 1478-1483

Kobet E, Zeng X, Zhu Y, Keller D, Lu H (2000) MDM2 inhibits p300-mediated p53 acetylation and activation by forming a ternary complex with the two proteins. *Proc Natl Acad Sci U S A* **97:** 12547-12552

Kruse JP, Gu W (2009) Modes of p53 regulation. *Cell* **137:** 609-622

Kubbutat MH, Jones SN, Vousden KH (1997) Regulation of p53 stability by Mdm2. *Nature* **387:** 299-303

Kussie PH, Gorina S, Marechal V, Elenbaas B, Moreau J, Levine AJ, Pavletich NP (1996) Structure of the MDM2 oncoprotein bound to the p53 tumor suppressor transactivation domain. *Science* **274:** 948-953

Lain S, Hollick JJ, Campbell J, Staples OD, Higgins M, Aoubala M, McCarthy A, Appleyard V, Murray KE, Baker L, Thompson A, Mathers J, Holland SJ, Stark MJ, Pass G, Woods J, Lane DP, Westwood NJ (2008) Discovery, in vivo activity, and mechanism of action of a small-molecule p53 activator. *Cancer Cell* **13:** 454-463

Lara E, Mai A, Calvanese V, Altucci L, Lopez-Nieva P, Martinez-Chantar ML, Varela-Rey M, Rotili D, Nebbioso A, Ropero S, Montoya G, Oyarzabal J, Velasco S, Serrano M, Witt M, Villar-Garea A, Imhof A, Mato JM, Esteller M, Fraga MF (2009) Salermide, a Sirtuin inhibitor with a strong cancer-specific proapoptotic effect. *Oncogene* **28:** 781-791

Lavu S, Boss O, Elliott PJ, Lambert PD (2008) Sirtuins--novel therapeutic targets to treat age-associated diseases. *Nat Rev Drug Discov* **7:** 841-853

Li M, Luo J, Brooks CL, Gu W (2002) Acetylation of p53 inhibits its ubiquitination by Mdm2. *J Biol Chem* **277:** 50607-50611

Luo J, Nikolaev AY, Imai S, Chen D, Su F, Shiloh A, Guarente L, Gu W (2001) Negative control of p53 by Sir2alpha promotes cell survival under stress. *Cell* **107:** 137-148

Luo J, Su F, Chen D, Shiloh A, Gu W (2000) Deacetylation of p53 modulates its effect on cell growth and apoptosis. *Nature* **408:** 377-381

Lynch CJ, Shah ZH, Allison SJ, Ahmed SU, Ford J, Warnock LJ, Li H, Serrano M, Milner J (2010) SIRT1 undergoes alternative splicing in a novel auto-regulatory loop with p53. *PloS one* **5:** e13502

Maya R, Balass M, Kim ST, Shkedy D, Leal JF, Shifman O, Moas M, Buschmann T, Ronai Z, Shiloh Y, Kastan MB, Katzir E, Oren M (2001) ATM-dependent phosphorylation of Mdm2 on serine 395: role in p53 activation by DNA damage. *Genes Dev* **15:** 1067-1077

Montes de Oca Luna R, Wagner DS, Lozano G (1995) Rescue of early embryonic lethality in mdm2-deficient mice by deletion of p53. *Nature* **378:** 203-206

Morris GM, Huey R, Olson AJ (2008) Using AutoDock for ligand-receptor docking. *Curr Protoc Bioinformatics* **Chapter 8:** Unit 8 14

Nakae J, Cao Y, Daitoku H, Fukamizu A, Ogawa W, Yano Y, Hayashi Y (2006) The LXXLL motif of murine forkhead transcription factor FoxO1 mediates Sirt1-dependent transcriptional activity. *J Clin Invest* **116:** 2473-2483

Nasrin N, Kaushik VK, Fortier E, Wall D, Pearson KJ, de Cabo R, Bordone L (2009) JNK1 phosphorylates SIRT1 and promotes its enzymatic activity. *PloS one* **4:** e8414

North BJ, Schwer B, Ahuja N, Marshall B, Verdin E (2005) Preparation of enzymatically active recombinant class III protein deacetylases. *Methods* **36:** 338-345

Nosho K, Shima K, Irahara N, Kure S, Firestein R, Baba Y, Toyoda S, Chen L, Hazra A, Giovannucci EL, Fuchs CS, Ogino S (2009) SIRT1 histone deacetylase expression is associated with microsatellite instability and CpG island methylator phenotype in colorectal cancer. *Mod Pathol* **22:** 922-932

Oda K, Arakawa H, Tanaka T, Matsuda K, Tanikawa C, Mori T, Nishimori H, Tamai K, Tokino T, Nakamura Y, Taya Y (2000) p53AIP1, a potential mediator of p53-dependent apoptosis, and its regulation by Ser-46-phosphorylated p53. *Cell* **102:** 849-862

Onel K, Cordon-Cardo C (2004) MDM2 and prognosis. *Mol Cancer Res* **2:** 1-8

Paull TT, Rogakou EP, Yamazaki V, Kirchgessner CU, Gellert M, Bonner WM (2000) A critical role for histone H2AX in recruitment of repair factors to nuclear foci after DNA damage. *Curr Biol* **10:** 886-895

Peck B, Chen CY, Ho KK, Di Fruscia P, Myatt SS, Coombes RC, Fuchter MJ, Hsiao CD, Lam EW (2010) SIRT inhibitors induce cell death and p53 acetylation through targeting both SIRT1 and SIRT2. *Mol Cancer Ther* **9:** 844-855

Popowicz GM, Czarna A, Rothweiler U, Szwagierczak A, Krajewski M, Weber L, Holak TA (2007) Molecular basis for the inhibition of p53 by Mdmx. *Cell Cycle* **6:** 2386-2392

Shangary S, Qin D, McEachern D, Liu M, Miller RS, Qiu S, Nikolovska-Coleska Z, Ding K, Wang G, Chen J, Bernard D, Zhang J, Lu Y, Gu Q, Shah RB, Pienta KJ, Ling X, Kang S, Guo M, Sun Y, Yang D, Wang S (2008) Temporal activation of p53 by a specific MDM2 inhibitor is selectively toxic to tumors and leads to complete tumor growth inhibition. *Proc Natl Acad Sci U S A* **105:** 3933-3938

Shieh SY, Ikeda M, Taya Y, Prives C (1997) DNA damage-induced phosphorylation of p53 alleviates inhibition by MDM2. *Cell* **91:** 325-334

Shvarts A, Steegenga WT, Riteco N, van Laar T, Dekker P, Bazuine M, van Ham RC, van der Houven van Oordt W, Hateboer G, van der Eb AJ, Jochemsen AG (1996) MDMX: a novel p53-binding protein with some functional properties of MDM2. *EMBO J* **15:** 5349-5357

Sun XX, Dai MS, Lu H (2007) 5-fluorouracil activation of p53 involves an MDM2-ribosomal protein interaction. *J Biol Chem* **282:** 8052-8059

Tang Y, Luo J, Zhang W, Gu W (2006) Tip60-dependent acetylation of p53 modulates the decision between cell-cycle arrest and apoptosis. *Mol Cell* **24:** 827-839

Tang Y, Zhao W, Chen Y, Zhao Y, Gu W (2008) Acetylation is indispensable for p53 activation. *Cell* **133:** 612-626

Tanny JC, Dowd GJ, Huang J, Hilz H, Moazed D (1999) An enzymatic activity in the yeast Sir2 protein that is essential for gene silencing. *Cell* **99:** 735-745

Trapp J, Meier R, Hongwiset D, Kassack MU, Sippl W, Jung M (2007) Structure-activity studies on suramin analogues as inhibitors of NAD+-dependent histone deacetylases (sirtuins). *ChemMedChem* **2:** 1419-1431

Tseng RC, Lee CC, Hsu HS, Tzao C, Wang YC (2009) Distinct HIC1-SIRT1-p53 loop deregulation in lung squamous carcinoma and adenocarcinoma patients. *Neoplasia* **11:** 763-770

van Leeuwen I, Lain S (2009) Sirtuins and p53. *Advances in cancer research* **102:** 171-195

Vassilev LT, Vu BT, Graves B, Carvajal D, Podlaski F, Filipovic Z, Kong N, Kammlott U, Lukacs C, Klein C, Fotouhi N, Liu EA (2004) In vivo activation of the p53 pathway by small-molecule antagonists of MDM2. *Science* **303:** 844-848

Vaziri H, Dessain SK, Ng Eaton E, Imai SI, Frye RA, Pandita TK, Guarente L, Weinberg RA (2001) hSIR2(SIRT1) functions as an NAD-dependent p53 deacetylase. *Cell* **107:** 149-159

Velasquez DA, Martinez G, Romero A, Vazquez MJ, Boit KD, Dopeso-Reyes IG, Lopez M, Vidal A, Nogueiras R, Dieguez C (2011) The central Sirtuin 1/p53 pathway is essential for the orexigenic action of ghrelin. *Diabetes* **60:** 1177-1185

Vogelstein B, Lane D, Levine AJ (2000) Surfing the p53 network. *Nature* **408:** 307-310

Vousden KH, Prives C (2009) Blinded by the Light: The Growing Complexity of p53. *Cell* **137:** 413-431

Wade M, Wang YV, Wahl GM (2010) The p53 orchestra: Mdm2 and Mdmx set the tone. *Trends Cell Biol* **20:** 299-309

Wales MM, Biel MA, el Deiry W, Nelkin BD, Issa JP, Cavenee WK, Kuerbitz SJ, Baylin SB (1995) p53 activates expression of HIC-1, a new candidate tumour suppressor gene on 17p13.3. *Nat Med* **1:** 570-577

Wu X, Bayle JH, Olson D, Levine AJ (1993) The p53-mdm-2 autoregulatory feedback loop. *Genes Dev* **7:** 1126-1132

Zeng SX, Jin Y, Kuninger DT, Rotwein P, Lu H (2003) The acetylase activity of p300 is dispensable for MDM2 stabilization. *The Journal of biological chemistry* **278:** 7453-7458

Zhang Y, Lu H (2009) Signaling to p53: ribosomal proteins find their way. *Cancer Cell* **16:** 369-377

Zhang Y, Xiong Y, Yarbrough WG (1998) ARF promotes MDM2 degradation and stabilizes p53: ARF-INK4a locus deletion impairs both the Rb and p53 tumor suppression pathways. *Cell* **92:** 725-734

Goodwin KD, Lewis MA, Tanious FA, Tidwell RR, Wilson WD, Georgiadis MM, Long EC (2006) A high-throughput, high-resolution strategy for the study of site-selective DNA binding agents: analysis of a "highly twisted" benzimidazole-diamidine. *J Am Chem Soc* **128:** 7846-7854

He L, He X, Lim LP, de Stanchina E, Xuan Z, Liang Y, Xue W, Zender L, Magnus J, Ridzon D, Jackson AL, Linsley PS, Chen C, Lowe SW, Cleary MA, Hannon GJ (2007) A microRNA component of the p53 tumour suppressor network. *Nature* **447:** 1130-1134

Lain S, Hollick JJ, Campbell J, Staples OD, Higgins M, Aoubala M, McCarthy A, Appleyard V, Murray KE, Baker L, Thompson A, Mathers J, Holland SJ, Stark MJ, Pass G, Woods J, Lane DP, Westwood NJ (2008) Discovery, in vivo activity, and mechanism of action of a small-molecule p53 activator. *Cancer Cell* **13:** 454-463

Li M, Luo J, Brooks CL, Gu W (2002) Acetylation of p53 inhibits its ubiquitination by Mdm2. *J Biol Chem* **277:** 50607-50611

Riccardi C, Nicoletti I (2006) Analysis of apoptosis by propidium iodide staining and flow cytometry. *Nat Protoc* **1:** 1458-1461

Sun XX, Dai MS, Lu H (2007) 5-fluorouracil activation of p53 involves an MDM2-ribosomal protein interaction. *J Biol Chem* **282:** 8052-8059

Wei D, Tao R, Zhang Y, White MF, Dong XC (2010) Feedback regulation of hepatic gluconeogenesis through modulation of SHP/Nr0b2 gene expression by Sirt1 and FoxO1. *Am J Physiol Endocrinol Metab*

Zeng X, Chen L, Jost CA, Maya R, Keller D, Wang X, Kaelin WG, Jr., Oren M, Chen J, Lu H (1999) MDM2 suppresses p73 function without promoting p73 degradation. *Mol Cell Biol* **19:** 3257-3266

[00140] While the novel technology has been illustrated and described in detail in the figures and foregoing description, the same is to be considered as illustrative and not restrictive in character, it being understood that only the preferred embodiments have been shown and described and that all changes and modifications that come within the spirit of the novel technology are desired to be protected. As well, while the novel technology was illustrated using specific examples, theoretical arguments, accounts, and illustrations, these illustrations and the accompanying discussion should by no means be interpreted as limiting the technology. All patents, patent applications, and references to texts, scientific treatises, publications, and the like referenced in this application are incorporated herein by reference in their entirety.

CLAIMS

1. A method of treating abnormal cell growth, comprising the steps of:

contacting a cell with at least one compound, or a pharmaceutically acceptable salt thereof according to the formula:

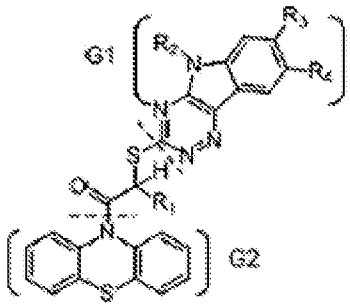

Compound A.

wherein: R_1 is –H, or $–CH_2CH_3$;

R_2 is -H, or $-CH_3$;

R_3 is H, or a halogen; and

R_4 is H or halogen.

2. The method according to claim 1, wherein:

R_1 $–CH_2CH_3$,

R_2 is H_5;

R_3 is H; and

R_4 is H.

3. The method according to claim 1, wherein the eukaryotic cell is a cancer cell.

4. The method according to claim 1, wherein the eukaryotic cell is a pre-cancerous cell.

5. The method according to claim 1, wherein the eukaryotic cell is a normal cell.

6. The method according to claim 1, wherein said contacting step occurs *in vitro*.

7. The method according to claim 1, wherein said contacting step occurs *in vivo*.

8. A method of modulating cellular activity, comprising the steps of:

contacting a deacylase with an effective amount of compound; or a pharmaceutally acceptable salt thereof of said compound, wherein said compound is:

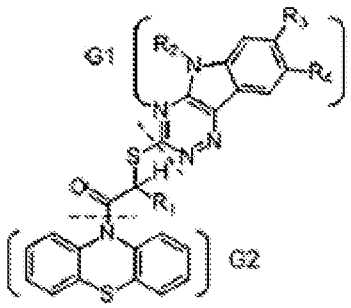

Compound A.

wherein: R_1 is –H, or $–CH_2CH_3$;

R_2 is -H, or $-CH_3$;

R_3 is H, or a halogen; and

R_4 is H or halogen.

10. The method according to claim 8, wherein the deacetylase is SIRT1.

11. The method according to claim 8, wherein the contacting step occurs in *vitro*.

12. The method according to claim 8, wherein the contacting step occurs in *vivo*.

13. The method according to claim 8, wherein the contacting step occurs in a tumor cell.

14. The method according to claim 8, wherein the contacting step occurs in an abnormal cell.

15. The method according to claim 14, wherein the abnormal cell is a cancer cell.

16. The method according to claim 8, wherein the contacting step occurs in a normal cell.

17. The method according to claim 8, wherein the cell is a mammalian cell.

18. A method of treating a patient, comprising the steps of:

administering a patient in need thereof, a therapeutically effective dose of at least one compound according to Compound A or a pharmaceutically acceptable salt thereof:

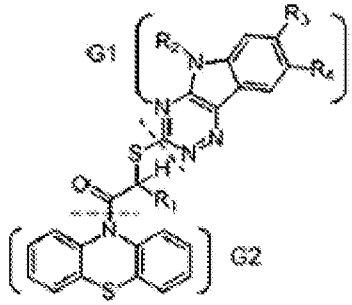

Compound A.

wherein: R_1 is –H, or $–CH_2CH_3$;

R_2 is -H, or $-CH_3$;

R_3 is -H, or a halogen; and

R_4 is -H or halogen.

19. The method according to claim 18, wherein:

R_1 is $–CH_2CH_3$,

R_2 is H;

R_3 is H; and

R_4 is H.

20. The method according to claim 18, wherein the patient is a mammal.

21. The method according to claim 18, wherein the patient is a human being.

22. The method according to claim 18, wherein the therapeutically effective dose is about 30 mg kg^{-1} of the mammals' body weight.

23. The method according to claim 18, wherein the patient is diagnosed with cancer.

24. The method according to claim 18, wherein the patient is diagnosed with breast cancer.

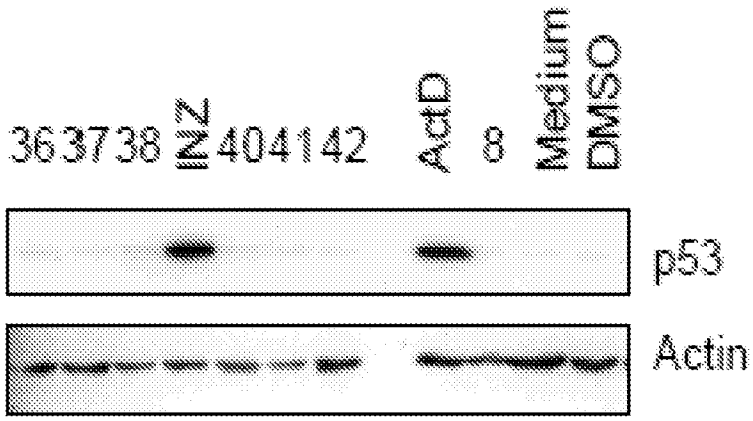

FIG.1A

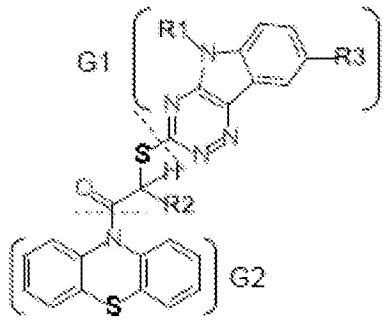

Inauhzin (INZ)

ID	R1	R2	R3
INZ	H	C_2H_5	H
INZ1	CH_3	C_2H_5	H
INZ2	H	H	F
INZ3	H	H	H
INZ4	CH_3	H	H
INZ5	CH_3	C_2H_5	Br

FIG.1B

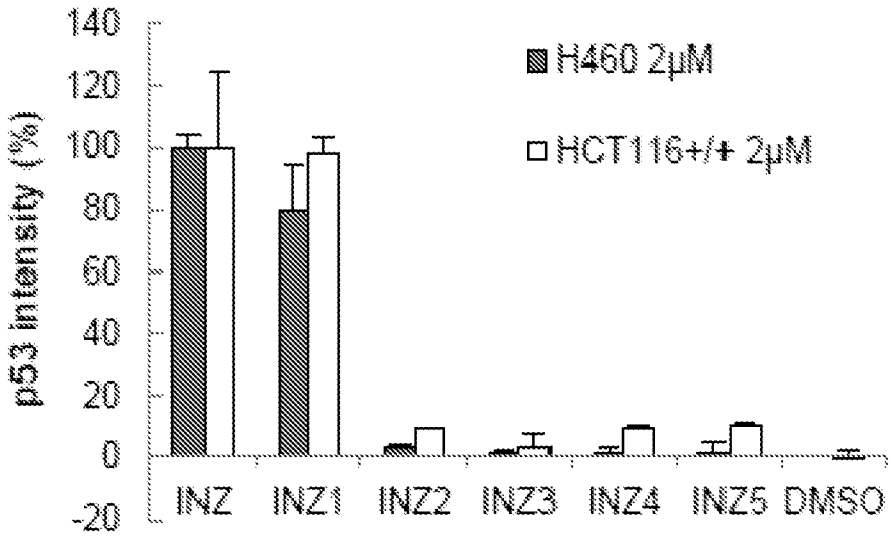
140
120
100
80
60
40
20
0
-20
p53 intensity (%)
H460 2μM
HCT116+/+ 2μM
INZ
INZ1
INZ2
INZ3
INZ4
INZ5
DMSO

FIG.1C

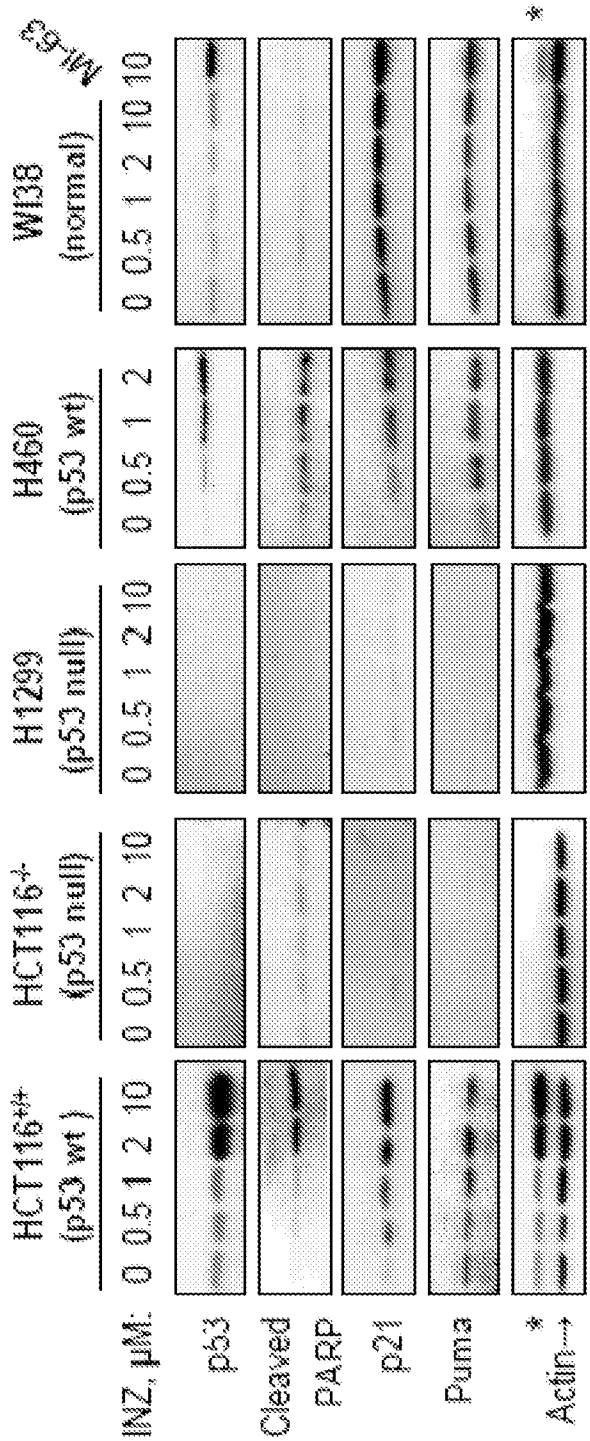
HCT116+/+ (p53 wt)
HCT116-/- (p53 null)
H1299 (p53 null)
H460 (p53 wt)
WI38 (normal)
INZ, μM: 0 0.5 1 2 10 0 0.5 1 2 10 0 0.5 1 2 10 0 0.5 1 2 0 0.5 1 2 10 10
MW-kD
p53
Cleaved PARP
p21
Puma
* Actin→

FIG.1D

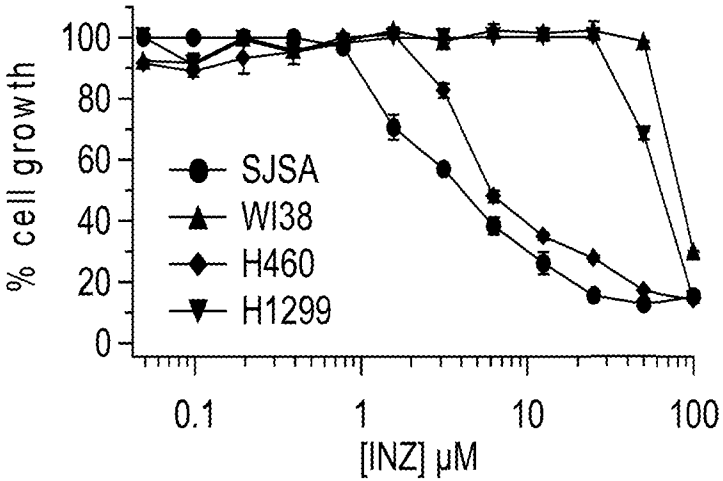

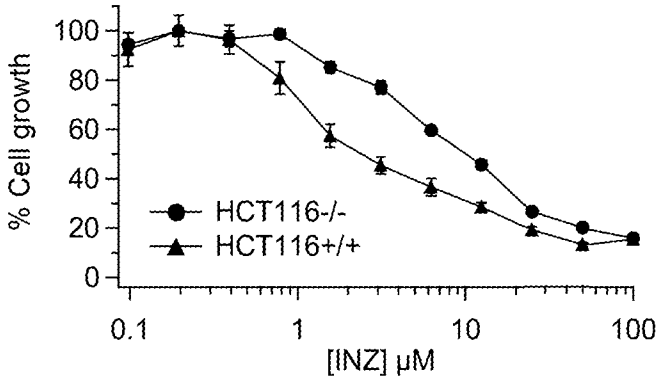

Cell line	IC_{50} (µM)
H460	9.2
H1299	60
SJSA	2.1
WI38	> 100
HT29	>100
$HCT116^{+/+}$	1.9
$HCT116^{-/-}$	15.9

FIG. 1E

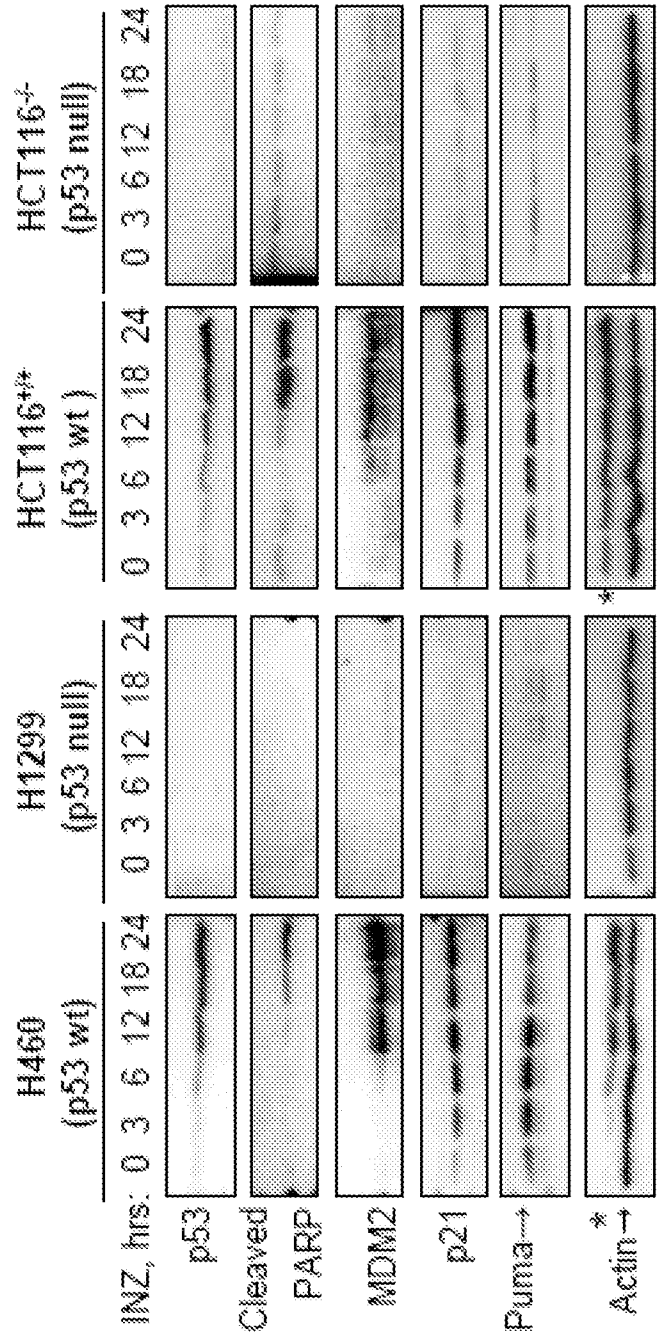
H460 (p53 wt)
H1299 (p53 null)
HCT116+/+ (p53 wt)
HCT116-/- (p53 null)
INZ, hrs: 0 3 6 12 18 24
0 3 6 12 18 24
0 3 6 12 18 24
0 3 6 12 18 24
p53
Cleaved PARP
MDM2
p21
Puma→
Actin→
*
*

FIG.2A

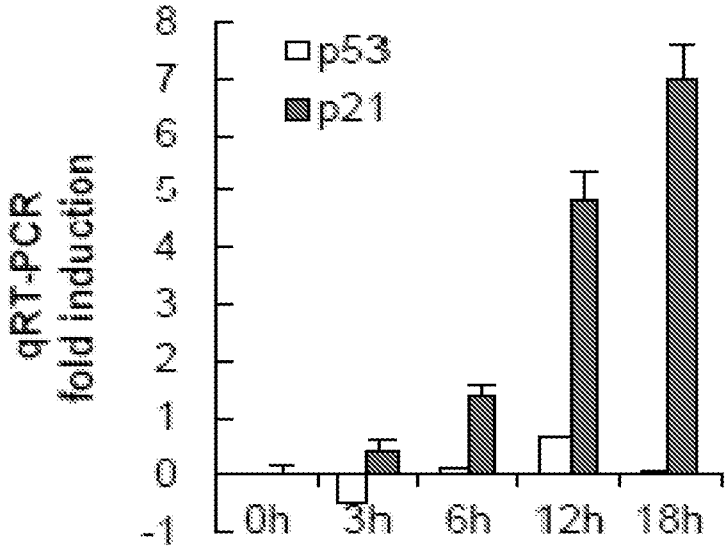
qRT-PCR
fold induction
8
7
6
5
4
3
2
1
0
-1
p53
p21
0h
3h
6h
12h
18h

FIG.2B

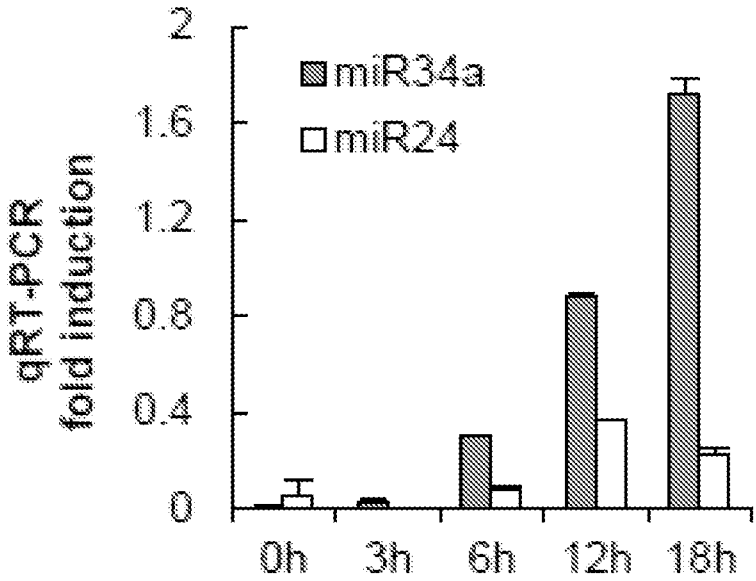
qRT-PCR
fold induction
2
1.6
1.2
0.8
0.4
0
miR34a
miR24
0h
3h
6h
12h
18h

FIG.2C

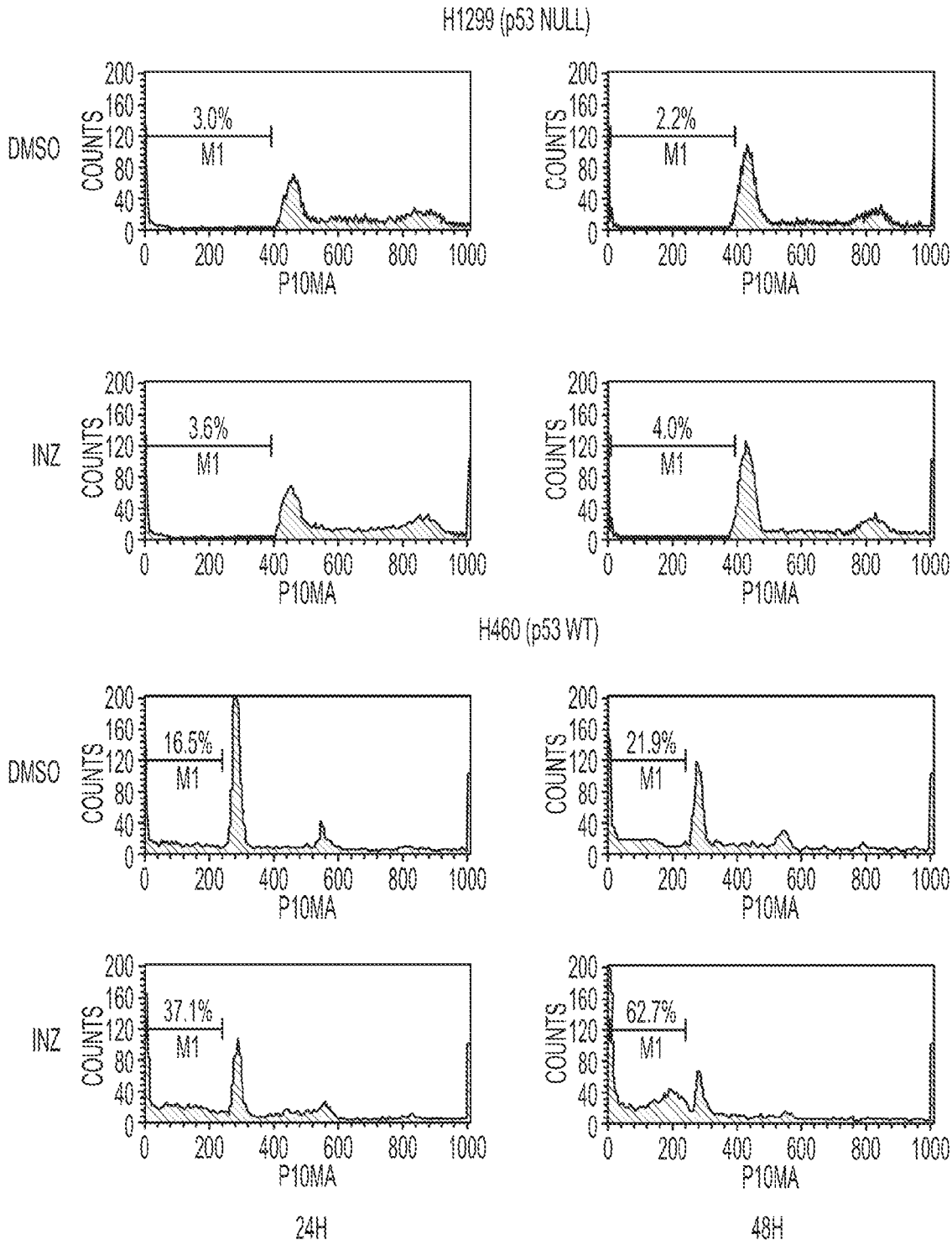
H1299 (p53 NULL)
DMSO
INZ
COUNTS
P10MA
M1
3.0%
2.2%
3.6%
4.0%
H460 (p53 WT)
16.5%
21.9%
37.1%
62.7%
0
40
80
120
160
200
400
600
800
1000
24H
48H

FIG. 2D

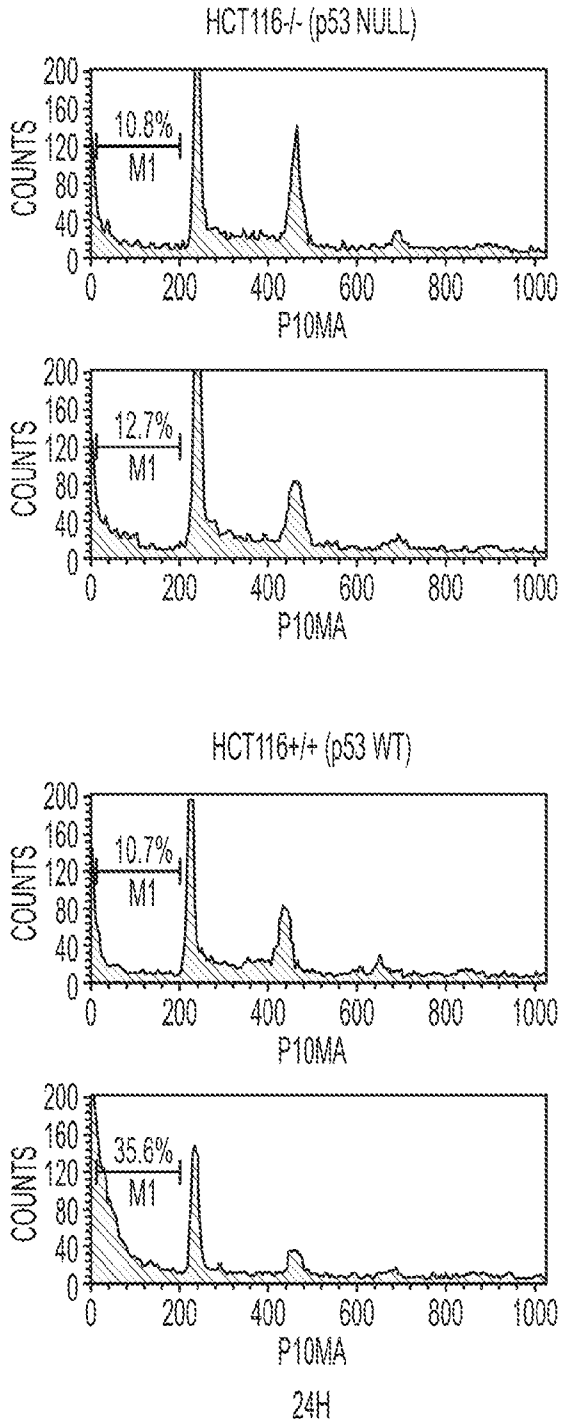

FIG. 2D
CONTINUED

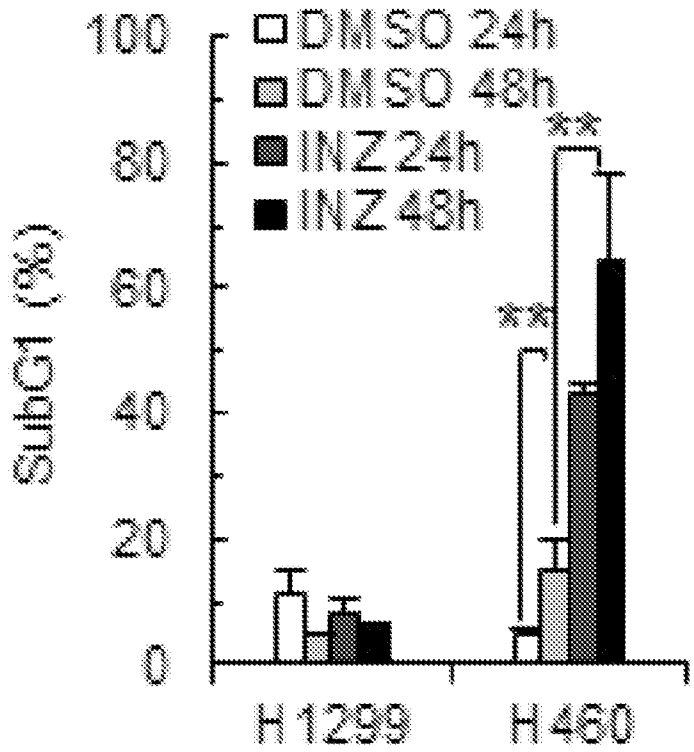
100
80
60
40
20
0
SubG1 (%)
DMSO 24h
DMSO 48h
INZ 24h
INZ 48h
**
**
H1299
H460

FIG.2E

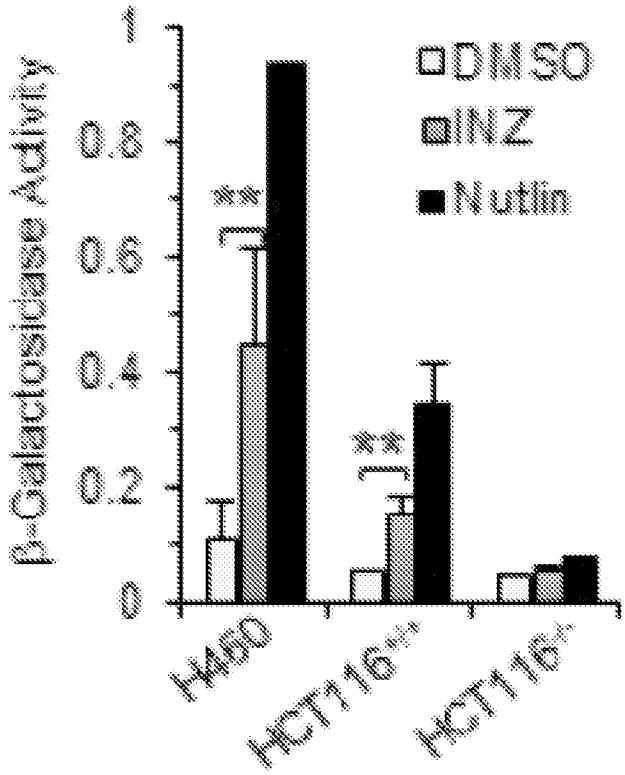
β-Galactosicase Activity
0
0.2
0.4
0.6
0.8
1
DMSO
INZ
Nutlin
**
**
H460
HCT116+/+
HCT116-/-

FIG.2F

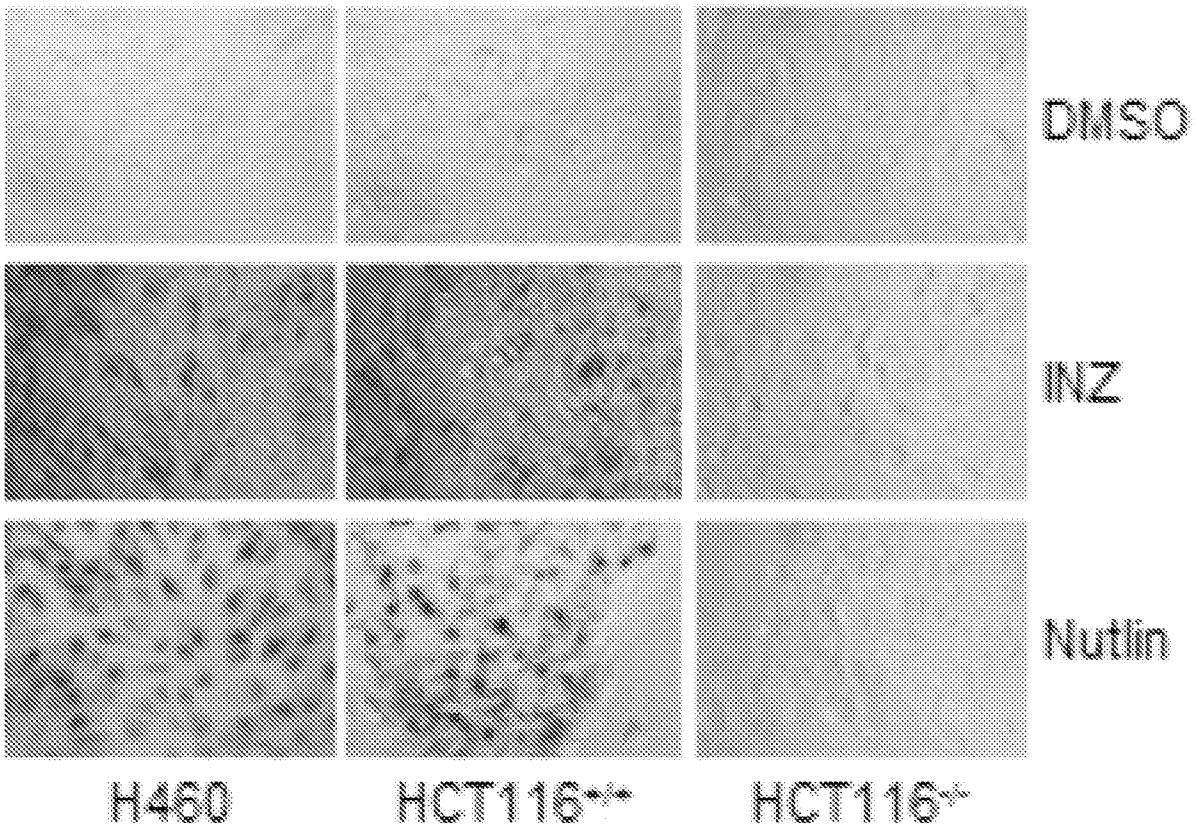

FIG.2G

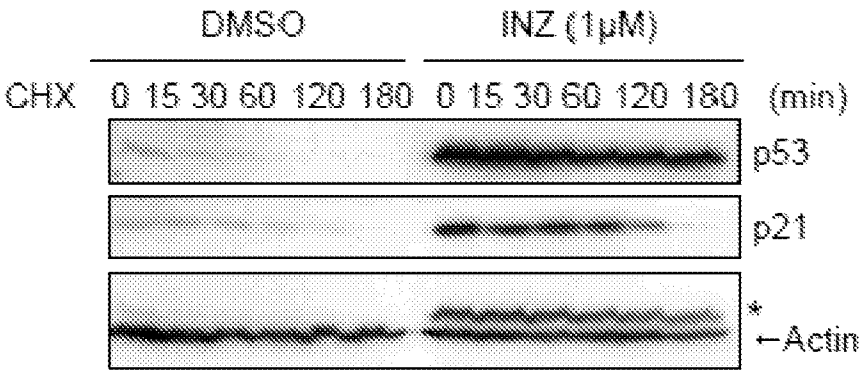
DMSO
INZ (1μM)
CHX 0 15 30 60 120 180 0 15 30 60 120 180 (min)
p53
p21
*
←Actin

FIG.3A

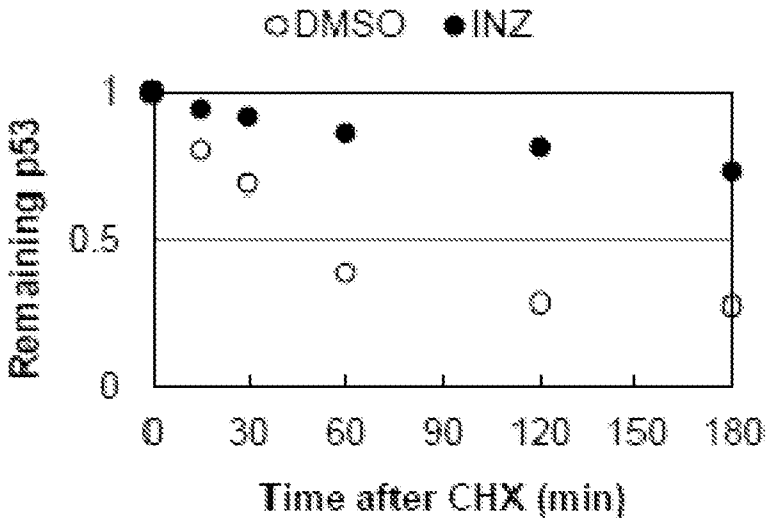
○DMSO ●INZ
Remaining p53
1
0.5
0
0 30 60 90 120 150 180
Time after CHX (min)

FIG.3B

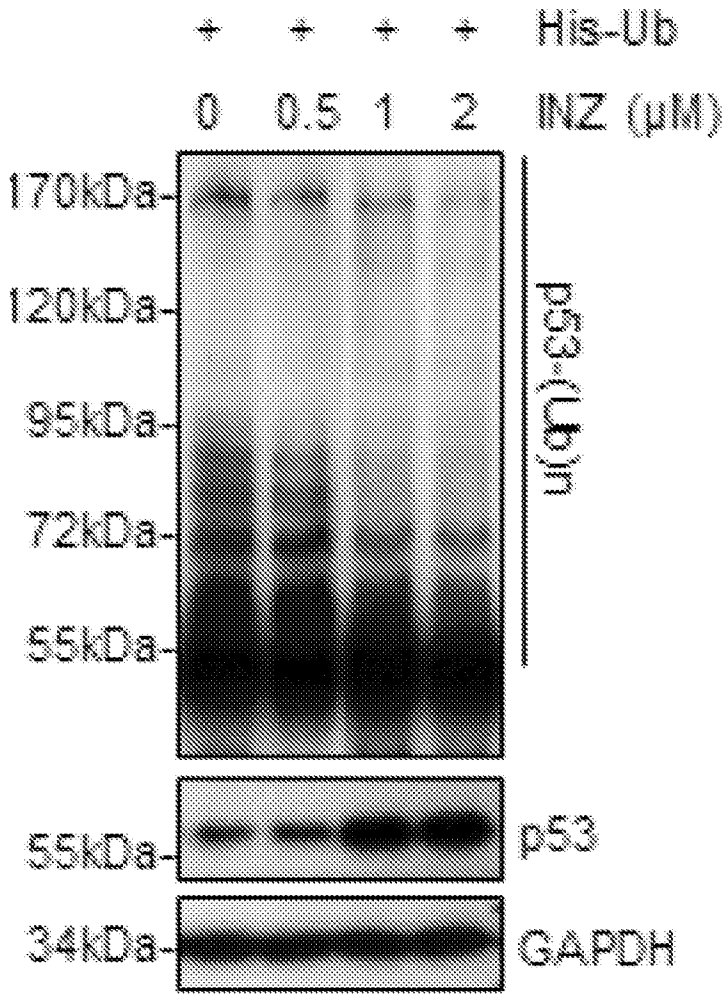
+ + + + His-Ub
0 0.5 1 2 INZ (μM)
170kDa-
120kDa-
95kDa-
72kDa-
55kDa-
p53-(Ub)n
55kDa-
p53
34kDa-
GAPDH

FIG.3C

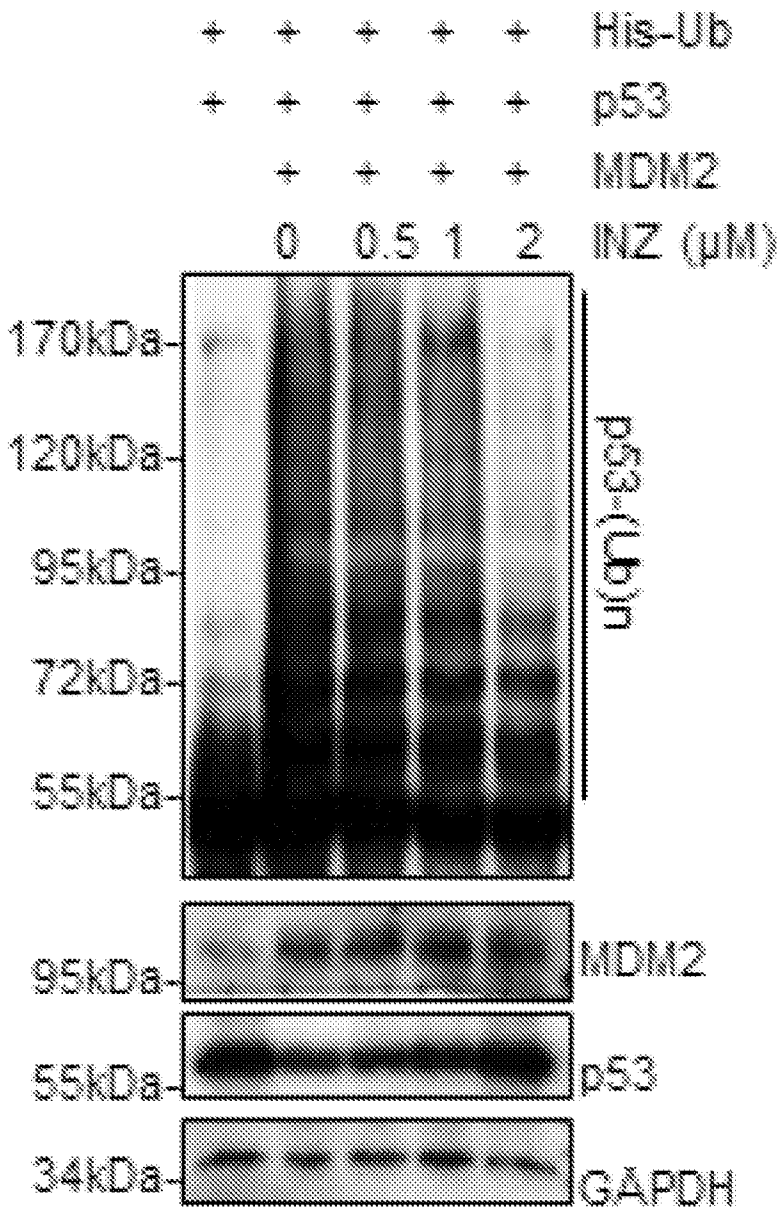
+ + + + + His-Ub
+ + + + + p53
+ + + + MDM2
0 0.5 1 2 INZ (μM)
170kDa
120kDa
95kDa
72kDa
55kDa
p53-Ub(n)
95kDa
MDM2
55kDa
p53
34kDa
GAPDH

FIG.3D

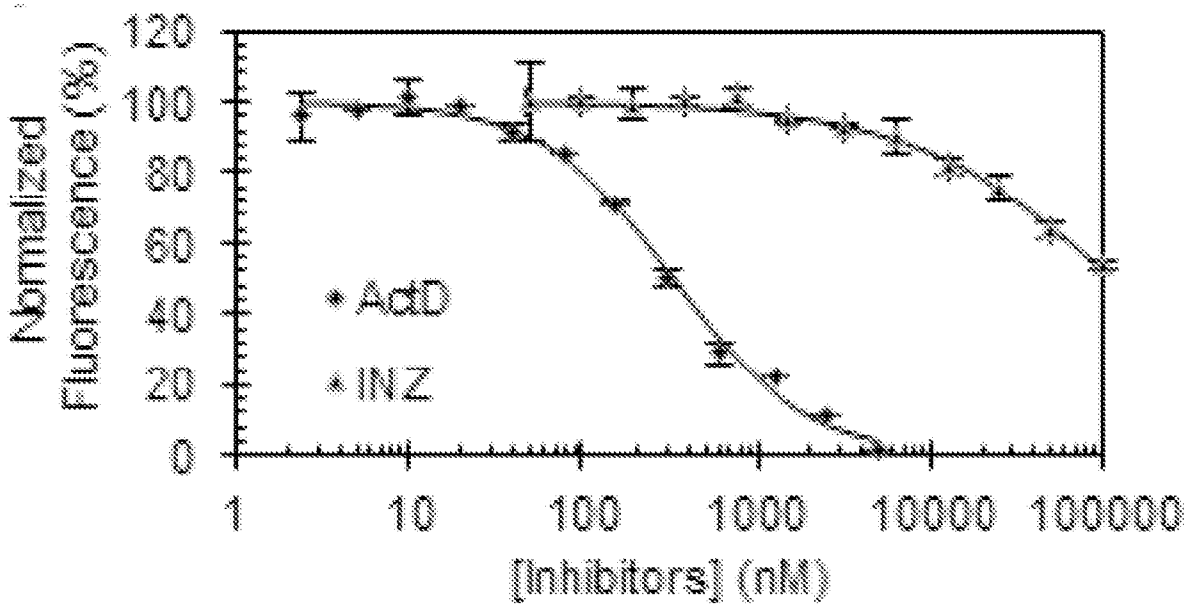
Normalized Fluorescence (%)
120
100
80
60
40
20
0
AcD
INZ
1
10
100
1000
10000
100000
[Inhibitors] (nM)

FIG.4A

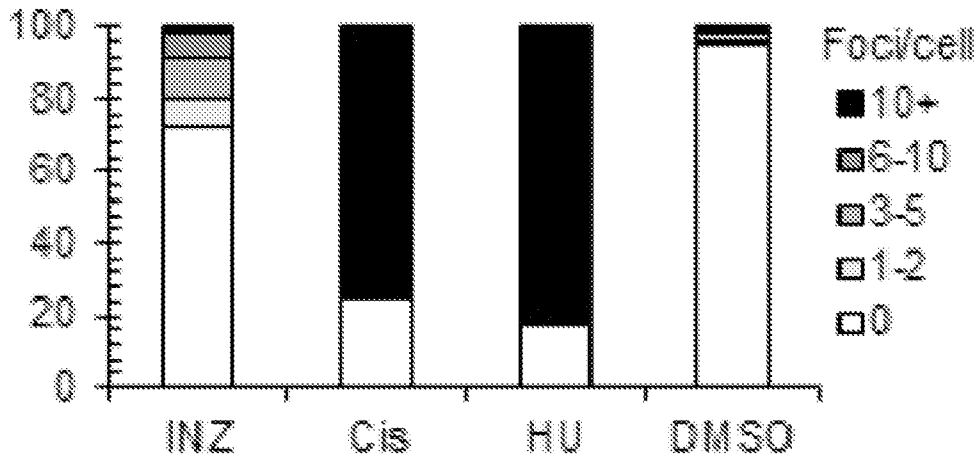
100
80
60
40
20
0
INZ
Cis
HU
DMSO
Foci/cell
10+
6-10
3-5
1-2
0

FIG.4B

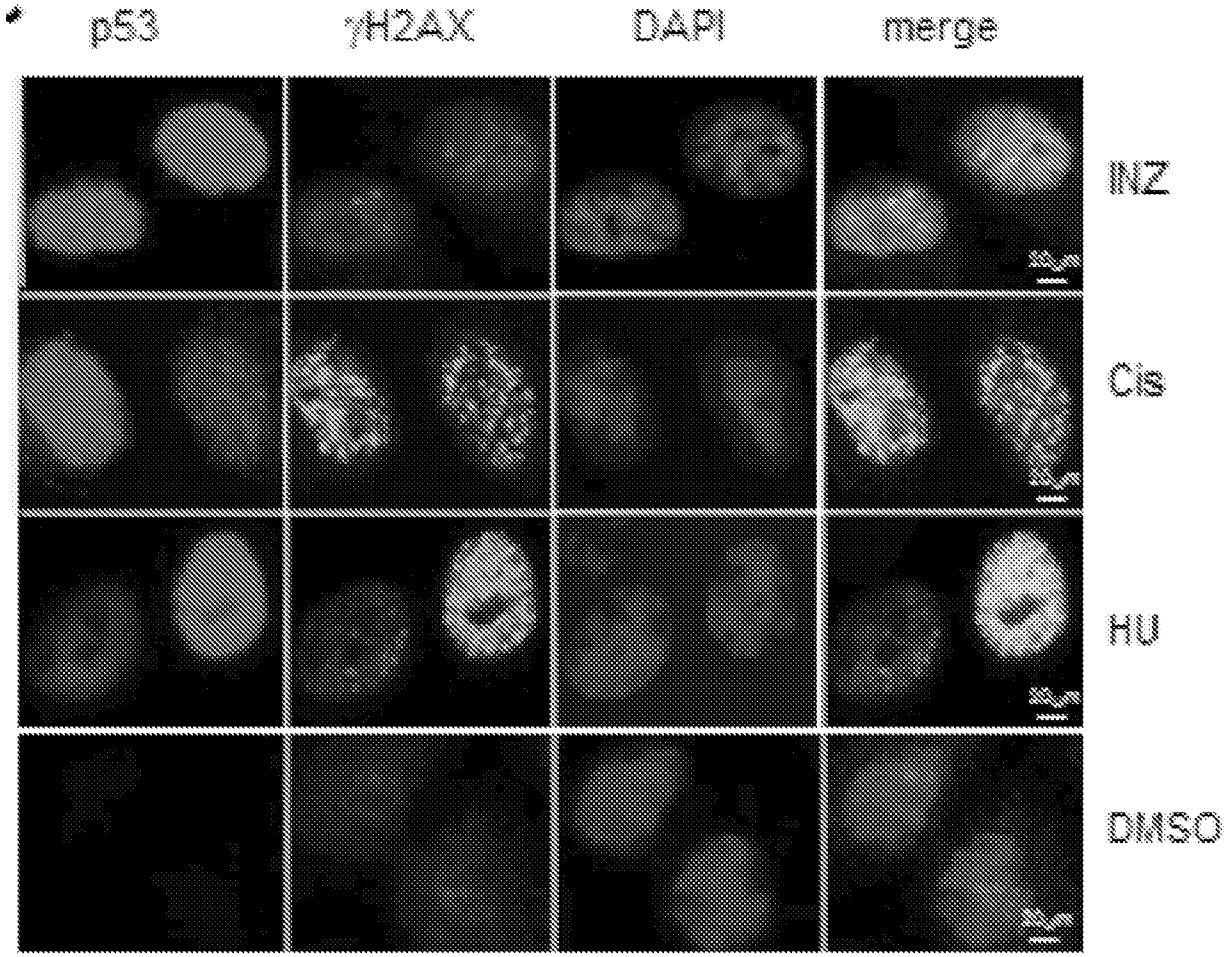

FIG.4C

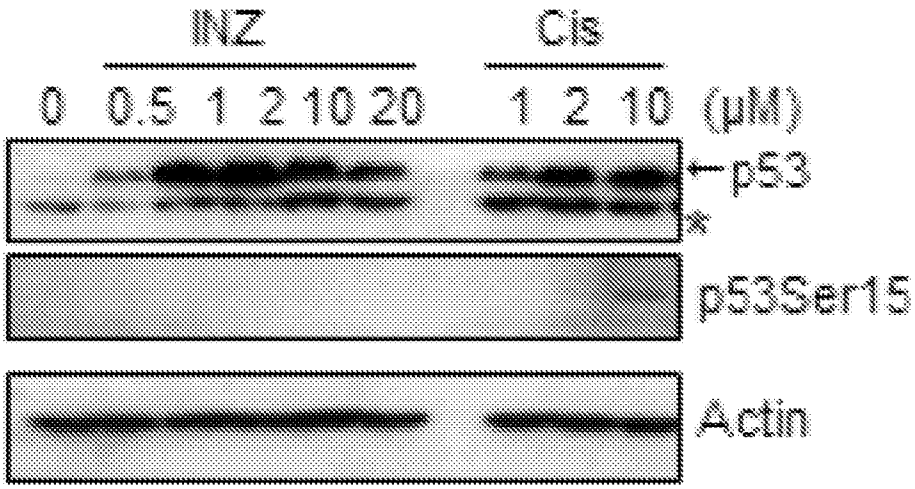
INZ
Cis
0 0.5 1 2 10 20 1 2 10 (μM)
p53
*
p53Ser15
Actin

FIG.4D

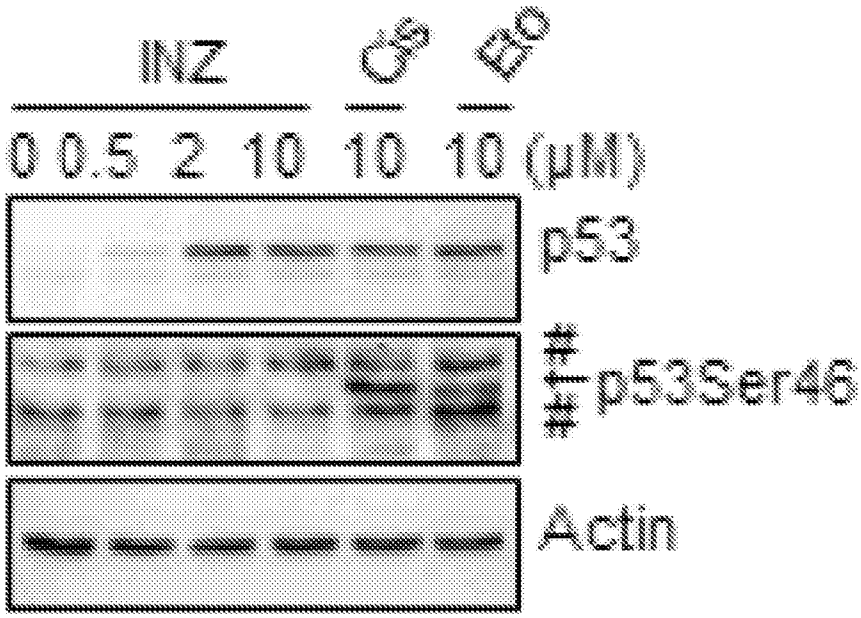
INZ
0 0.5 2 10 10 10 (μM)
p53
##
p53Ser46
Actin

FIG.4E

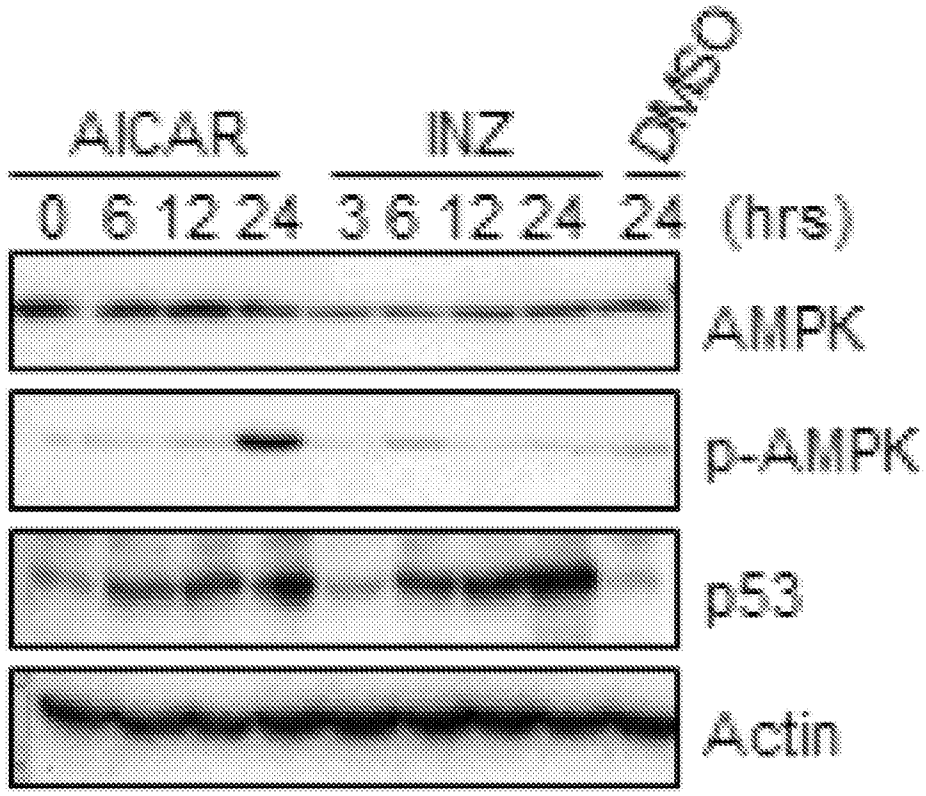

FIG.4F

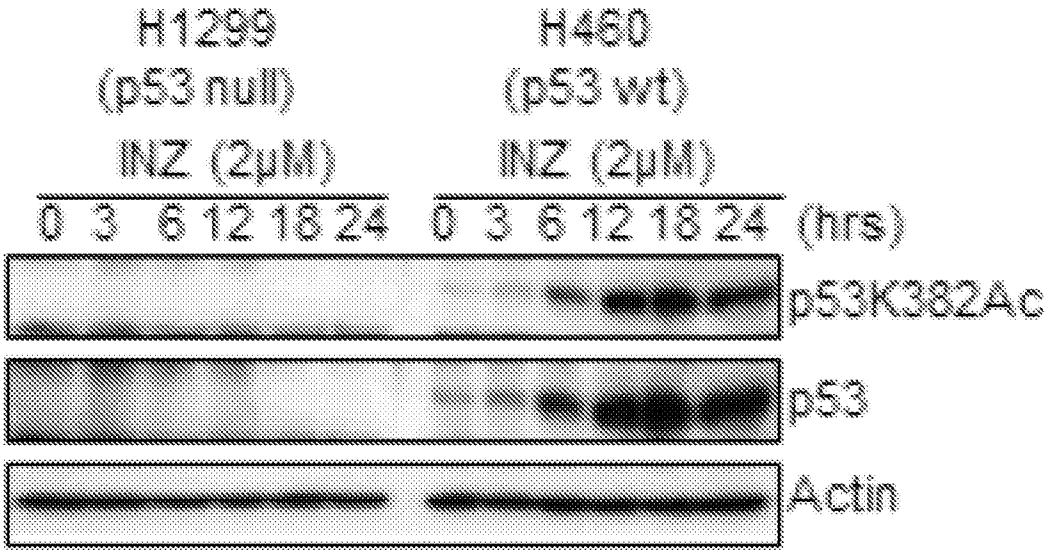
H1299
(p53 null)
INZ (2μM)
0 3 6 12 18 24
H460
(p53 wt)
INZ (2μM)
0 3 6 12 18 24 (hrs)
p53K382Ac
p53
Actin

FIG.5A

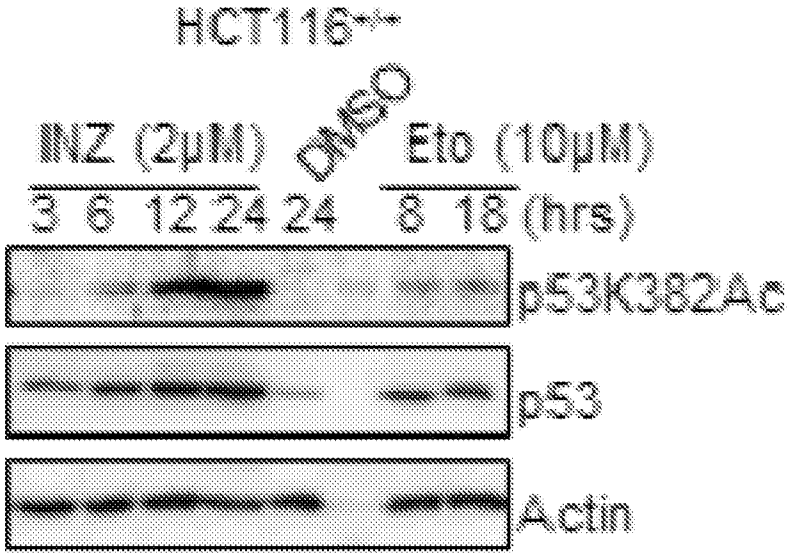
HCT116+/+
INZ (2μM)
DMSO
Eto (10μM)
3 6 12 24 24 8 18 (hrs)
p53K382Ac
p53
Actin

FIG.5B


H460
INZ
Eto
0 1 2 10 10 (μM)
MDM2
p53K382Ac
p53
Actin

FIG.5C

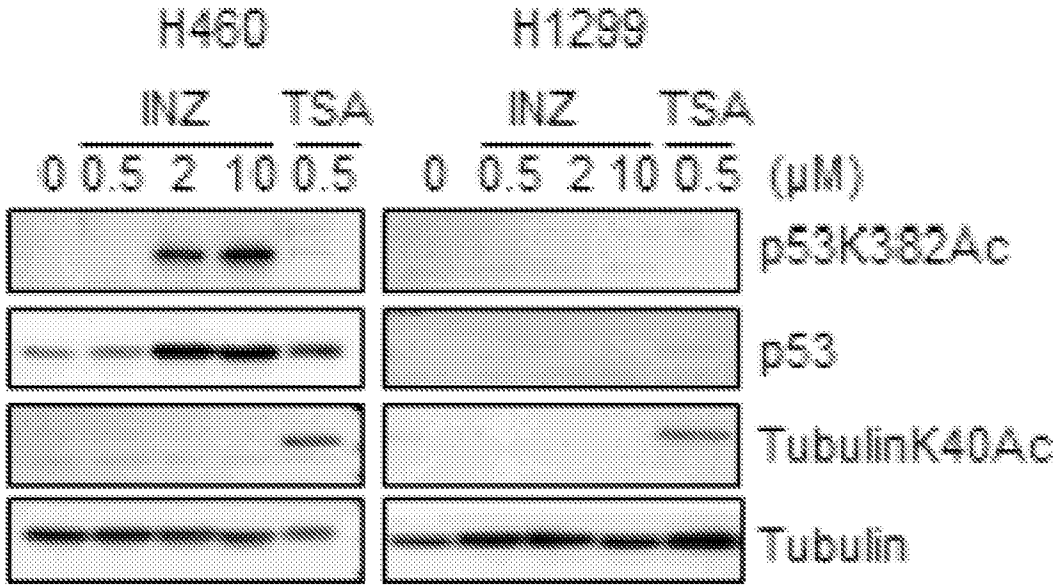
H460
H1299
INZ
TSA
INZ
TSA
0 0.5 2 10 0.5 0 0.5 2 10 0.5 (μM)
p53K382Ac
p53
TubulinK40Ac
Tubulin

FIG.5D

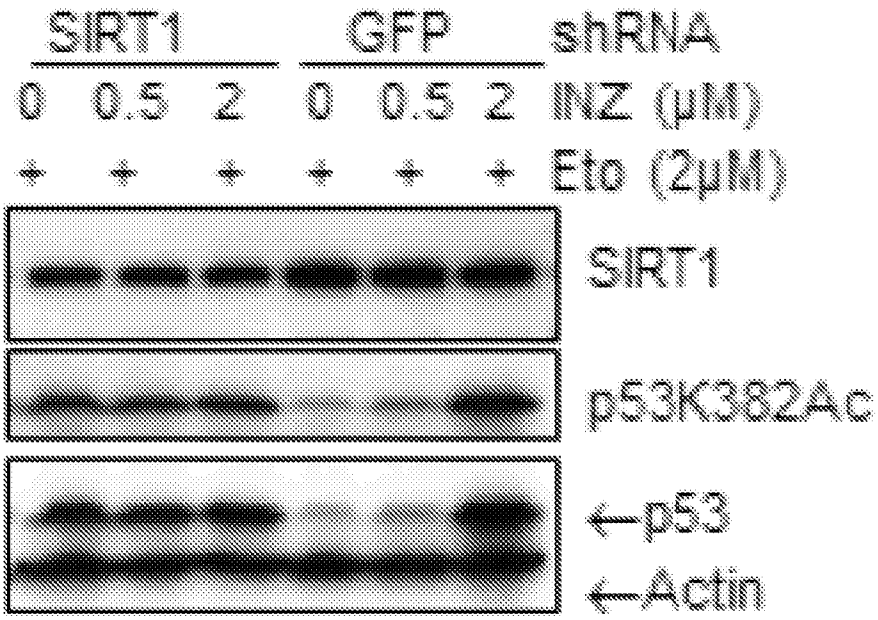
SIRT1
GFP
shRNA
0 0.5 2 0 0.5 2
INZ (μM)
+ + + + + +
Eto (2μM)
SIRT1
p53K382Ac
←p53
←Actin

FIG.5E

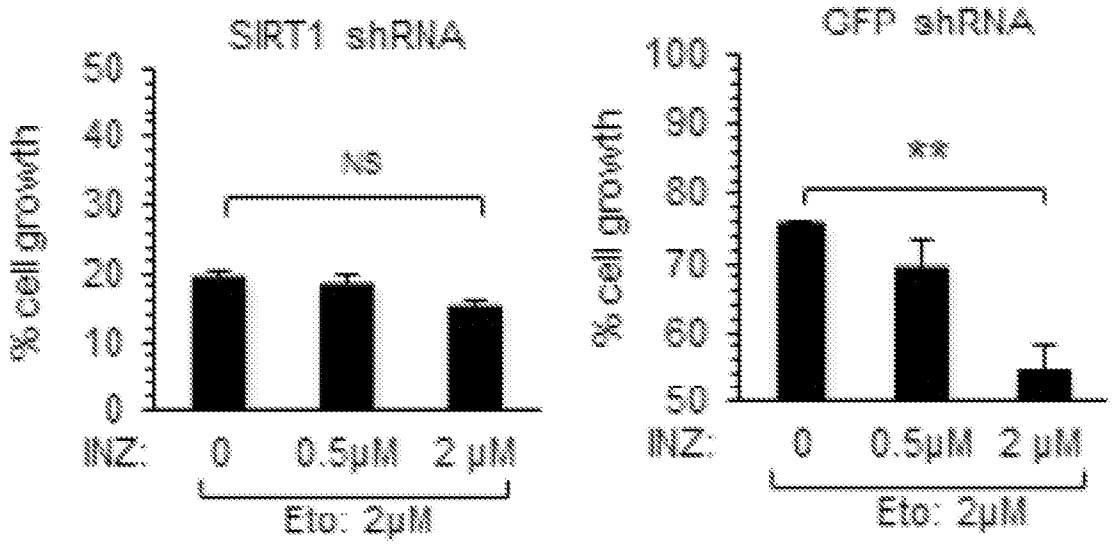
SIRT1 shRNA
% cell growth
50
40
30
20
10
0
NS
INZ: 0 0.5μM 2 μM
Eto: 2μM
GFP shRNA
100
90
80
70
60
50
**
INZ: 0 0.5μM 2 μM
Eto: 2μM

FIG.5F

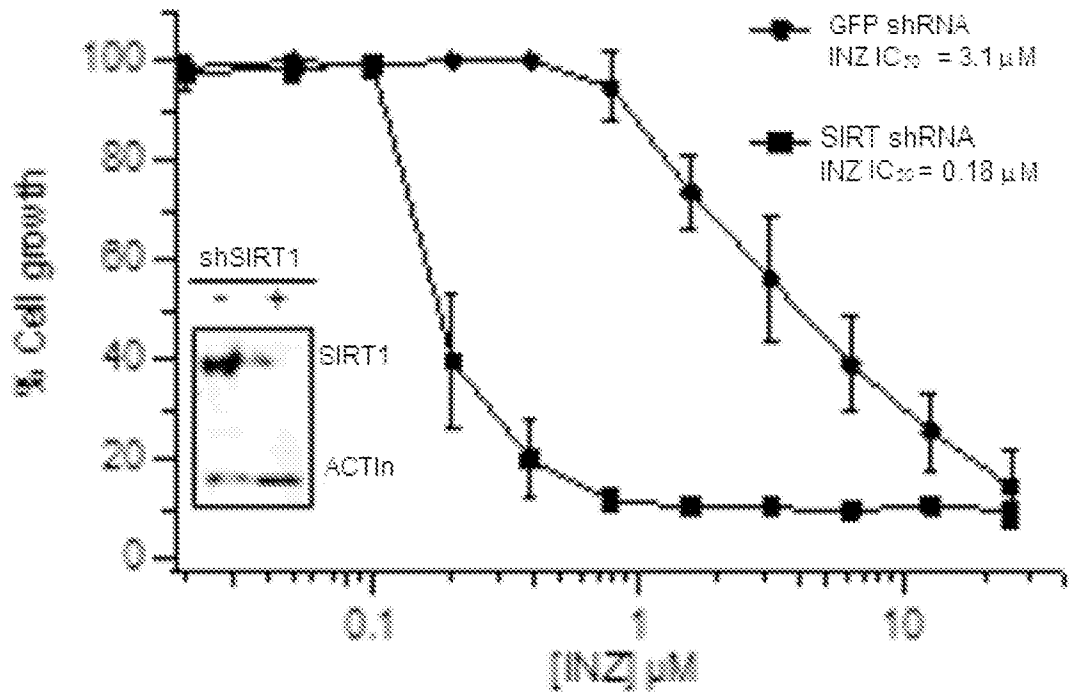
% Cell growth
100
80
60
40
20
0
shSIRT1
-
+
SIRT1
ACTIn
0.1
1
10
[INZ] μM
GFP shRNA
INZ IC50 = 3.1 μM
SIRT shRNA
INZ IC50 = 0.18 μM

FIG.5G

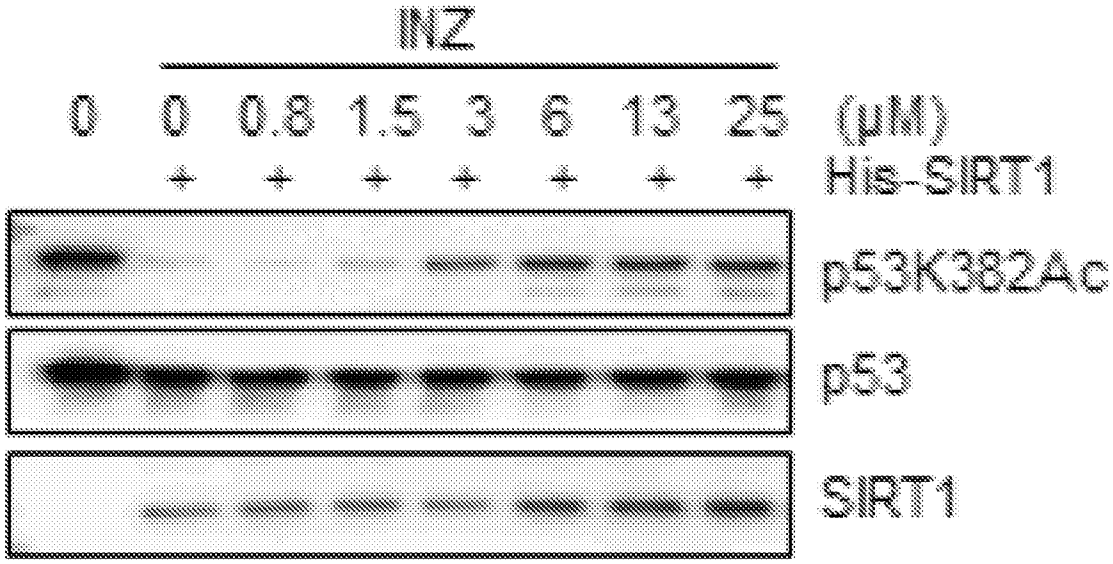
INZ
0 0 0.8 1.5 3 6 13 25 (μM)
+ + + + + + + His-SIRT1
p53K382Ac
p53
SIRT1

FIG.6A

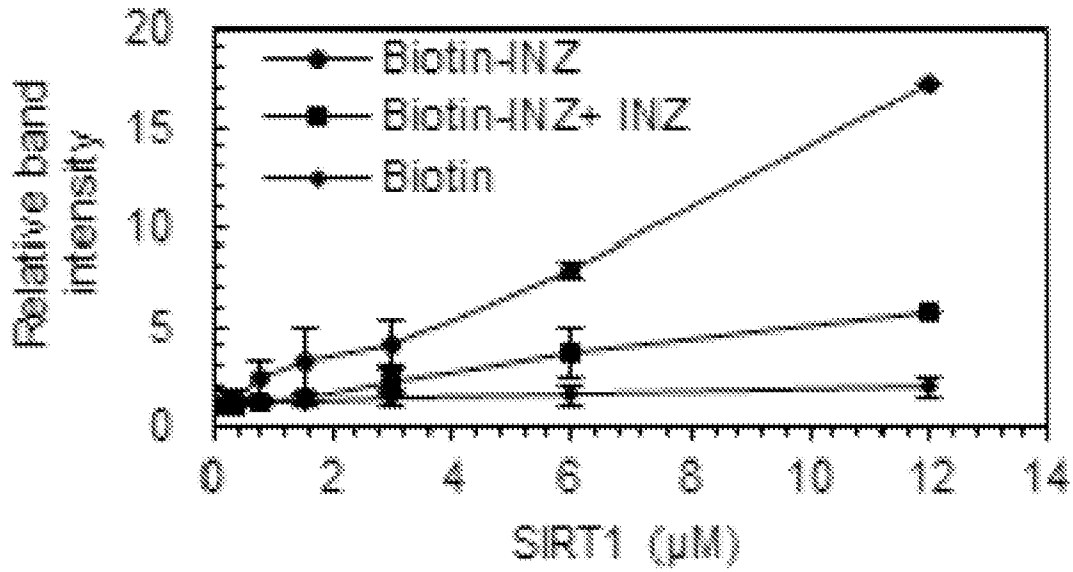
Relative band intensity
20
15
10
5
0
Biotin-INZ
Biotin-INZ+ INZ
Biotin
0 2 4 6 8 10 12 14
SIRT1 (μM)

FIG.6B

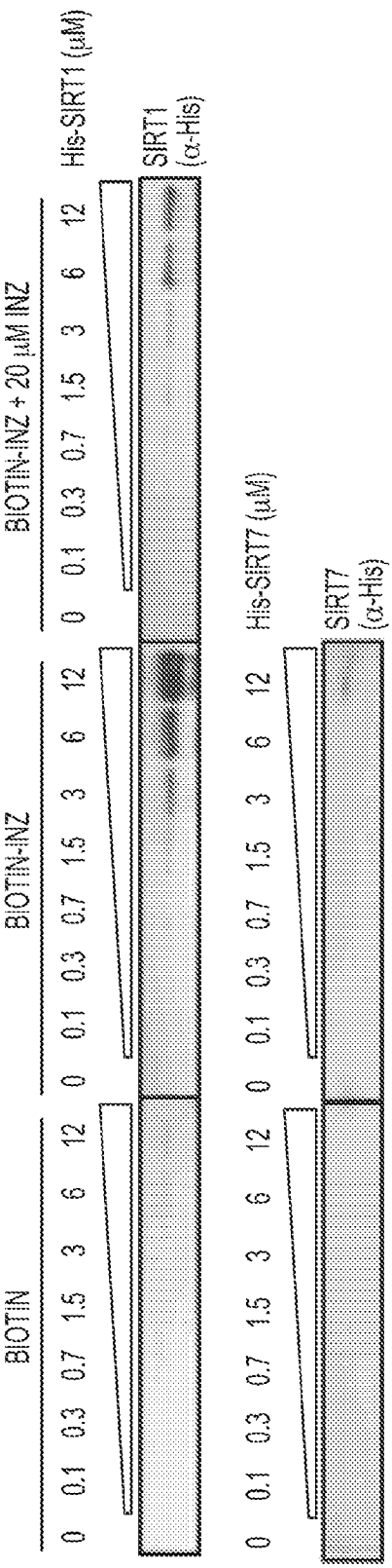
BIOTIN
0 0.1 0.3 0.7 1.5 3 6 12
BIOTIN-INZ
0 0.1 0.3 0.7 1.5 3 6 12
BIOTIN-INZ + 20 µM INZ
0 0.1 0.3 0.7 1.5 3 6 12
His-SIRT1 (µM)
SIRT1 (α-His)
His-SIRT7 (µM)
0 0.1 0.3 0.7 1.5 3 6 12
SIRT7 (α-His)

FIG. 6C

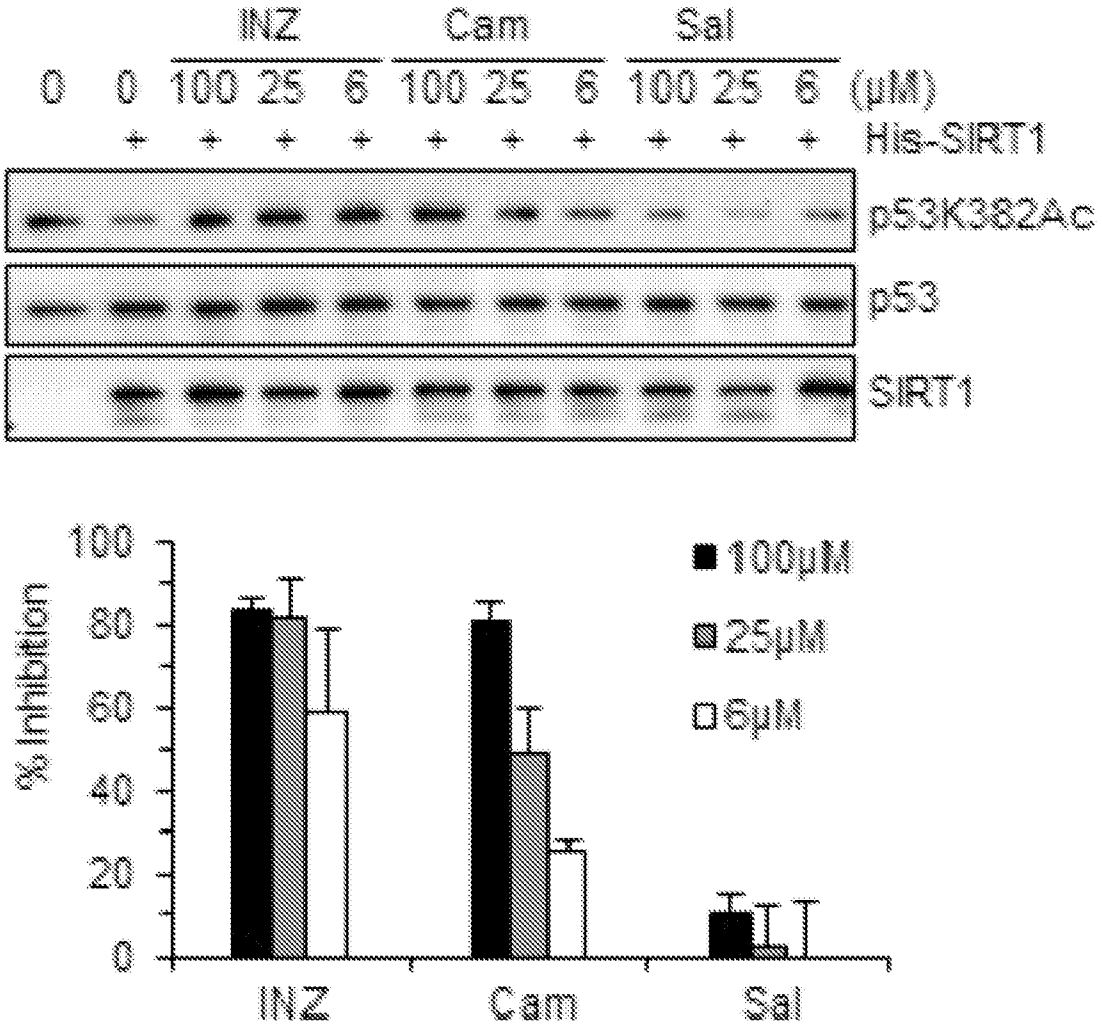
INZ
Cam
Sal
0 0 100 25 6 100 25 6 100 25 6 (μM)
+ + + + + + + + + + His-SIRT1
p53K382Ac
p53
SIRT1
% Inhibition
100
80
60
40
20
0
100μM
25μM
6μM
INZ
Cam
Sal

FIG.6D

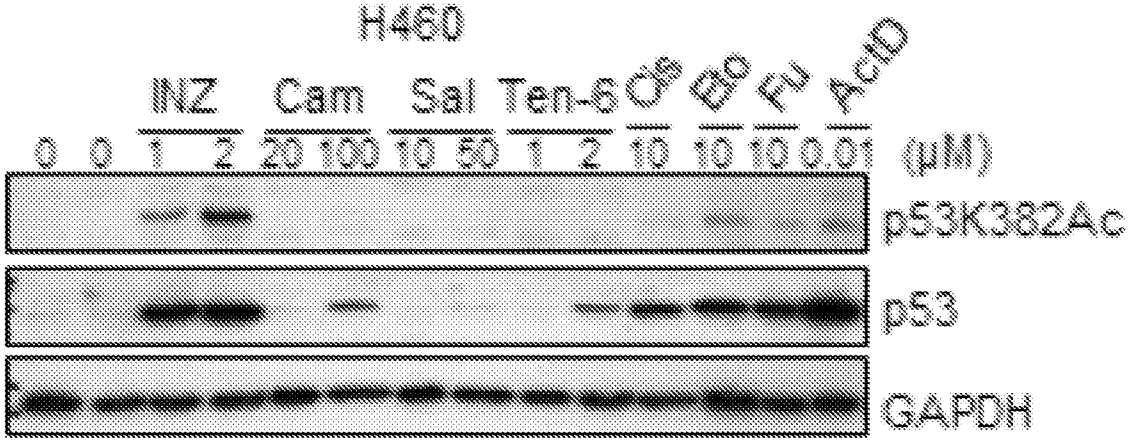
H460
INZ
Cam
Sal
Ten-6
0 0 1 2 20 100 10 50 1 2 10 10 10 0.01 (μM)
p53K382Ac
p53
GAPDH

FIG.6E

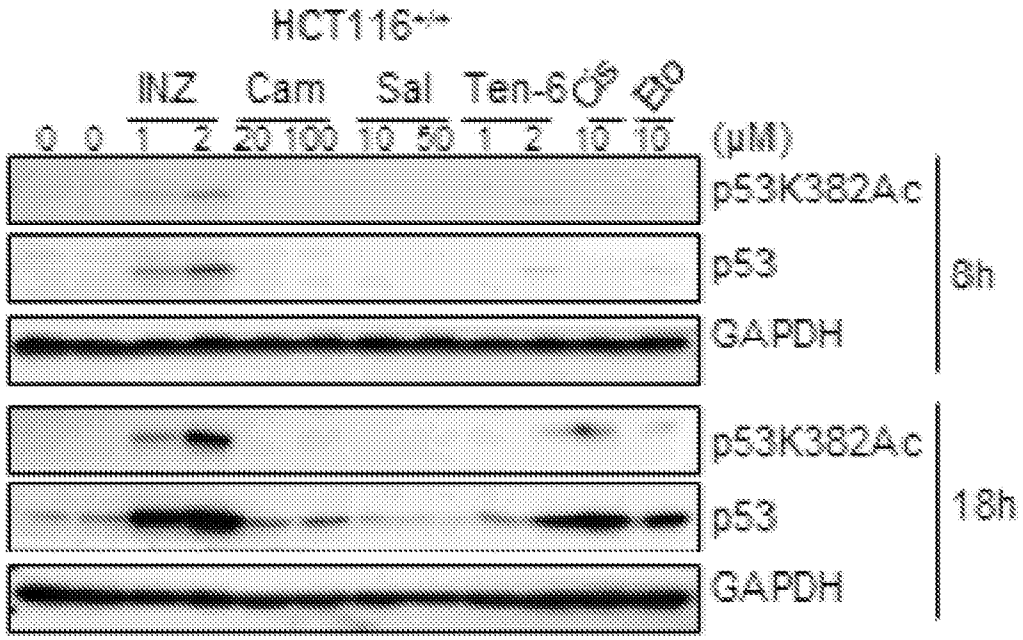
HCT116
INZ
Cam
Sal
Ten-6
0 0 1 2 20 100 10 50 1 2 10 10 (μM)
p53K382Ac
p53
GAPDH
8h
p53K382Ac
p53
GAPDH
18h

FIG.6F

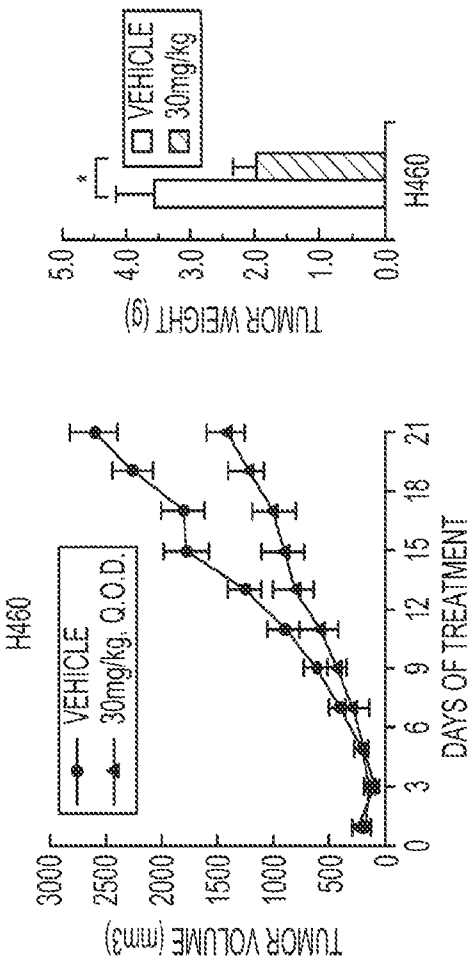
H460
VEHICLE
30mg/kg, Q.O.D.
TUMOR VOLUME (mm3)
3000
2500
2000
1500
1000
500
0
0 3 6 9 12 15 18 21
DAYS OF TREATMENT
TUMOR WEIGHT (g)
5.0
4.0
3.0
2.0
1.0
0.0
*
VEHICLE
30mg/kg
H460

FIG. 7A

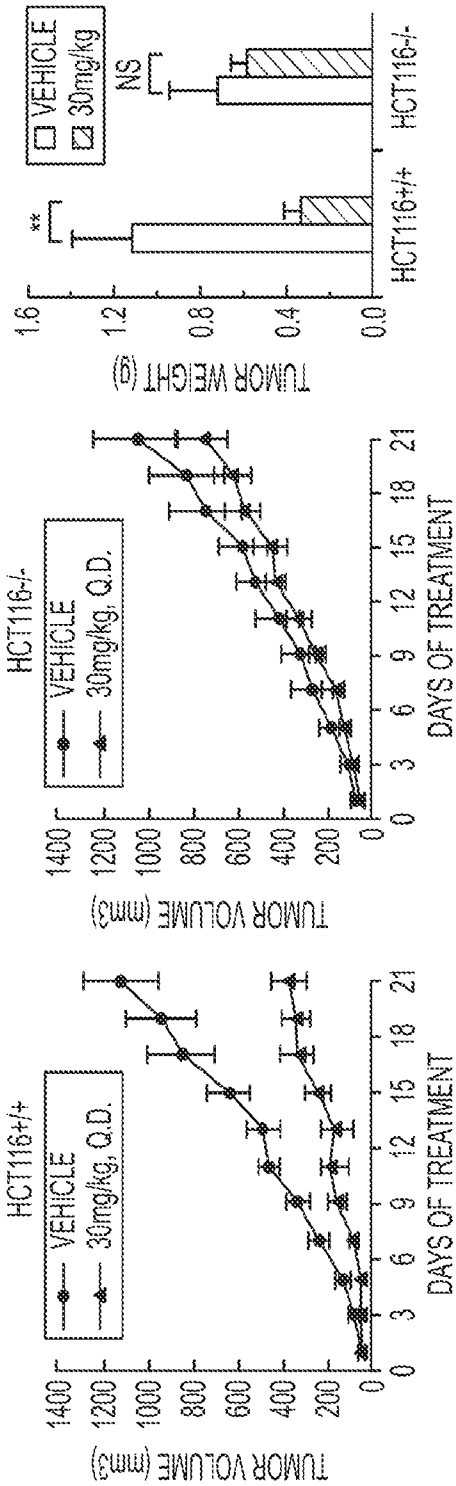
HCT116+/+
VEHICLE
30mg/kg, Q.D.
HCT116-/-
VEHICLE
30mg/kg, Q.D.
TUMOR VOLUME (mm3)
1400
1200
1000
800
600
400
200
0
0 3 6 9 12 15 18 21
DAYS OF TREATMENT
TUMOR WEIGHT (g)
1.6
1.2
0.8
0.4
0.0
**
NS
VEHICLE
30mg/kg
HCT116+/+
HCT116-/-

FIG. 7B

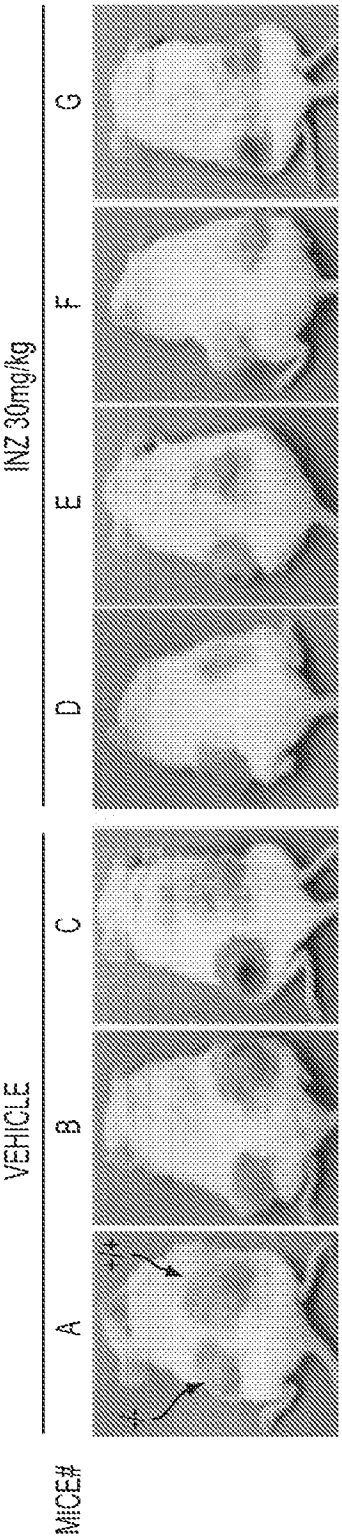
MICE#
VEHICLE
INZ 30mg/kg
A
B
C
D
E
F
G

FIG. 7C

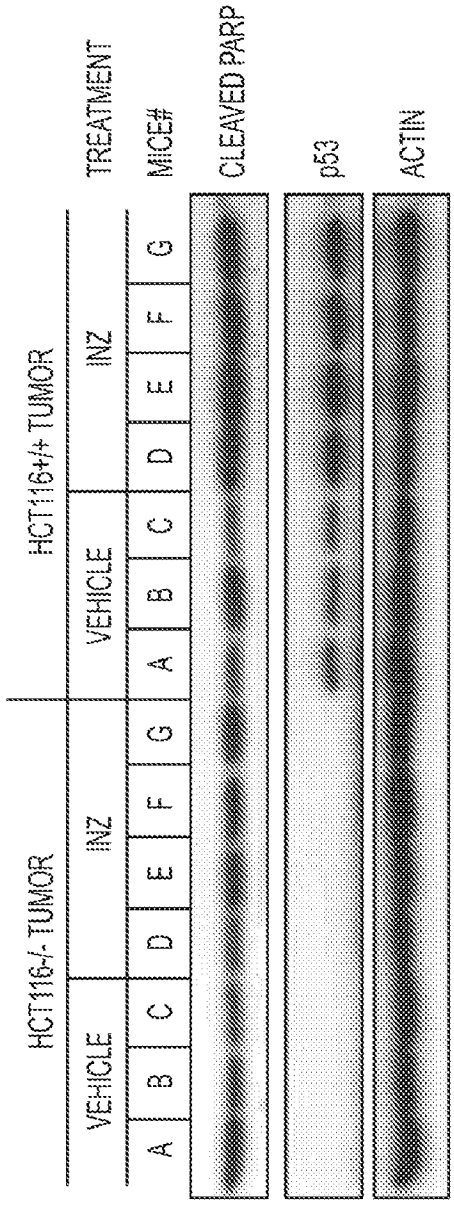
HCT116-/- TUMOR
HCT116+/+ TUMOR
TREATMENT
VEHICLE
INZ
VEHICLE
INZ
MICE#
A B C D E F G A B C D E F G
CLEAVED PARP
p53
ACTIN

FIG. 7D

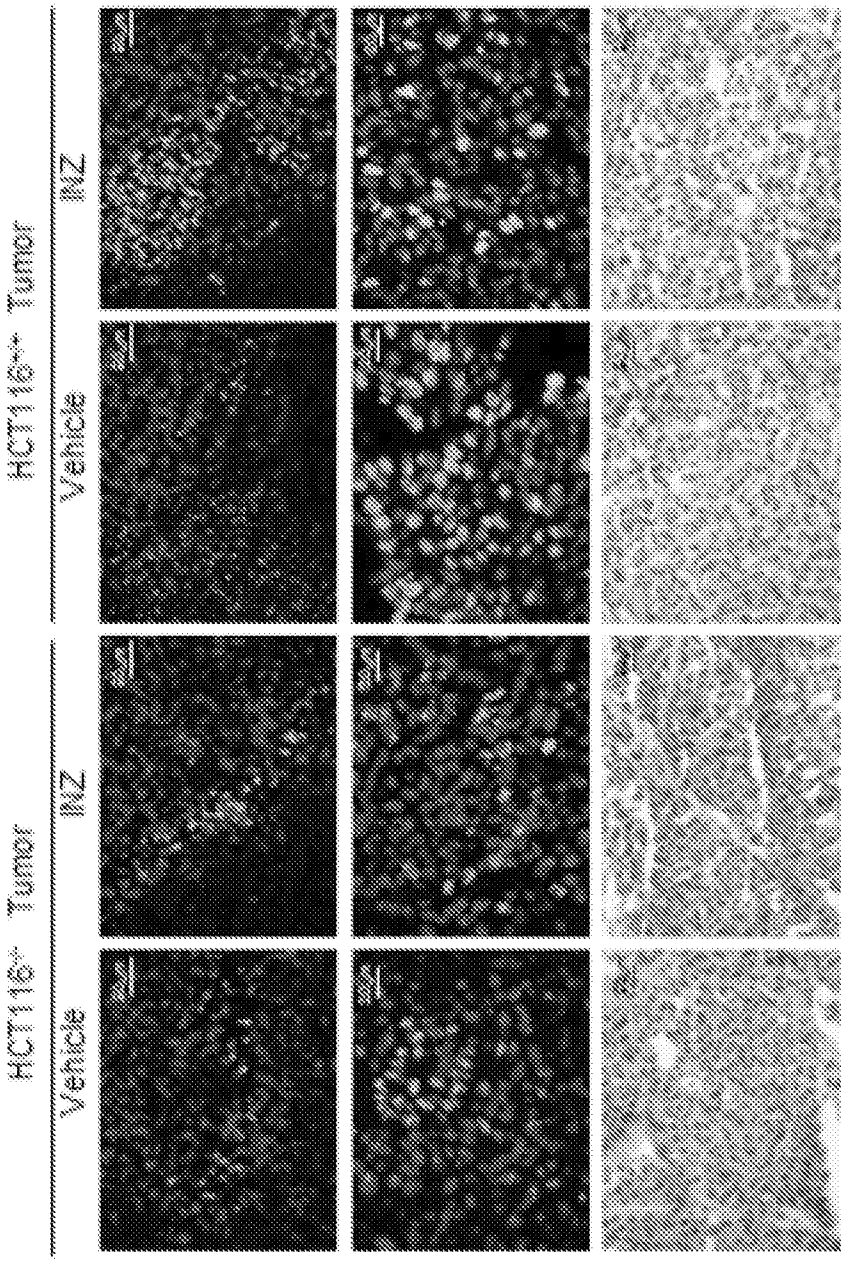
HCT116-/- Tumor
Vehicle
IRIZ
HCT116+/+ Tumor
Vehicle
IRIZ
TUNEL/DAPI
(20x)
BrdU/pS3/DAPI
(40x)
H&E
(20x)

FIG.7E

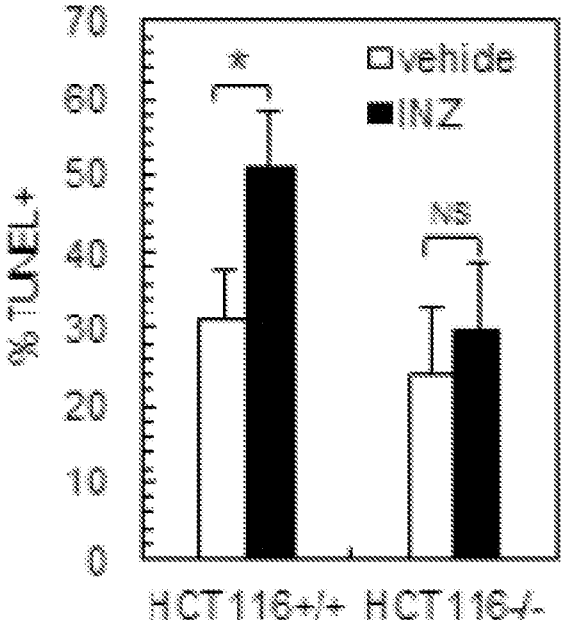
70
60
50
40
30
20
10
0
% TUNEL+
*
vehicle
INZ
Ns
HCT116+/+
HCT116-/-

FIG.7F

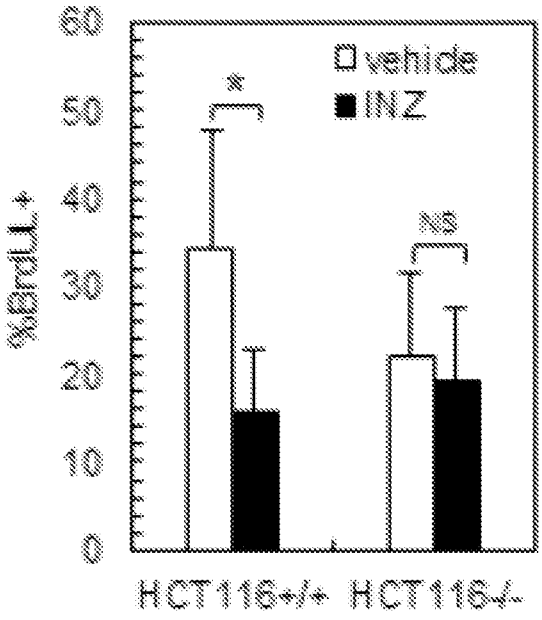
60
50
40
30
20
10
0
%BrdU+
*
vehicle
INZ
Ns
HCT116+/+
HCT116-/-

FIG.7G

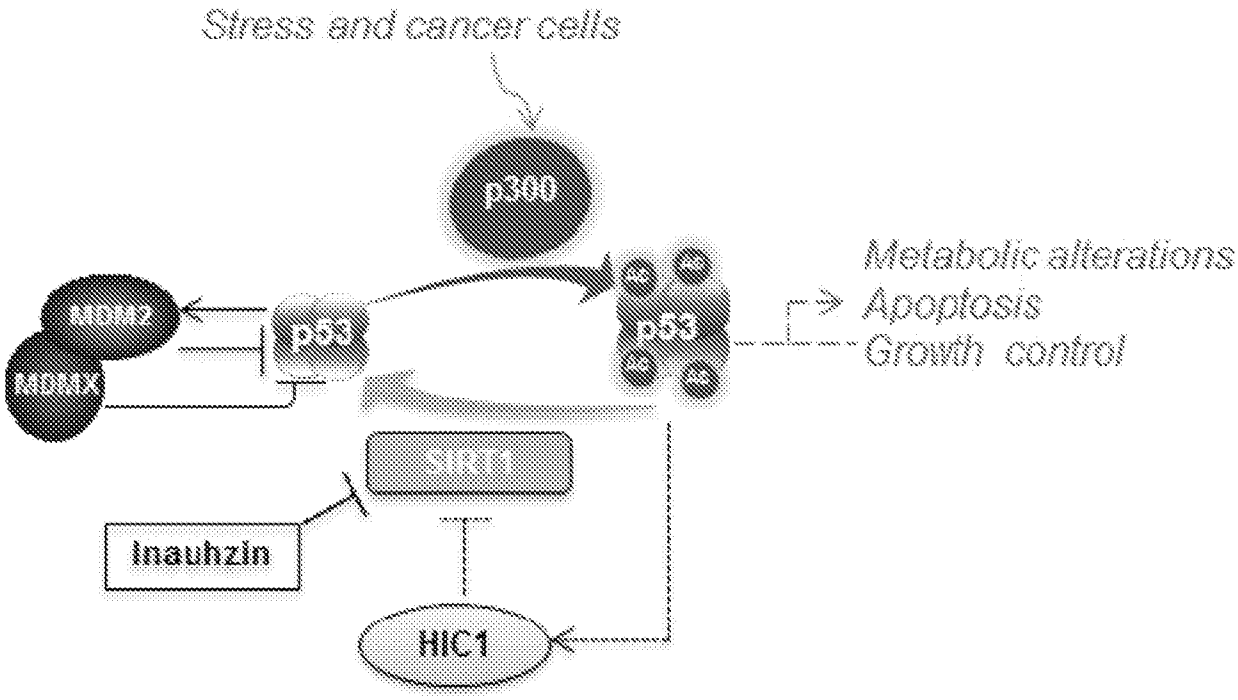
Stress and cancer cells
p300
MDM2
MDMX
p53
p53
Metabolic alterations
Apoptosis
Growth control
SIRT1
Inauhzin
HIC1

FIG.8

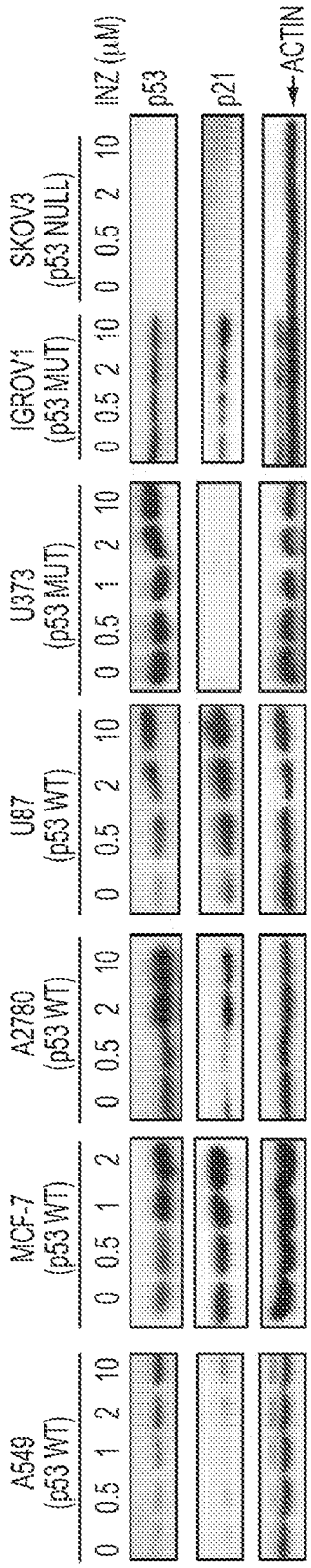
A549 (p53 WT)
0 0.5 1 2 10
MCF-7 (p53 WT)
0 0.5 1 2
A2780 (p53 WT)
0 0.5 2 10
U87 (p53 WT)
0 0.5 2 10
U373 (p53 MUT)
0 0.5 1 2 10
IGROV1 (p53 MUT)
0 0.5 2 10
SKOV3 (p53 NULL)
0 0.5 2 10
INZ (μM)
p53
p21
ACTIN

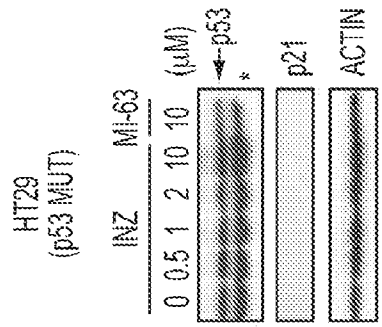
HT29 (p53 MUT)
INZ MI-63
0 0.5 1 2 10 10 (μM)
p53
p21
ACTIN

FIG. 9

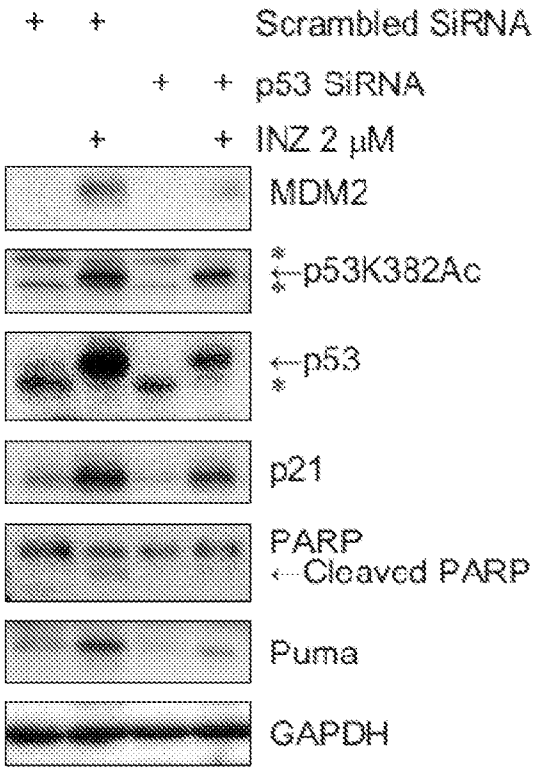

FIG.10A

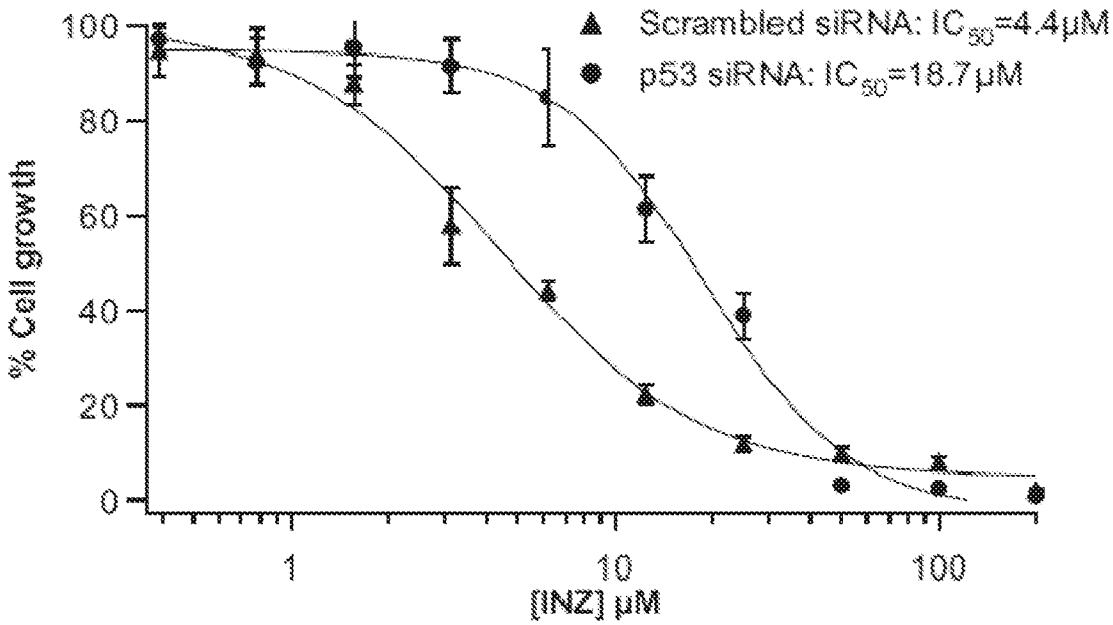

FIG.10B

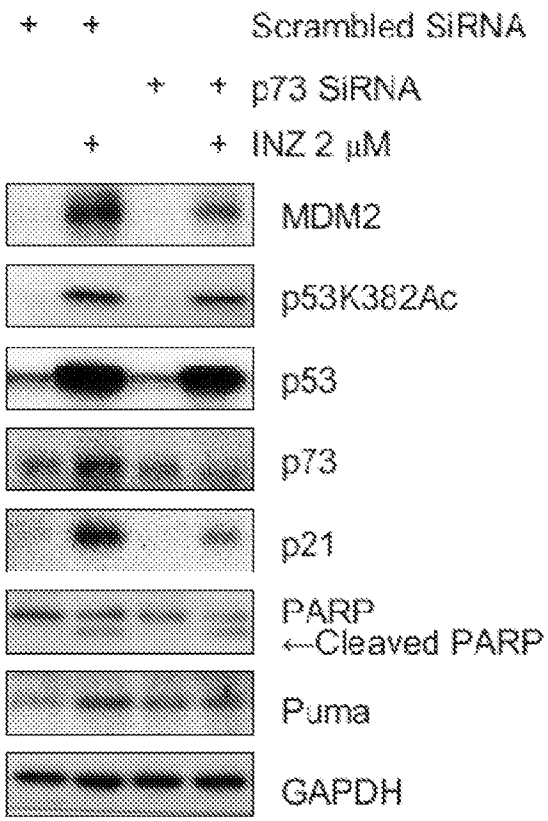
+ + Scrambled SiRNA
+ + p73 SiRNA
+ + INZ 2 μM
MDM2
p53K382Ac
p53
p73
p21
PARP
←Cleaved PARP
Puma
GAPDH

FIG.10C

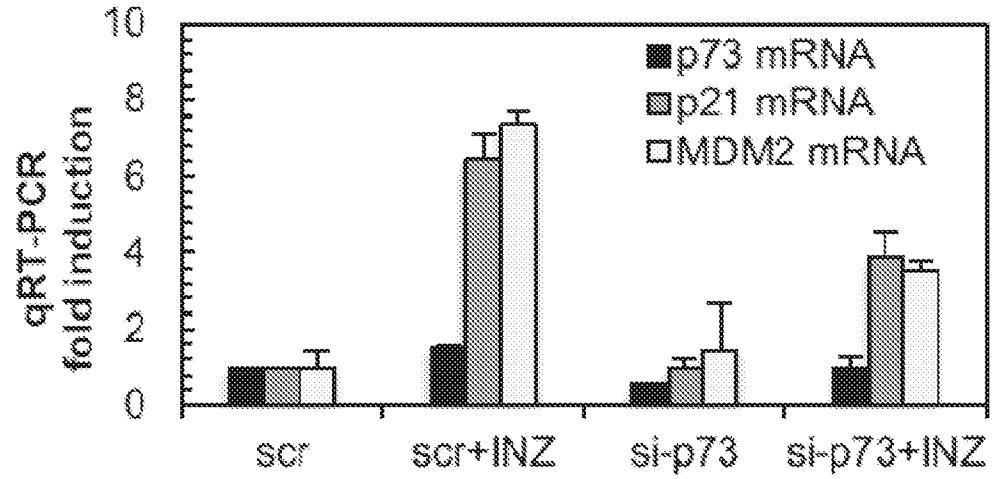

FIG.10D

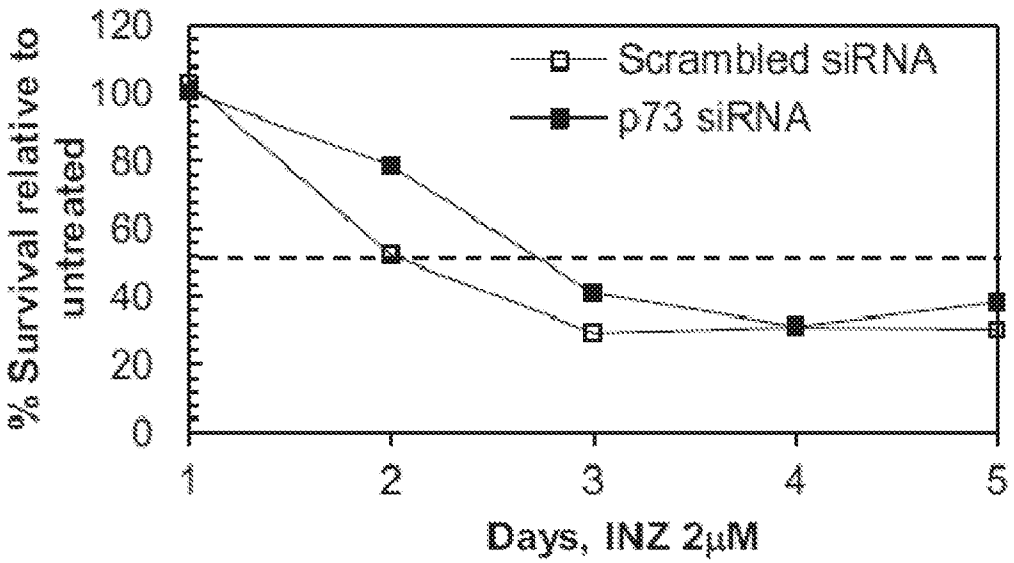

FIG.10E

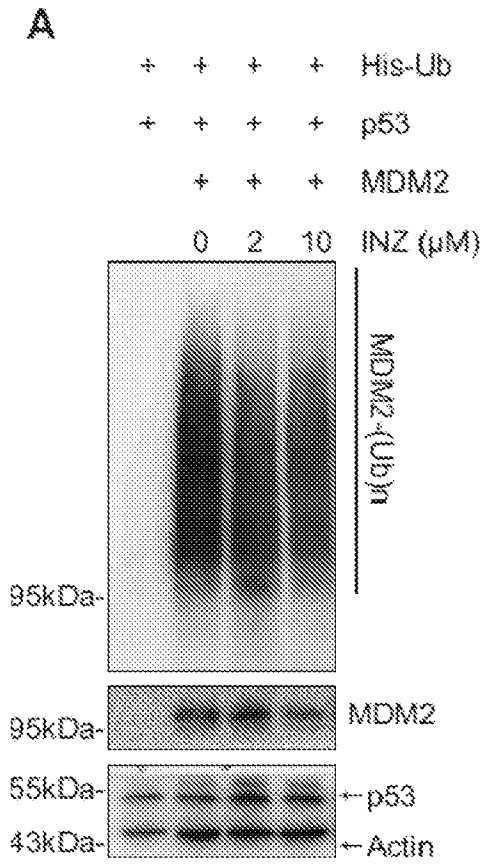

FIG.11A

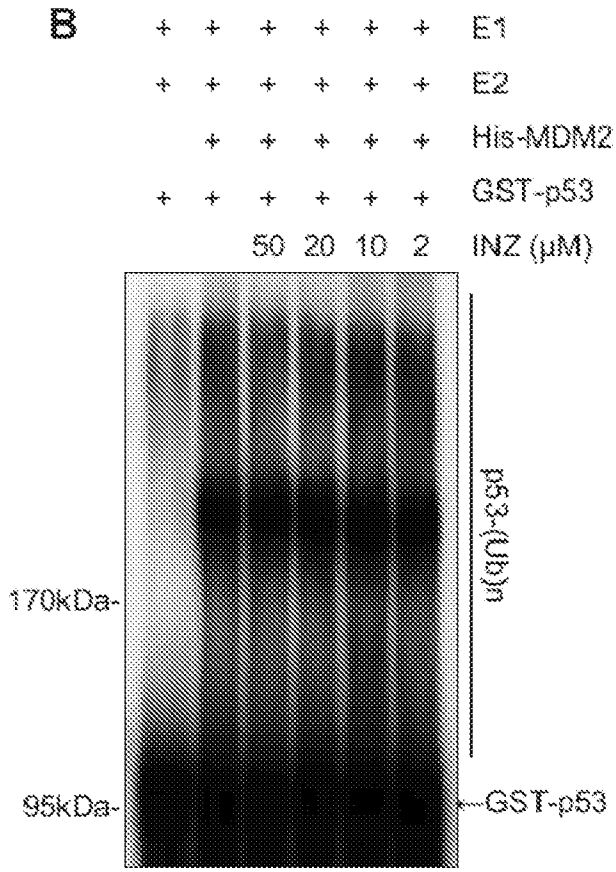

FIG.11B

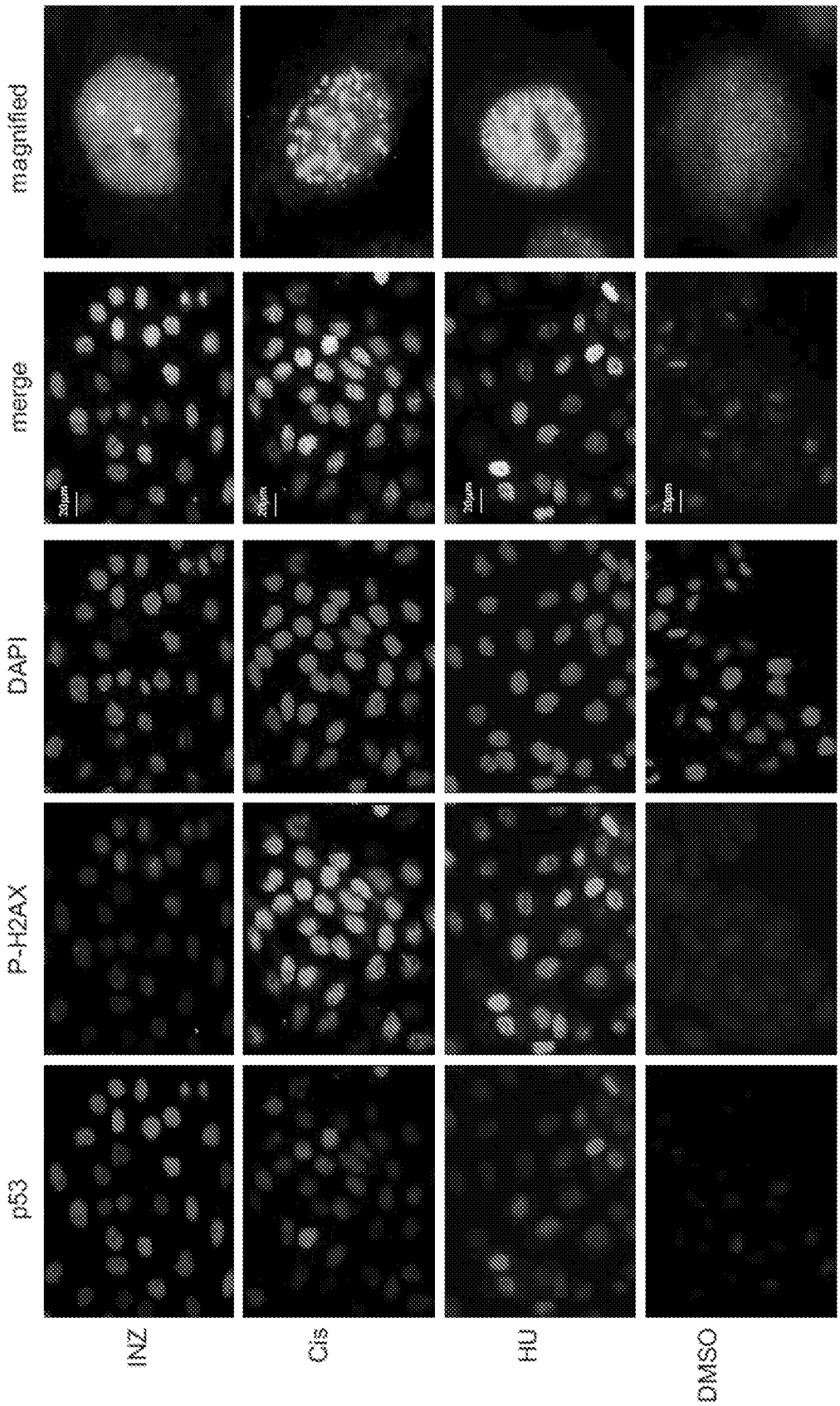

FIG.12A

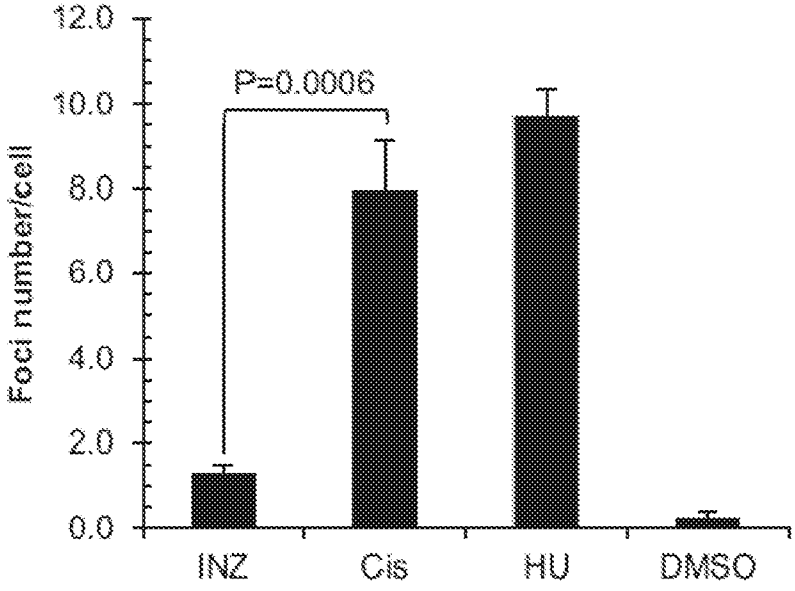

FIG.12B

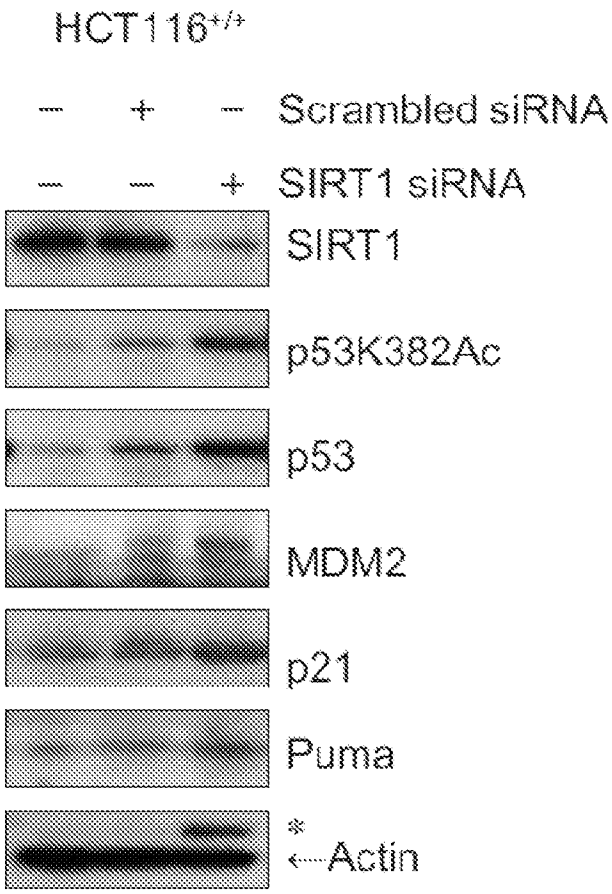

FIG.13A

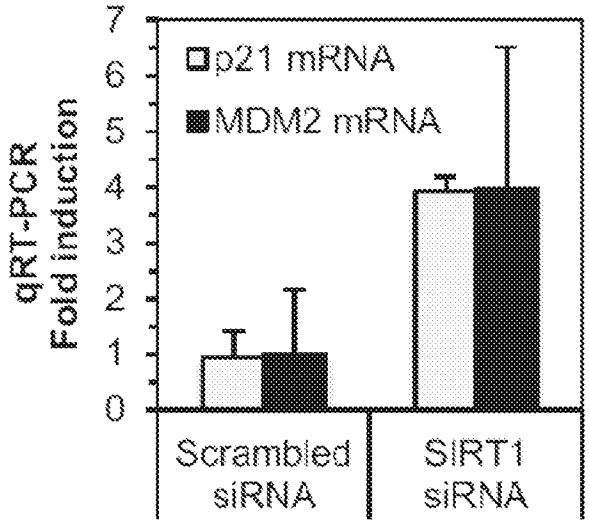

FIG.13B

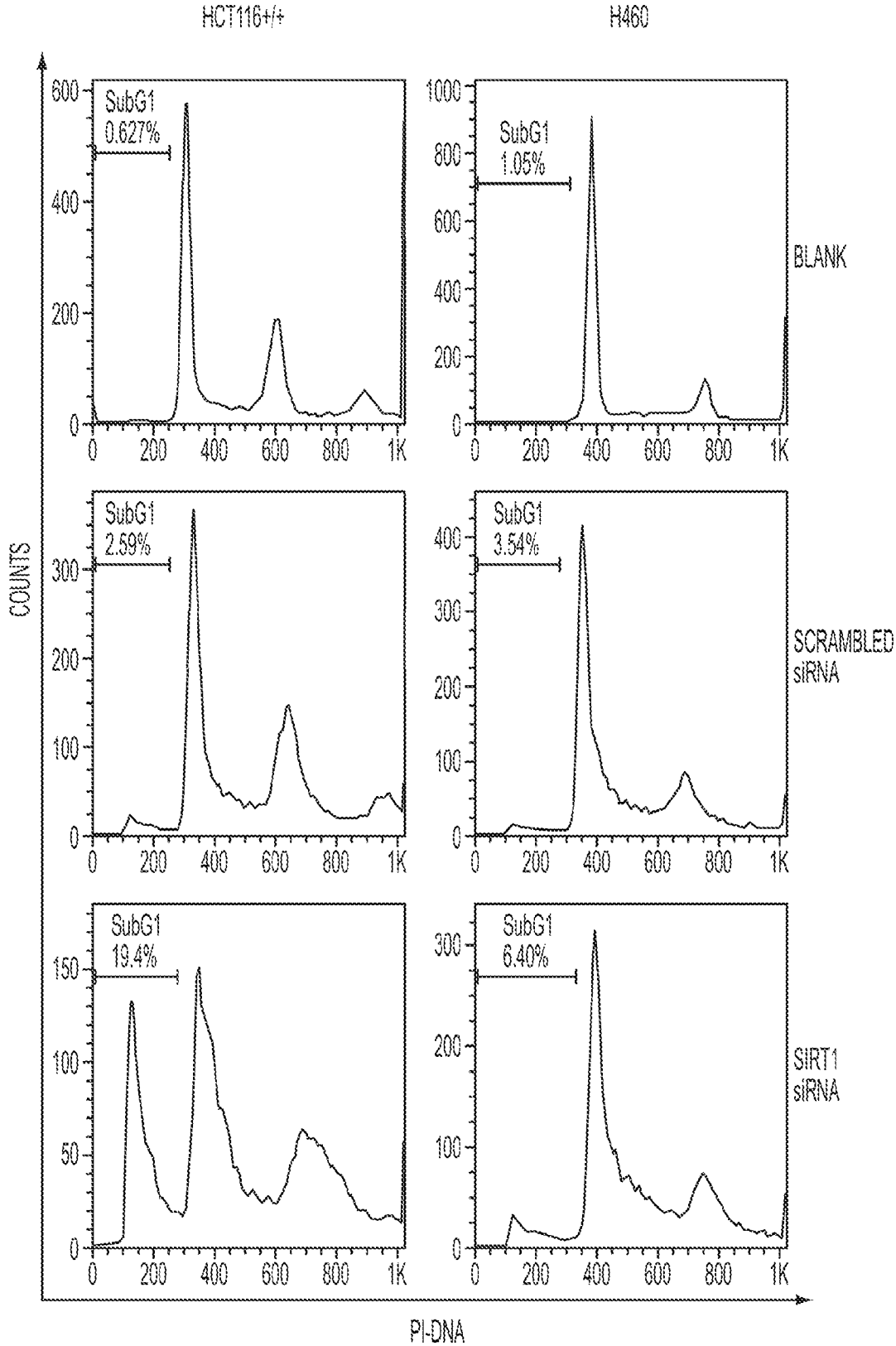
HCT116+/+
H460
SubG1
0.627%
SubG1
1.05%
BLANK
SubG1
2.59%
SubG1
3.54%
SCRAMBLED
siRNA
SubG1
19.4%
SubG1
6.40%
SIRT1
siRNA
COUNTS
PI-DNA

FIG. 13C

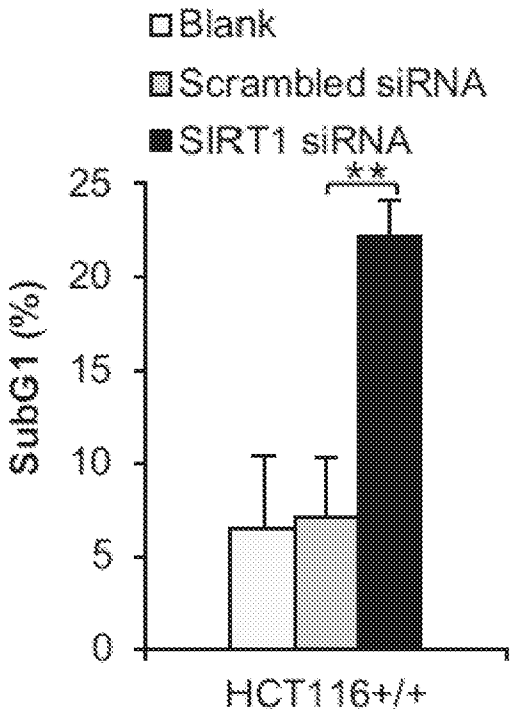

FIG.13D

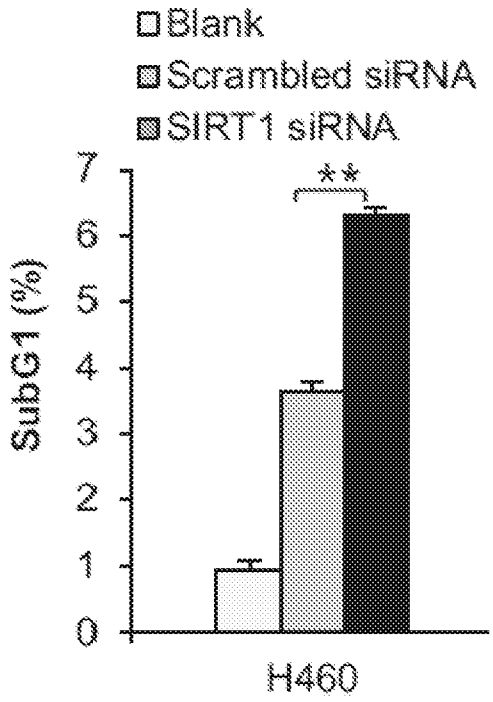

FIG.13E

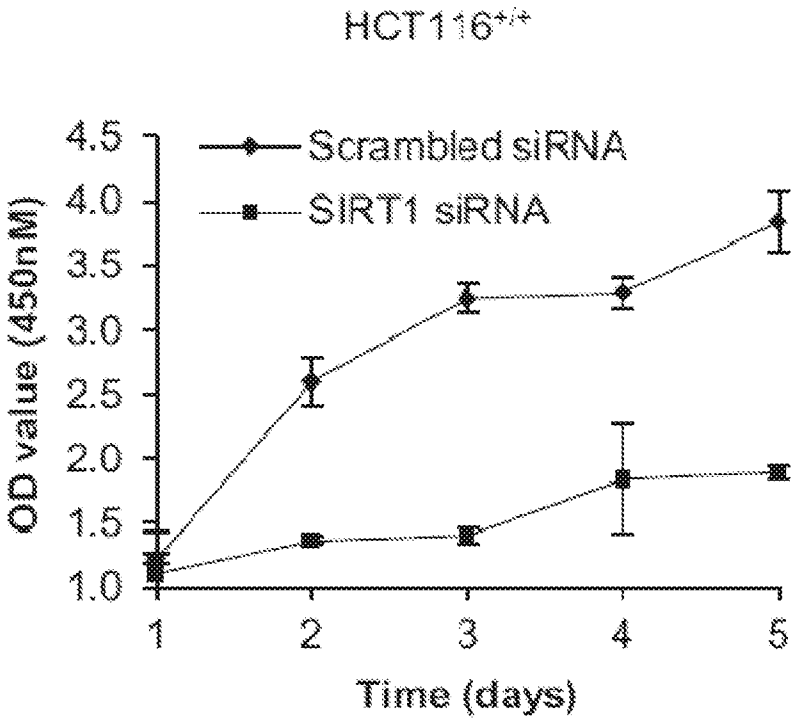

FIG.13F

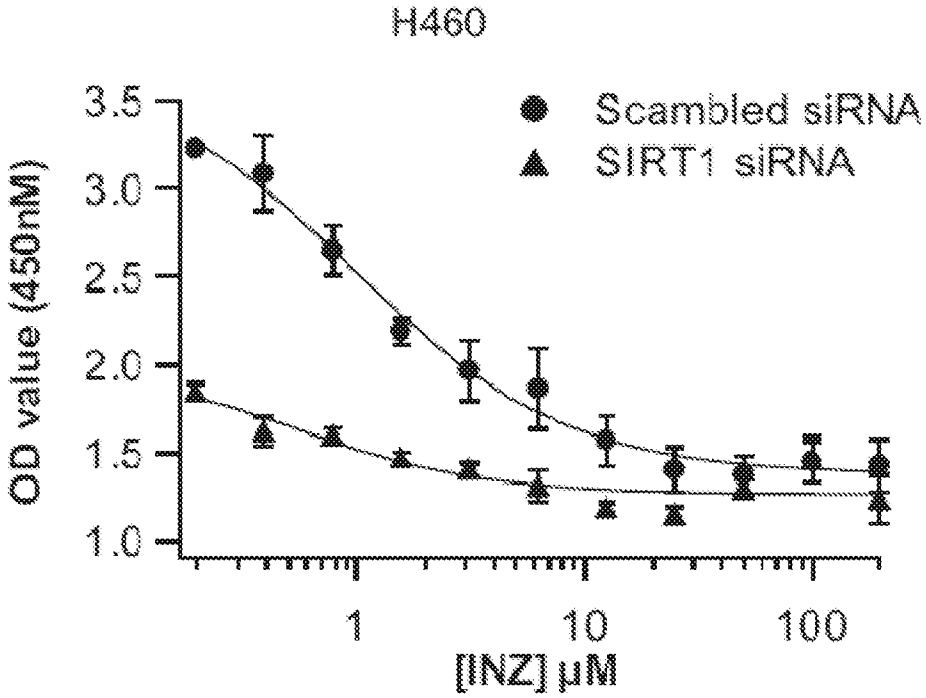

FIG.13G

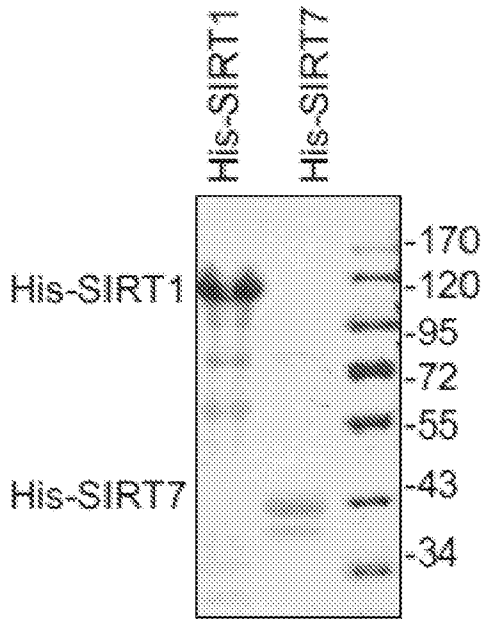

FIG.14A

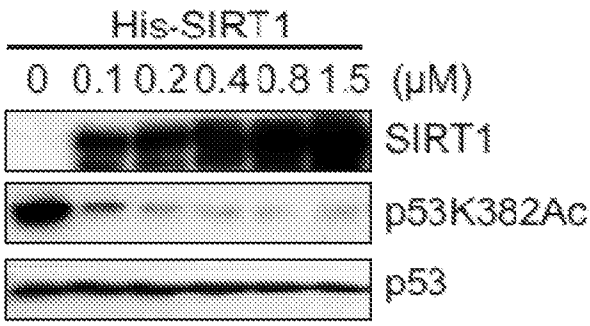

FIG.14B

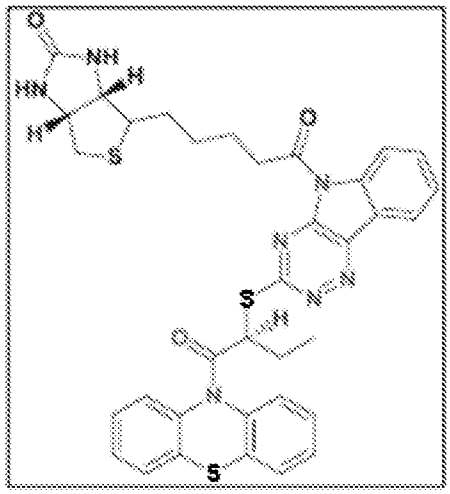

FIG.14C

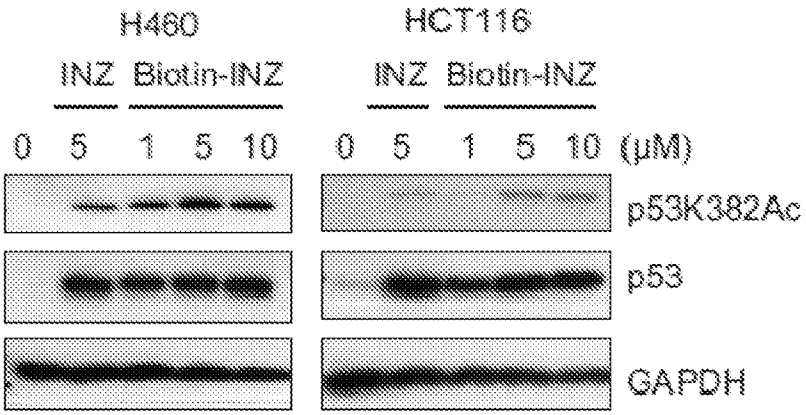

FIG.14D

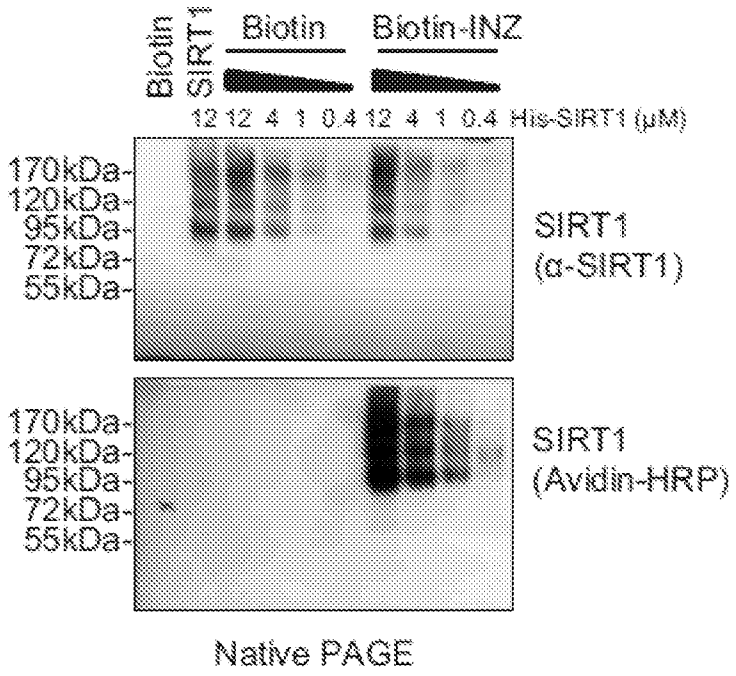
Biotin
SIRT1
Biotin
Biotin-INZ
12 12 4 1 0.4 12 4 1 0.4 His-SIRT1 (μM)
170kDa-
120kDa-
95kDa-
72kDa-
55kDa-
SIRT1
(α-SIRT1)
170kDa-
120kDa-
95kDa-
72kDa-
55kDa-
SIRT1
(Avidin-HRP)
Native PAGE

FIG.14E

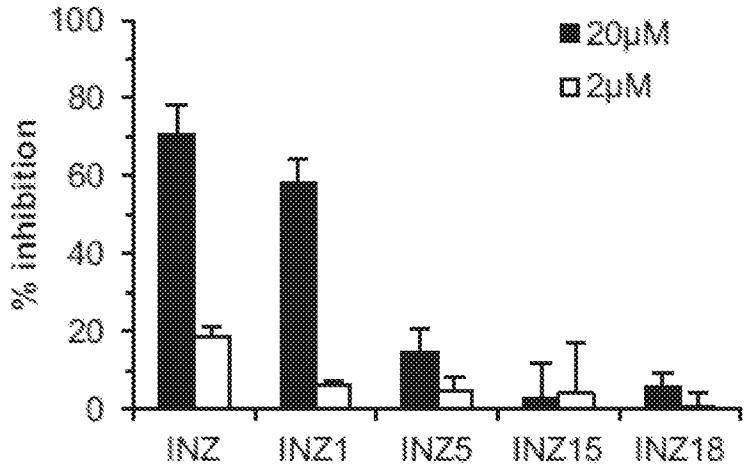

FIG.15A

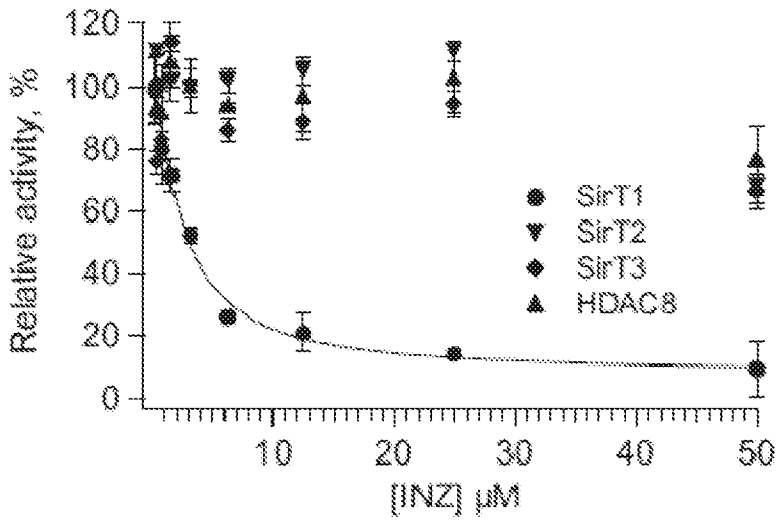

FIG.15B

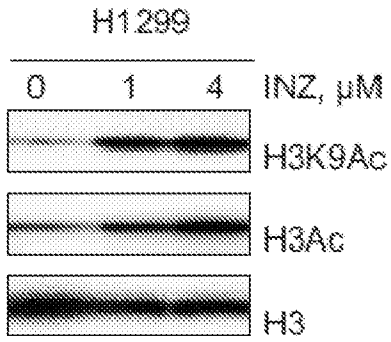

FIG.15C

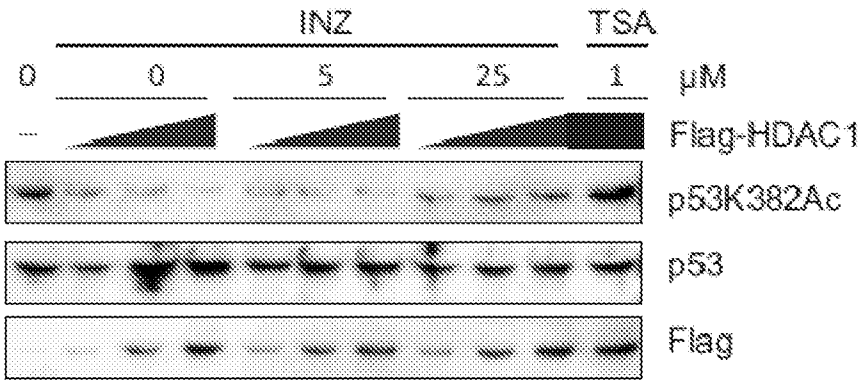

FIG.15D

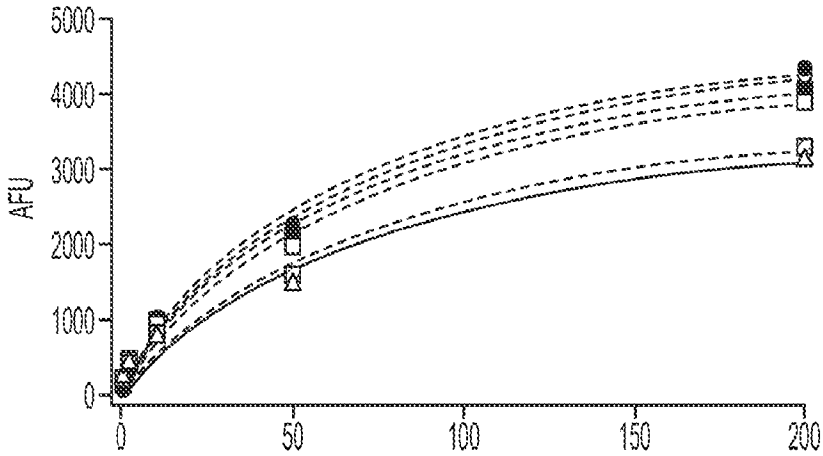

[FdL PEPTIDE] μM

INZ (μM)	%Km	%Vmax
0	100	100
0.8	110.9	100.8
1.6	118.2	105.9
3.1	99.2	91.7
6.3	106.4	89.9
12.5	120.9	75.6
25.0	121.1	70.8

FIG. 15E

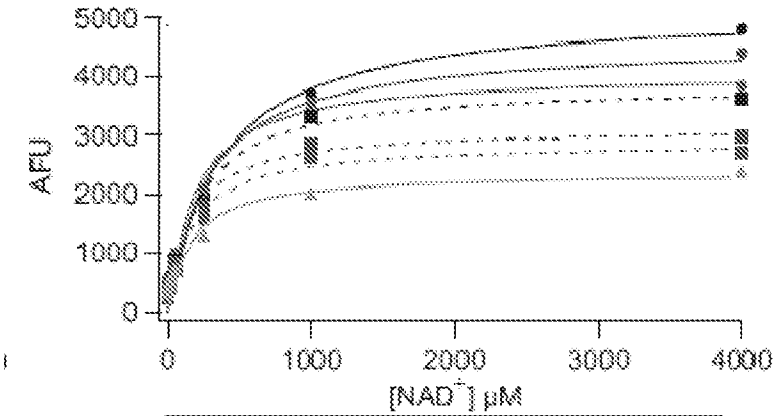

INZ (µM)	% Km	% Vmax
0	100	100
0.8	77.9	85.9
1.6	53.7	74.2
3.1	60.9	69.0
6.3	42.4	51.2
12.5	46.5	45.4
25.0	45.2	33.3

FIG.15F

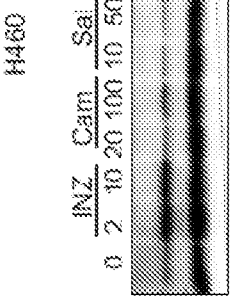

FIG.16A

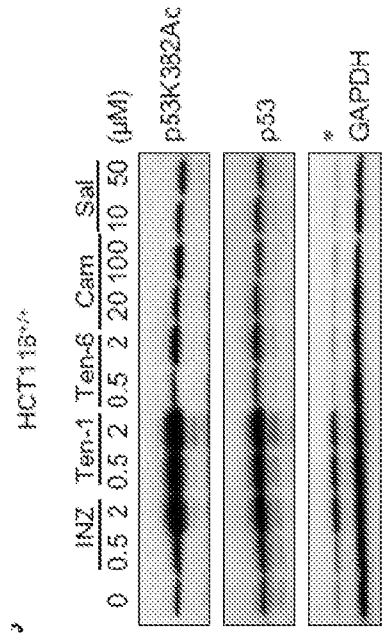

FIG.16B

Structure	Compound	IC_{50} (μM)[a]						
		H460	HCT116	SJSA	A549	AZ784	NHF	W138
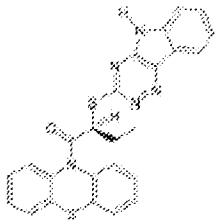	Inauhzin	5.4	2.0	30	3.2	1.67	>100	>100
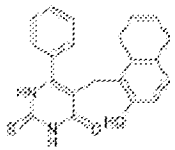	Cambinol	~100	>100	15	>100	>100	>100	>100
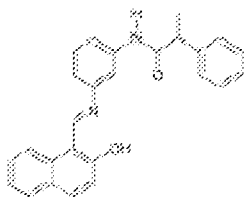	Salermide	55	>100	> 50	30	24.7	54	49.5
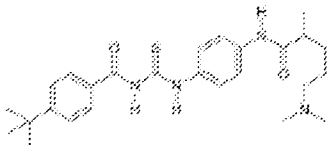	Tenovin-6	3.2	1.3	> 50	3	1.36	8.5	6.8

[a] Relative standard deviations are <20% in all values.

FIG.16C

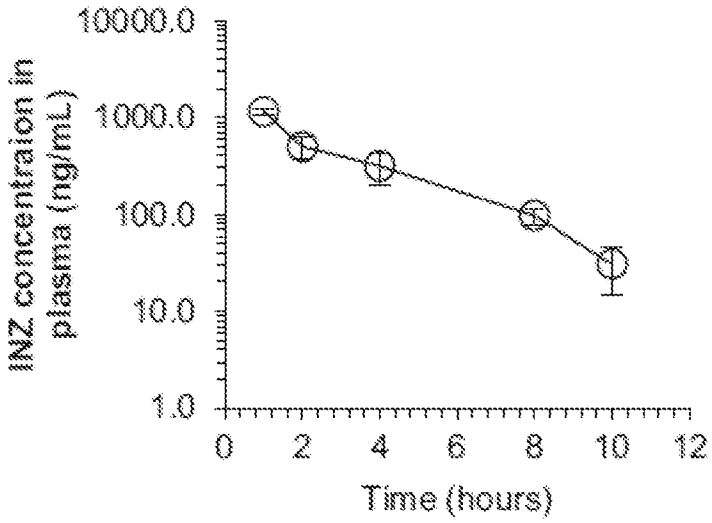

FIG.17A

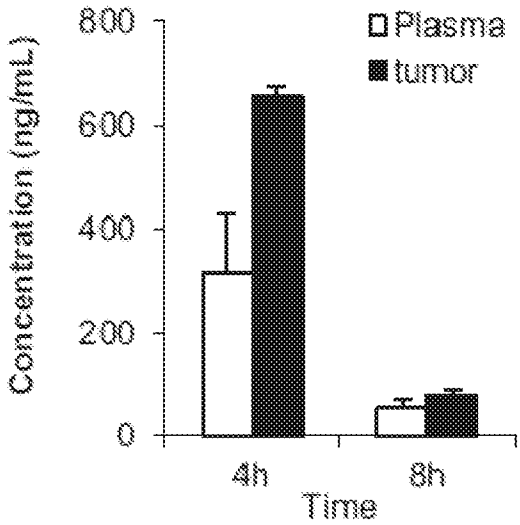

FIG.17B

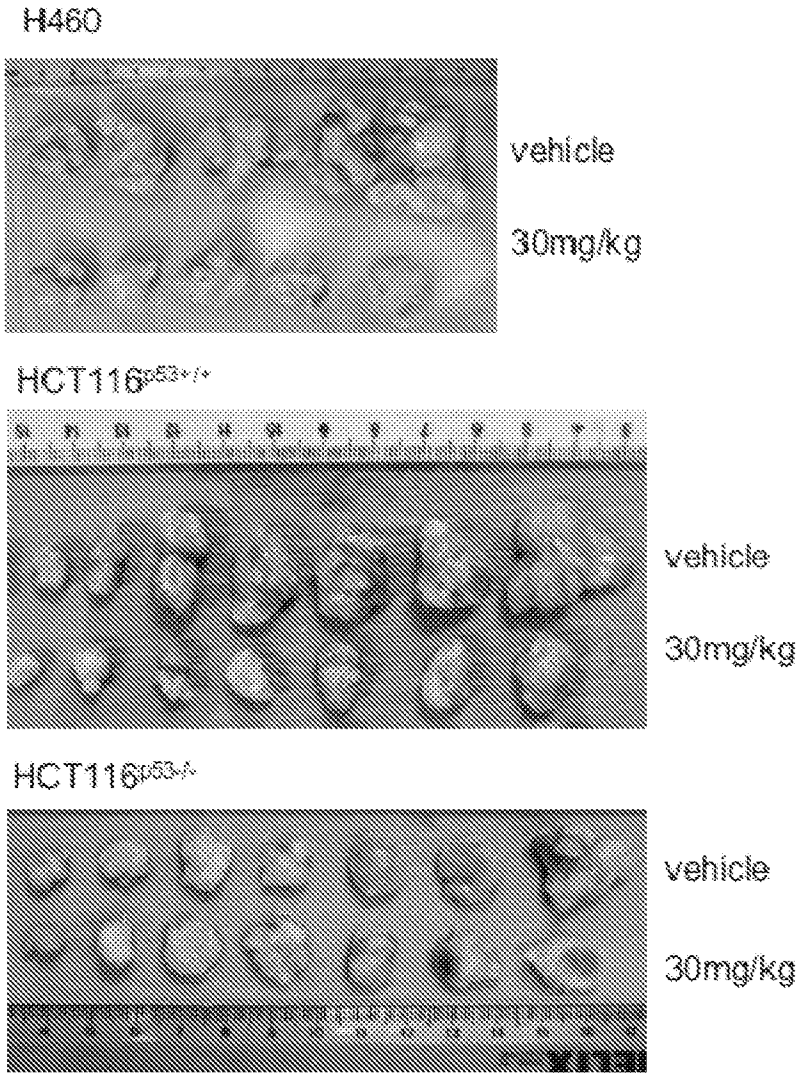
H460
vehicle
30mg/kg
HCT116p53+/+
vehicle
30mg/kg
HCT116p53-/-
vehicle
30mg/kg

FIG.17C

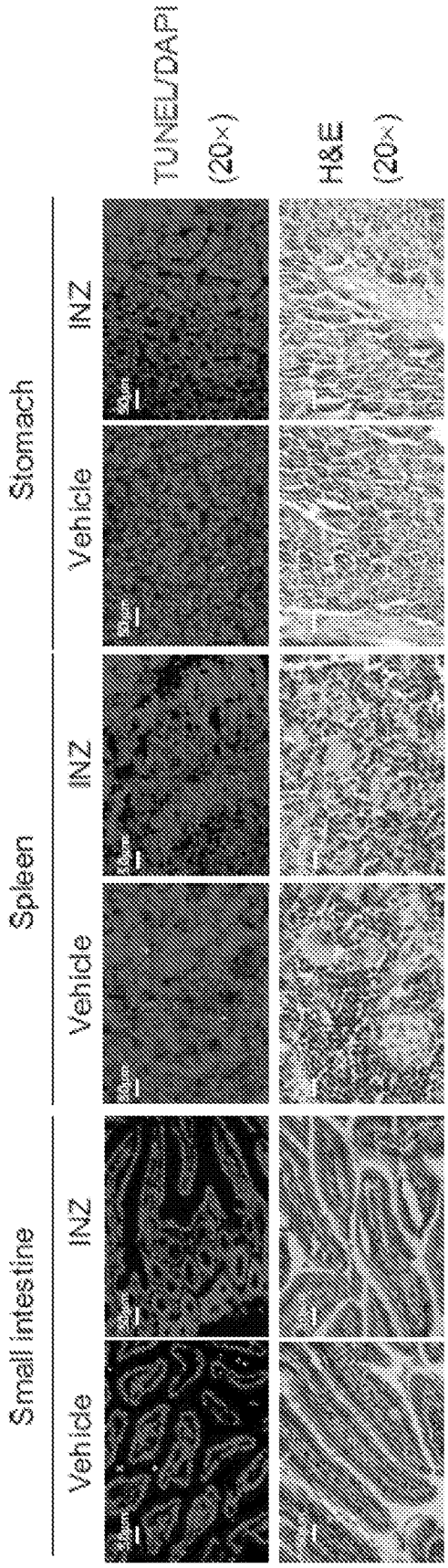
Small intestine
Spleen
Stomach
Vehicle
INZ
Vehicle
INZ
Vehicle
INZ
TUNEL/DAPI (20×)
H&E (20×)

FIG. 17D